EVALUATING TECHNIQUES FOR ONLINE DETECTION OF GENERATOR EARTH-BRUSH FAULTS

A dissertation submitted to the Faculty of Engineering and Built Environment, University of the Witwatersrand, Johannesburg, in fulfilment of the requirements for the degree of Master of Science in Engineering

by

Oupa Mailula

1777690

School of Electrical and Information Engineering

University of the Witwatersrand

Johannesburg, South Africa

Project Supervisor: Prof. W. Cronje (Willie.Cronje@wits.ac.za)

Co-Project Supervisor: Dr. Lesedi Masisi (Lesedi.Masisi@wits.ac.za)

Johannesburg, 2021

Declaration

I declare that this dissertation, Evaluating Techniques for Online Detection of Generator Earth-brush Faults, is my own, unaided work, except where otherwise acknowledged. It is being submitted for the degree of Master of Science in Engineering at the University of the Witwatersrand, Johannesburg. It has not been submitted before for any degree or examination at any other university.

Signed this _01_ day ____June___of 2022

____

Oupa Mailula

ABSTRACT

Poor performance of shaft earthing system is caused by a wide range of factors such as the high wear rates of earth-brushes, which reduces shaft earthing contact, the environmental contamination of brushes by seal oil, and carbon dust contamination. This study evaluates online shaft-signal based techniques to classify different earth-brush fault types using shaft current and voltage measurements during operation to monitor the condition of synchronous generator earthing brushes. The effects of shaft earthing brush faults on shaft voltages/currents were successfully determined through physical measurements and experiments using a two-pole, 20 kVA synchronous generator which was designed and built to mimic a full-sized 600 MW turbo generator. Measurements on a two-pole synchronous generator found that the shaft voltages and current characteristics are responsive to the earth-brush faults. The results of an investigation indicated that the shaft voltages and current characteristics have effects on earth-brush fault types. The harmonics of the shaft voltage show a definite trend for the 3^{rd}, 5^{th}, and 9^{th} harmonics which is significant in the diagnosis of an earthing brush fault system. Therefore, it is possible to determine the earth-brush condition from shaft voltage and current measurement given that baseline information is available. The evaluation of shaft-signal based fault detection techniques such as warning criteria, threshold checking and frequency spectral analysis techniques indicated that the frequency spectral analysis technique is the most suitable technique for generator shaft earthing system condition monitoring and exhibits best earthing-brush fault detection capabilities than any of the others. The technique provides a holistic overview of the performance of shaft earthing brushes and does not depend on initially set or benchmark threshold values of the measured quantities.

Key words/ Key terms

- *Bearing current, earth-brush, performance problems, spectrum analysis, shaft currents, shaft earthing, shaft voltages, worn-out brushes*

Acknowledgements

I would like to thank my supervisors Prof Willie Cronje and Dr. Lesedi Masisi for their patience, advice and support in all forms. I would like to also thank my industrial supervisor Dr. Simon Higgins for his technical guidance and for motivating me, and I am very grateful for Eskom for financial assistance. Lastly, I would like to further extend my gratitude to my wife Vinolia and Jesus Christ for their invariable support and love at every moment of my life.

Contents

LIST OF FIGURES

LIST OF TABLES

LIST OF SYMBOLS

A cross-sectional area (m^2)

B Magnet flux density [T]

Ɛ Induced voltage (V)

f frequency (Hz)

H Magnetic field intensity [A/m]

I Current (A)

L Length (m)

R Resistor (Ω)

t time (s)

μ Magnetic permeability [H/m]

ϕ Magnetic flux [Wb]

LIST OF ABBREVIATIONS

AC	Alternating current
DC	Direct current
DE	Drive end
EE	Exciter end
FFT	Fast fourier transform
IR	Insulation resistance
I_{RMS_peak}	RMS peak current
$I_{RMS\_average}$	RMS average current
IP	Intermediate pressure
kVA	Kilovolt-ampere
kW	Kilowatt
NDE	Non-drive end
OEM	Original equipment manufacturer
RMS	Root mean square
RPM	Revolutions per minute
V_{dc}	DC voltage
V_{rms_peak}	RMS peak voltage
$V_{RMS\_average}$	RMS average voltage

Chapter 1

Introduction

Overview

Earthing brushes are used as contact mediums to earth generator shaft journals and can also be employed for measuring and monitoring the condition of generators. The earthing brush is connected to an earthing cable through a current-measuring shunt resistor to allow stray shaft currents on the shaft to discharge to the earthing mat.

Utilities' turbine generators are guarded against the damage caused by excessive shaft voltages or currents by using conventional earthing brushes (usually carbon, silver/gold and copper braided brushes) as they are designed to direct and release stray shaft currents and voltages on a shaft to the earth mat [1] [2]. The current brush is normally installed at the drive end of the generator to avoid the creation of ground loops, and this location has been found to be effective in removal of stray currents or electrostatic charges, as well as shaft voltages originating in generator [1] [3]. The current brush should protect the generator bearings and hydrogen seals from damage by providing a low-impedance path to earth for stray shaft currents.

However, due to poor asset management and abnormal operating conditions, the integrity of these brushes can be compromised. If they are not properly maintained, shaft earthing brushes fail to protect generator bearings, gears and hydrogen seals, and this result in serious and costly damage to the components of a turbine generator (in other words, bearing, seals and gears) [2] [3].

Earlier researchers have discovered that shaft-signal data from generators exhibit characteristic harmonic changes when the generator is under abnormal operating conditions [4] [5] [6].In particular, it has been found that by analysing the generator's shaft-signal data, inferences can be made about certain generator fault conditions. This is achieved through signal processing, analysis and interpretation, and then detection of the fault conditions [4] [5] [6].

The project presented in this thesis aimed at evaluating techniques for classifying faults in earth-brushes, which use online voltage and current data from shaft signals. Effective shaft-signal based techniques are needed to monitor the condition of earthing systems while online; this project aimed to increase the effectiveness of physical shaft-signal analyses and interpretation in order to detect earth-brush inception faults and maintain effective generator earthing system performance.

This report documents the different project phases, beginning with a background to the origins of generator-shaft voltages and currents, moving to earth-brush performance problems, utilities' experiences of operational failure, background to the existing techniques for monitoring shaft-signal data, and physical experiments carried out with a standard miniature two-pole synchronous generator. This leads to techniques of classifying faults using shaft voltage and current data, and a general conclusion. The research aim and objectives are outlined in the next section.

1.1 Research Aims and Objectives

The main goal of this research study was to evaluate different shaft-signal based techniques to determine online, *in situ* earthing brush performance. The study further investigated the effects of earthing brush performance from shaft-signal (i.e. shaft voltages/currents) characteristics. The aim was to advance the efficiency of earthing system condition-monitoring and forestall premature component failures. The key objectives of the research are to:

- Investigate the effect of good and poor earth-brush shaft contacts, using shaft voltage and current measurements
- Investigate the effect of a lost shaft ground circuit or loss of earthing continuity, using shaft voltage and current measurements
- Investigate the effect of earth-brushes' exposure to oil and dust, using shaft voltage and current measurements
- Evaluate an effective online shaft-signal based technique for monitoring the condition of the shaft earthing system
- Developed a method for online Earth-brush fault detection

The outcomes of this study will feed into the improvement of the monitoring systems of utilities' generating plants globally. This knowledge will add value to proactive condition-monitoring by reliably distinguishing problems as they develop in shaft earthing systems.

The plant personnel will then be able to use this knowledge to plan remedial actions well in advance and schedule corrective action during planned outages. By using such knowledge, imminent component damage and unplanned outages can be minimised.

1.2 Dissertation Outline and Contributions

1.2.1 Chapter 2 – Literature Survey

The work of Ziemianek [1], Hoffe [6], Sohre [19], and Nippes [25-27] is presented and discussed. Three shaft-signal based fault detection techniques, namely frequency spectral analysis, warning criteria and threshold checking are discussed.

This chapter further presents generator earthing brush application philosophy, general overview of the existing generator condition-monitoring systems and associated generator shaft-signal based analytical techniques. The application of shaft-signal based techniques to detect and interpret impending generator faults is explained. A background is then provided of the historical application of the shaft-signal based techniques to analyse, diagnose and early warning detection of generator failures.

1.2.2 Chapter 3 – Theory

Chapter 3 presenting the four main causes of shaft voltages and currents in a synchronous turbine generator. It explains the basic theoretical concepts of shaft voltages/currents generation and gives a detailed explanation of the four main causes of shaft voltages and currents in an operating synchronous generator.

1.2.3 Chapter 4 – Miniature Synchronous Generator Experimental Set-up

Chapter 4 presents the experimental set-up, shaft current and voltage measurement techniques and measurement error analysis. Results analysis and interpretation using a signal processing tool such the fast Fourier Transform (FFT) and current scatter plot are elucidated.

1.2.4 Chapter 5 – Test Performance and results

This chapter presents test performance and experimental results analysis. The effects of shaft earthing brush faults on the shaft-signals (i.e., shaft currents and voltages) were investigated through physical measurements and experiments on a 2-pole, 20 kVA synchronous generator. Experiments were conducted for different earth-brush faults at four different earth-brush faults scenarios. The results of an investigation of the shaft voltage and current effects in the frequency domain were obtained in these four scenarios under different earth-brush fault conditions. The results obtained in these scenarios are presented and discussed. Obtained results are analysed and interpreted by performing signal-processing on the measured shaft currents and voltages. It is concluded that the shaft voltages and currents characteristics are responsive to earth-brush faults.

1.2.5 Chapter 6 – Evaluating Online Fault Detection Techniques

This chapter presents different shaft-signal based fault detection techniques that will be applied to the test performance and results in Chapter 5. The method employed utilises shaft current and voltage characteristics to determine online, and *in situ*, the condition of earth-brushes. Different shaft-signal based techniques were considered for analysis of the earth-brush condition. Online earth-brush early warning fault detection and streamlined flowchart for earthing system fault detection are proposed.

1.2.6 Chapter 7 – Conclusion and Recommendations

This chapter provides a general overview and conclusions of the research presented in this document. A summary of the suggested future recommended research projects is presented.

Chapter 2 Literature Survey

2.1 Literature Survey

Previous researchers working on generator rotor shaft earthing systems [4] [5] [6] have conducted a number of studies and published results on shaft voltage and current signal-based techniques. Other research studies in the recent past have investigated the use of shaft signature faults and frequency spectral analysis as a diagnostic tool for electrical machines [3] [4] [5] [6]. These studies have dealt with specific faults on generators and the effects thereof on shaft voltages. The most common technique of assessing these effects is by analysing the variants in the harmonic components of the shaft voltage signature when a fault occurs. It was discovered that these techniques can be used for generator fault diagnosis and prognosis. These machine operational fault-frequency relationship techniques have brought about a better understanding of fault diagnosis and prognosis.

Nippes [7] also studied the shaft current-voltage relationship. He investigated the effects of shaft voltage on earthing resistance by inserting different earthing resistors in the shaft grounding circuit. He discovered a significant reduction in shaft voltage as the resistors were inserted into the brush earthing cable [7]. These tests provided insightful information on the relation of the shaft-signal effects on the earthing brush system.

Ziemianek [1], Nippes [2] and Sohre [8] investigated different types of earthing brush performance in various environmental and operational conditions. They also discovered that carbon brushes have a greater current-carrying capacity than other conventional brushes (silver-graphite, metal fibre), however, deposit residues increased contact resistance, eventually making the earthing system completely ineffective [1] [2].

Recent studies have investigated the use of shaft signals as a diagnostic tool by using harmonics content [9] [10]. Hoffe [4] and Doorsamy [6] investigated the subject of synchronous generator diagnosis using shaft voltage signal measurements. It was proved that shaft voltage signatures could be used to diagnose eccentricity and generator field faults.

Several research papers were published about the condition monitoring of electrical machines using the frequency spectral analysis technique [6] [9] [10]. The frequency spectral analysis technique described in Stone [3] , Higgins [9] and Thompson [10] uses the harmonic component of the shaft-voltage signal as information that will allow the source of the fault to be identified.

It has been shown that the harmonic content of a shaft voltage signature contains information that will allow the source of the shaft voltage to be identified [3] [4] [6] [9]. Traditionally, this shaft-signal based monitoring technique entails fast Fourier Transform (FFT), analysis, and interpretation. This is the most widely used analysis and interpretation technique by many power utilities for generator fault diagnosis and is gaining popularity in the field of condition monitoring [6] [9]. The most common approach of analysis and interpretation of the FFT signal is by assessing the change in harmonic content when a fault occurs.

Previous researchers have provided shaft-signal based techniques and the work of Nippes [11] and Posedel [12] provide warning criteria of the developing problems in shaft earthing systems. Doorsamy and Cronje [13] have experimentally demonstrated that the magnetic asymmetry that is due to manufacturing imperfections, such as variable air gaps, rotor misalignment and core imperfections, introduces relatively high nominal values of 5^{th} and 6^{th} harmonics.

Another technique for analysis and interpretation is shown in Posedel [12] where structured evaluation logics are developed based on measured shaft voltage and current measurements. The measured currents and voltages are baselined and based on theoretically- and practically-acquired threshold values to produce a binary combination of measured variables to define the condition of the machine.

In previous years, researchers have focused on issues involving diagnosis of rotating machines and mechanisms that lead to faults arising from shaft-voltages. Through a review of previous literature and after consultation with experienced system engineers, it became clear that there are uncertainties about earth-brush faults types and interpretation and analysis of earthing brush performance. Thus this research is concerned with earthing brush performance, analysis, and interpretation. The performance of an earthing brush depends on whether it is making proper contact, is misaligned or contaminated.

2.2 Problem Statement

This section provides a review of industrial and utility experience of earth-brush performance and associated problems. It highlights reasons for the great need of effective online shaft-signal based fault detection techniques to determine online, *in situ* earthing brush condition.

The high failure rate of generator components as a result of poor earthing has created a significant need to improve the effectiveness of techniques of analysing the performance of earthing systems, in order to avert premature failures.

To assist the reader in understanding the need for a more effective methods of earthing systems and monitoring their condition, the section presents a brief general overview of common turbine generator bearing damage due to shaft voltages and currents, utilities' experiences of operational failures and the existing condition-monitoring systems.

2.2.1 Problem Description

Shaft earthing brushes are usually applied on both ends of the generator shaft to minimise potential shaft voltage build-up. However, turbine generators still experience high shaft voltage build-up because of poor shaft earthing system performance caused by problems such as worn-out earth-brushes, floating or disconnected earth-brushes and contamination of brushes. These problems cause the generator to experience high shaft voltages/currents, shaft magnetisation, hydrogen seal failures, bearing failures and gear failures as a result of poor earthing systems. [3]

If these problems are not monitored, they can cause costly generator component failures [3]. The most prevalent bearing damage types are due to stray shaft currents and voltages, as discussed in subsection 1.3 below.

Shaft earthing problems result from poor asset management and maintenance [1]. It was discovered that poor performance of earthing brushes is one of the biggest reasons for shaft voltage build-up [3].

Shaft earthing brush performance problems are a subject of interest in the utility industry and academic community [1] [8] [9]. The research trend is to focus on methods to measure and identify generator operational faults, shaft brush application and various brush technology evaluation, analysis and interpretation techniques. In these investigations, some researchers have refined the use of shaft voltage and current measurements to diagnose machine faults, categorise generator fault types, and analyse various shaft voltage/current interpretation techniques.

The early identification of generator faults and the analysis of source failures in electrical machines is very important. Nipples [14] and Sohre [8] discuss the unreliability of conventional brushes made of carbon, silver, solid metals and copper braids and combinations of these materials. Different analyses and interpretations of shaft voltages have been employed in Sohre [8] to analyse and locate causes of earth-brush failures. Sohre lists the following causes as important:

- An excessive amount of brush dust from normal operation that is very conductive and extends to the adjacent area, and which requires frequent maintenance (requires frequent cleaning or replacement)
- An excessive amount of brush dust, which increases brush contact resistance
- A high wear rate of brushes, which compromises the earthing brush performance
- Loss of brush contact and earthing integrity due to poor shaft contact resistance
- Earth-brushes are intolerance to seal oil, dirt, and other types of environmental contamination

Earthing brush performance tests have been investigated in Ziemianek [1] and Sohre [8] and it was found that conventional shaft earth-brushes are intolerant to oil, brush residue, dirt and other types of environmental contamination. Researchers have found that worn earth-brushes provide zero or non-existent brush contact with the shaft surface. Worn earth-brushes were found to be providing zero conductivity and not making the required grounding. It was also discovered that worn earth-brushes accumulated an excessive amount of conductive dust, which increased the grounding resistance.

Ziemianek [1] found that a great deal of maintenance is required to keep carbon brushes in good operational condition. According to Ziemianek [1], frequent maintenance for cleaning, removing brush deposits from the shaft and foreign material worn off from the brushes is required to ensure that the grounding system is in a sound operational condition. However, this maintenance is required at unpredictable intervals.

With a focus on safety, the on-load maintenance of generator earthing systems is becoming a major issue as maintenance personnel have to work very close to rotating shafts spinning at 3 000 rpm. According to Ziemianek [1], this reality affects the regular maintenance of shaft earth-brushes as it is difficult to perform such maintenance while generators are in service.

2.3 Bearing damage due to shaft voltages and currents

Earth-brushes are key components that are used to control and discharge the circulating shaft currents in the electrical generators. In literature, it was found that effective earth-brushes installed on both ends of generator shaft reduce the shaft voltage and restricts the flow of circulating shaft current [15]. If earth-brushes are not effective, circulating shaft currents can cause discharges through key components such as bearings, hydrogen seals and gears [1] [8]. These shaft-signal discharges over time have caused detrimental damage to bearings, hydrogen seals, and even costly generator component failures [1] [2] [8]. As a result, the need to monitor the performance of these earth-brushes, as proposed in this study, is of great significance to ensure that brushes are always in an effective operational condition so that impending danger can be averted.

Previous researchers have provided insightful information on bearing damage from shaft current and voltage [1] [16]. The following factors have been identified as a source of bearing failures, namely frosting, pitting, spark tracks, and welding.

- Frosting bearing damage known as frosting is the most usual type of bearing damage due to shaft voltages. This damage is due to the breakdown, by electrostatic discharge, of the resistance of the oil film that lubricates the bearing between the shaft and inner casing. The frosting damage is invisible to the naked eye but can be seen through a microscope.

- Pitting bearing damage to a bearing is similar to frosting damage but the irregularities are much larger because of the strength of the source. Pitting is uncommon and when it happens it does not extend to the whole area as frosting does.

- Spark tracks bearing damage on a bearing are visible to the naked eye. The spark tracking is due to impurities in the lubrication oil caused by electrical arcing by the circulation current. The spark track has the same depth over its entire surface and is often skewed to the direction of rotation.

- Welding bearing damage is visible to the naked eye and can be detected by visual inspection. It occurs due to extremely high circulation currents. This phenomenon is known as "self-excitation".

2.4 Utility Operational Experience

In the past five years, problems that result from shaft earthing system failures have been experienced in various utility companies [1] [3][17]. All the identified failure mechanisms of these cases are listed in *Table 1* and were caused by circulating shaft currents due to poor shaft earthing brush performance. The list of incidents is as follows:

Table 1: Operational utility failure incidents due to poor shaft earthing [17]

Cases	Incident date	What happened
#Case 1 125 MW Generator 7	8 May 2012	Unit 7 tripped due to high bearing vibrations. The cause of failure was established to be electrical stray current discharges because of a poor earthing system.
#Case 2 200 MW Generator 1	3 July 2012	Unit 1 tripped due to an H_2 seal failure. The cause of failure was electrical arcing between the seal surfaces because of a poor earthing system
# Case 3 600 MW Generator 3	26 September 2012	The H_2 seal failed in service, resulting in high hydrogen consumption. An indication of electrical arcing was found; the earthing brush link was found to be open-circuited, which caused poor earthing system performance.
# Case 4 600 MW Generator 2	25 January 2013	The unit was shut down due to a failed H_2 seal. Damage was found on the hydrogen seal, which was caused by electrical arcing due to a damaged earthing brush or lost earthing circuit.
#Case 5 200 MW Generator 3	3 March 2013	The unit tripped due to a bearing 5 failure. The cause of failure was established to be circulating currents, resulting in electrical arcing between the journals and bearing surfaces because of a poor earthing system.
#Case 6 200 MW Generator 4	19 April 2013	The cause of failure was established to be electrical discharge in the bearing due to a possible loss of brush contact and oil contamination

# Case 7 600 MW Generator 5	3 August 2013	Failed bearing due to electrical arcing on the bearing shells. The earthing system and voltage monitoring brushes of the generator were severely contaminated.
#Case 8 200 MW Generator 2	20 June 2014	Frosting found on the main oil pump (MOP) drive bearing journals due to residual magnetism because of a poor earthing system.
# Case 9 600 MW Generator 2	23 July 2016	The cause of failure was worn-out brushes, creating poor contact between the earthing brushes and bearing 2.

It is evident from the literature, as seen in *Table 1*, that poor performance of shaft earthing brushes is an industrial problem and has caused many failures of major generator components.

The study evaluates online techniques for classifying faults based on data from shaft signals. The techniques must enable online, *in situ*, monitoring of the condition of earth-brushes. The study further investigates the effects of earthing brush performance from shaft voltages/currents characteristics.

2.5 Generator Shaft Earthing System

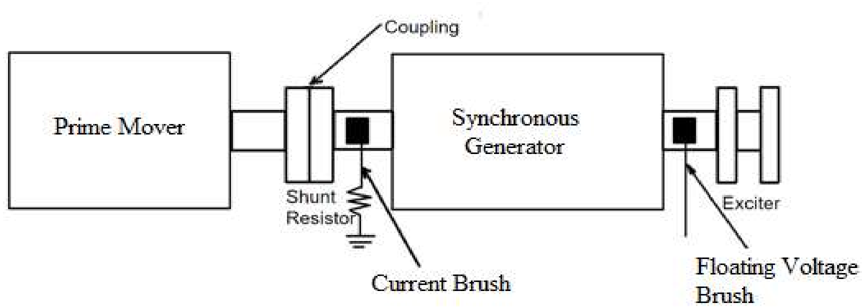

Figure 1: Generator rotor-shaft earthing configuration [3] [14]

Figure 1 shows the most frequently used protective earthing system configuration, which was also applied in Stone [3], Nippes [7], and Nippes [14]. There is no standardised philosophy for measuring shaft earthing, but the above configuration for protective shaft voltage earthing systems has been adopted by many utilities around the world [3] [18].

When the generator is in operation without earth-brushes in place, shaft voltages build up on the generator rotor shaft [3]. If this voltage discharges through generator components such as bearing-oil films, journals, gears, thrust bearings, and hydrogen seals, the current degrades the surfaces of these components and this can eventually cause costly component failures [7].

Protection against shaft voltage and current build-up is achieved by using earth-brushes as contact mediums to earth the generator rotor shaft, usually the current brush is located on the drive end side of the generator rotor shaft [1] [3] [7]. The shaft earthing brush serves as the return path to ground in the event of shaft charge build-up. This earth-brush discharges shaft stray currents from the rotor shaft to ground so that the accumulated charges do not flow through bearings and other components in contact with the shaft [7]. However, these earth-brushes lose their earthing ability over time, sometimes unpredictably, and regular maintenance and replacement is essential.

2.6 Generator Condition Monitoring

Generation plant condition monitoring systems are prevalent around the utility space due to the ever-increasing demand for improved reliability and fail-safe operational systems. Plant downtime can be averted with proactive maintenance strategy by measuring and monitoring vital generator parameters to discover imminent faults. The condition of the turbine generator is monitored/analysed using the characteristic signals present in the rotor/stator generated by the rotating magnetic fields. [15]

The magnetic field within rotating electrical machines splits into two flux paths and travel circumferentially (180^{o}) around the core [19]. Under ideal condition, if the generator core were magnetically perfectly uniform, that is, if the core contained no electrical defects, these magnetic fluxes will be symmetrical within the generator core [20]. In actual practice, no practical electrical machine can be constructed with a perfect balanced symmetry due to manufacturing variations within allowable tolerances, rotor static or dynamic eccentricity, shaft key-ways and joints between segmental laminations [20] [21]. Defects on either the rotor or stator interrupt the circumferential patterns of flux in the generator core. When this unbalanced rotating flux leaves the rotor/stator, it divides unevenly and subsequently induces shaft voltages in the generator shaft, ranging from micro-volts, to hundreds of volts [7].

This induced shaft voltage signal contains the fundamental and harmonics of the generator running speed. A complex fast Fourier Transform of this shaft voltage signal represents a fingerprint of the generator that symbolises the physical and magnetic variations within the generator [20]. Furthermore, any faults within the generator such as bearing faults, winding faults, segment looseness, or mechanical looseness can be detected and monitored outside the generator by applicable condition monitoring techniques.

Generator condition monitoring techniques can be categorised into four groups, namely chemical, mechanical, electrical and thermal [6] [19]. Thermal condition monitoring of a generator entails monitoring allowable temperature limits in components as per the recommendations of the original equipment manufacturer (OEM). Thermal monitoring is achieved by measuring local temperatures and it sometimes entails thermal modelling that measures hotspots in a machine.

Chemical condition monitoring entails the detection of gas, in other words, cyclo-octyl imide, dihexyl amic acid, and carbon monoxide to check if there is any degradation of insulation, core, or windings due to overheating [19].

Mechanical condition monitoring involves looking at defects associated with mechanical faults, such as segment looseness, air-gap eccentricity, bearing faults, end-winding vibrations, structural resonance, and cooling systems. Vibration, accoustic emissions, torque fluctuations, shock pulses, and bump tests are commonly used to measure and monitor symptoms of mechanical faults. [19]

Electrical condition monitoring of the stator and rotor entails stator/rotor field winding faults, air gap faults (dynamic and static eccentricity), slip ring or brush gear faults, circulating currents and earthing faults, partial discharge, end-winding vibrations, single/double earth leakage, stray flux and stator or terminal bushings [6].

2.7 Electrical Condition Monitoring Techniques

Electrical condition monitoring techniques can be divided into three types based on functionality, such as fault detection, fault diagnosis and fault prognosis. The fault-detection techniques determine if a specific generator fault has occurred or is about to occur. This proactive condition monitoring techniques also provide information about the specific fault type and location that enables for fault diagnosis. The fault-detection techniques utilise three fault analytical techniques in condition monitoring of the shaft earthing system, namely [6]:

- Frequency spectral analysis [9]
- Threshold checking [12]
- Warning criteria [11], [22]

2.7.1 Threshold checking (comparative logics) technique

In this technique, the various shaft voltage and current components that are measured on the generator grounding system are summarised. This analytical approach is generally done based on values gained from practical experience and literature [12].

The analysis is shown in Posedel, et al. [12] where structured evaluation logics were developed based on measured raw shaft voltage and shaft harmonic components.

The measured currents and voltages are baselined, and based on theoretically and practically acquired threshold values, a binary combination of measured variables is produced to define the machine condition.

The evaluation is defined in a logic form: each variable is assigned logic output signal "0" as long as its value remains below the threshold value and it is assigned a "1" when the said threshold value is exceeded [12]. Then these threshold values can be combined to analyse and interpret the machine's condition by comparatively simple structured evaluation logic. Indications of a problem developing are based on threshold values of measured variables. In this report, these maximum threshold values will be used to baseline the measured parameters for brush current and voltage values.

2.7.2 Warning criteria technique

The warning criteria technique is used for analysis and interpretation to detect and indicate the early occurrence of possible generator problems [11] [22]. Indicators of developing problems are based on parameter values of measured variables. These are key baseline parameters for specific fault types, as shown in Nippes [11] and [22], used to interpret and analyse the condition of the machine.

There is a technique of shaft-voltage signal interpretation defined in Nippes [11] and [22] that provides the warning criteria for developing problems associated with the synchronous generators.

2.7.3 Frequency spectral analysis technique

Many faults detection and diagnosis systems use techniques which require signal analysis and interpretation in the frequency domain. Frequency spectral analysis technique is used to identify unacceptable generator performance by examining harmonic component of the measured signal [19].

Transformation of the shaft voltage raw signal to the frequency domain is usually carried out using the fast Fourier Transform (FFT). The technique detects poor performance by recording deviations in the measured signal from a normal operating condition. An increase of a specific fault level in a generator is only made known by a definite increase in the n^{th} harmonic of the measured signal. [6]

Identification of harmonic components, and their amplitudes present in the shaft voltage raw signal is very useful for diagnostic and long-term trending [3]. *Figure 2* provides typical process flow-chart of a generator fault-diagnosis mechanism which uses frequency spectral analysis.

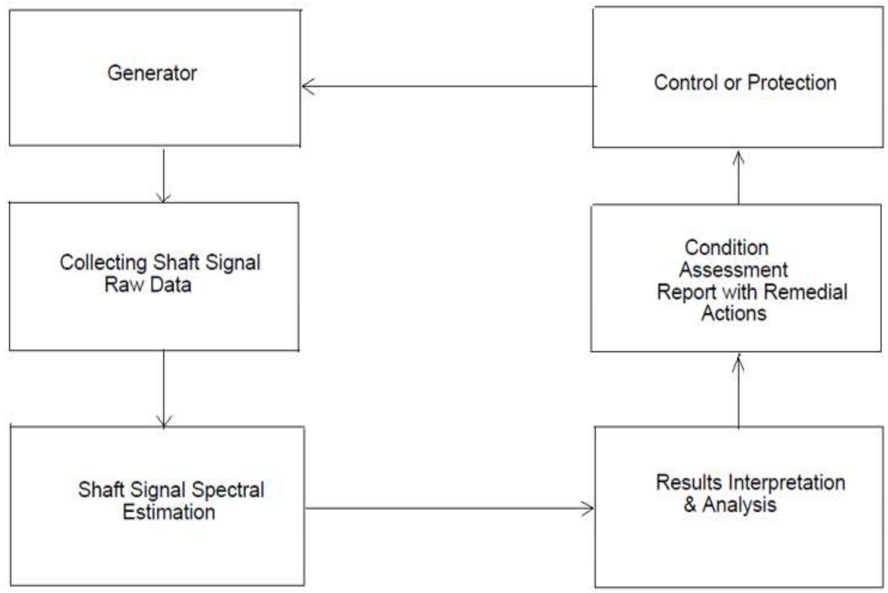

Figure 2: Typical fault diagnosis/prognosis mechanism on a generator using spectrum analysis [21]

A number of researchers have reported the identification of various frequencies associated with defects in synchronous generators, including Hoffe [4], De Cahna [5], and Doorsamy [6]. Higgins [9] described a generator shaft monitoring system that notifies a user of a generator fault condition based upon the frequency spectral analysis of a shaft voltage signal. The presence of various frequency components results from multiple reasons, such as design features (both stator and rotor), construction details and types of asymmetries occurring in the generator [3]. In order to summarise the prominent shaft-signal frequencies for a given generator fault, the following *Table 2* has been compiled [4] [5] [6] [23].

Table 2: Frequency spectral analysis of shaft voltage signals [4] [5] [6] [23]

Source	Characteristic component of shaft voltage
Static eccentricity of the rotor.	Static eccentricity exhibits increase in the 5^{th} harmonic
Vibration from mechanical sources such as a dynamic eccentricity of the rotor or misaligned components.	2^{nd} Harmonic (100 Hz) will be visible in low frequency time domain waveforms. Sometimes the level of 100 Hz signature fluctuates over a period of minutes.
Manufacturing imperfections, and rotor misalignment	Introduces high nominal values of 5^{th} and 6^{th} harmonics
Inter-turn short circuit in the rotor-winding.	Fundamental harmonic. Even harmonics. D.C. component. The level of 100 Hz will usually remain stable over medium term.
Negative sequence current	2^{nd} Harmonic
Saturation of the stator core	Fundamental, and 3^{rd} harmonic
Electric contacts between shaft and seals	Non-synchronous step-voltages
Magnetisation of the shaft	Increase in D.C. component. The 50 Hz component of the harmonic spectra may also be higher than usual. Cross check DC and 50 Hz measurement records.

Asymmetries in the excitation circuit	6^{th} Harmonic. Problems with the exciter can most clearly be seen in the time domain waveform from the exciter end voltage brush.
Large ground capacitances in the excitation circuit	Amplitude of high-frequency peaks

2.8 Conclusion

In this chapter, background information on historical application of shaft-signal based techniques to diagnose and detect generator failures and impending faults was provided. A literature review on earthing brush systems, shaft-signal analyses and interpretation and earthing system problems was also provided.

Philosophy of the application of generator earthing brush systems was presented, along with a general overview of the existing generator condition monitoring systems. Associated generator shaft-signal based analytical techniques were presented, as well as a general review of existing electrical condition monitoring systems, and a review of existing shaft-signal based techniques applied in condition monitoring of generators.

Chapter 3 Theory

3.1 Introduction

In order to understand how research questions in Chapter 1 were answered, there is a need to first understand the origin of shaft voltages and currents in the electrical rotating generator.

The following sub-sections give basic theoretical concepts of how shaft voltages/currents are generated and provides detailed explanation of the four main causes of shaft voltages and currents in a synchronous generator.

3.2 Generation of Shaft Voltages and Currents

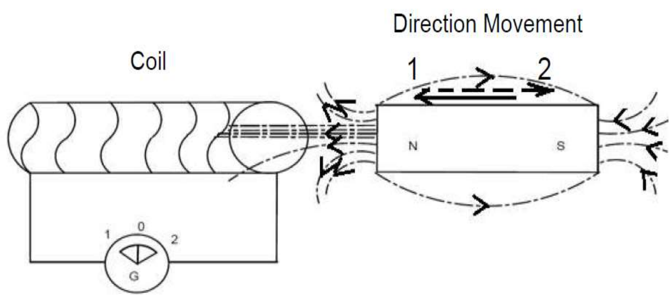

Figure 3: Faraday's Law of Electromagnetic Induction [24]

Figure 3 illustrates Faraday's set-up for demonstrating that a magnetic field can produce a current. When the coil moves towards the magnet, deflection will take place in the galvanometer (G). The deflection is an indication that the voltage (Ɛ) is induced across the coil in a changing magnetic field [24]. Faraday's Law states that the magnitude of the induced voltage (Ɛ) is equal to the time-based rate of change of magnetic flux (ϕ):

$$\varepsilon = -\frac{d\phi}{dt} \tag{2.1}$$

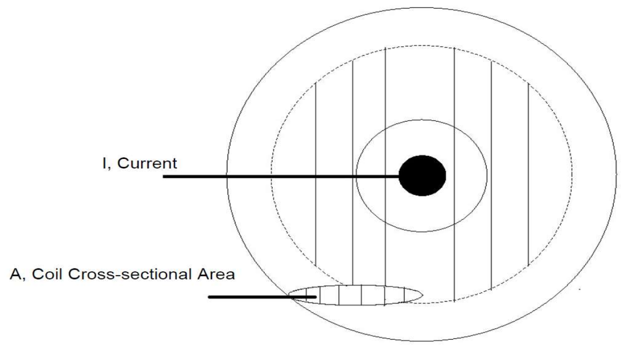

Figure 4: Coil outline [1]

An outline of a coil is shown in *Figure 4*, consider N as a number of turn coils carrying a time changing current (I) in a coil and (H) magnetic field intensity tangential to the cross-sectional area (A) of the coil. Applying Faraday's Law to the coil, the induced instantaneous voltage Ɛ in the coils is given by:

$$\mathcal{E} = -\frac{d}{dt}\left(\sum_{n=1}^{N} \phi_n\right) \tag{2.2}$$

Where ϕ_n is the instantaneous flux linking the n^{th} turn of N-turn coil, with the unit weber (Wb) or volt-second. The magnetic flux is surface integral

$$\phi_n = \iint B_n \, dA_n \tag{2.3}$$

Substituting for ϕ_n, equation 2.2 becomes

$$\mathcal{E} = -\frac{d}{dt}\left(\sum_{n=1}^{N} [\iint B_n dA_n]\right) \tag{2.4}$$

B_n is the magnetic flux density linking the n^{th} turn of N-turn coil and it is simply the flux per unit area, given in Tesla (Wb/m2) and the corresponding cross-sectional area of each turn of coil A_n. Where B_n in equation (2.5) is given

$$B_n = \mu_0 H_n = \frac{\mu_0 N I_n}{L_n} \tag{2.5}$$

H_n is the magnetic flux strength linking the n^{th} turn of N-turn coil, in amperes/meter. Where μ_0 is the permeability in the region of the coil and L_n is the length of the n^{th} turn of N-turn coil. Applying equation (2.5) and rearranging, equation (2.4) becomes

$$\mathcal{E} = -\frac{d}{dt}\left(\sum_{n=1}^{N}[\iint \frac{\mu_0 N I_n}{L_n} dA_n]\right) \tag{2.6}$$

By Ampere's law , the current I_n passing through a coil generates a perpendicular magnetic field intensity given by

$$I_n = \oint H_n dl \tag{2.7}$$

Faraday's Law in the equation effectively demonstrates the fundamental relationship between induced shaft voltage ($\mathcal{E}$) and generated flux (ϕ). The equation provides a concise summary of how an induced voltage may be generated by changing magnetic flux. When magnetic flux (ϕ) changes or becomes unbalanced because of magnetic field strength (B) changes due to rotor winding faults or deformed coil, these unbalanced magnetic flux will induce in it a voltage ($\mathcal{E}$).

If a coil is wound around the generator rotor shaft as rotor winding, changing magnetic fluxes will induce a voltage around the rotor shaft. As the generator rotor shaft is rotated, the magnetic fluxes crosses the air gap and cuts to the bearing surfaces. This magnetic flux will cause localised bearing currents to be induced in the rotor shaft and a serious problem develops when shaft and bearing currents reach levels that cause electrical arcing and erosion on the bearing surface [2].

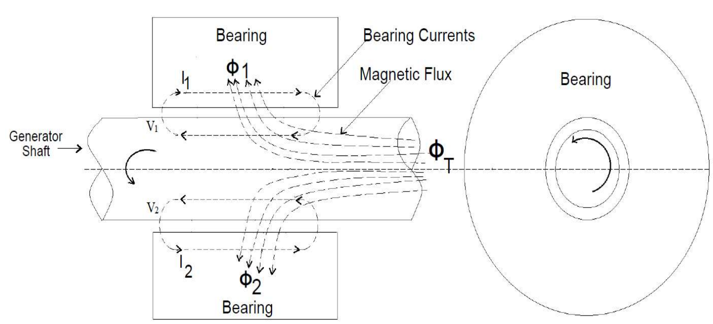

Figure 5: Flux causing circulating bearing currents [2]

Figure 5 it illustrates that the magnetic flux passing through the shaft will split into two components moving in opposite directions, namely clockwise and anticlockwise. The magnetic flux linkage passes across the rotor centreline through the bearings to the generator casing back to the shaft [1] [2]. The magnetic flux linkage generates localised voltages (V_1 and V_2) on the bearing surfaces and subsequently drive respective localised circulating currents (I_1 and I_2). The induced localised voltages in both bearings will be exactly equal in magnitude, provided the outgoing and returning magnetic fluxes are also equal [1] [2]. The magnetic flux ϕ_T enters and leaves at bearing points, generating fluxes ϕ_1 and ϕ_2. Therefore,

$$\phi_T = \phi_1 + \phi_2$$

(2.8)

and resultant induced emf ($\mathcal{E}$) or voltage is defined as:

$$\mathcal{E} = -\frac{d\Phi}{dt}$$

Therefore, the magnitude of the bearing localised voltages (V_1 and V_2) depends on the magnitude of the outgoing fluxes (ϕ_1 and ϕ_2), resultant flux ϕ_T. Thus, the total summation of the outgoing and entering fluxes is equal to zero, hence

$$V_1 + V_2 = 0 \qquad (2.9)$$

The induced localised voltages drive currents (I_1 and I_2) from the generator shaft through the bearing surfaces/seals back to the shaft. The localised currents developed as a result of induced localised voltages develop self-excitation from the internal region of the generator rotor. The results of localised bearing currents if not monitored can cause damage to the bearing surfaces/seals [1] [2] [3].

Thus, unbalanced magnetic fluxes (ϕ_T) in alternating current machines will cause current to be induced in the shaft. This unequal distribution of the magnetic flux can result from the introduction of unequal distributions of joints in the stator core. Uniform permeability in each flux path is impossible to obtain due to geometry, inconsistencies in manufacturing, etc. and consequently, as the flux pattern shift around the machine, the varying reluctance will result in changes in the magnitude of the flux. The reluctances of the flux paths through the joints are higher than for other paths. The magnitudes of magnetic flux densities in the flux paths through the joints will be less dense than other paths. [21]

Shaft currents/voltages can also originate from many different sources. As a results of combination of various sources of shaft voltages, up to 150 *Vrms_peak* can be generated on the rotor shaft and damage to bearing surfaces, gears and oil seals can occur [3] [20]. The most common problem is bearing pitting damage that is due to mechanical damage resulting from arcing between rotor shaft and bearing surfaces. Arcing between two surfaces causes very high temperature at contact points and results in vaporization of metal. [3] The four main causes of shaft voltages/currents sources in a synchronous turbine generator are summarised below [1] [16] [17]:

3.2.1 Electrostatic charge (Direct Current)

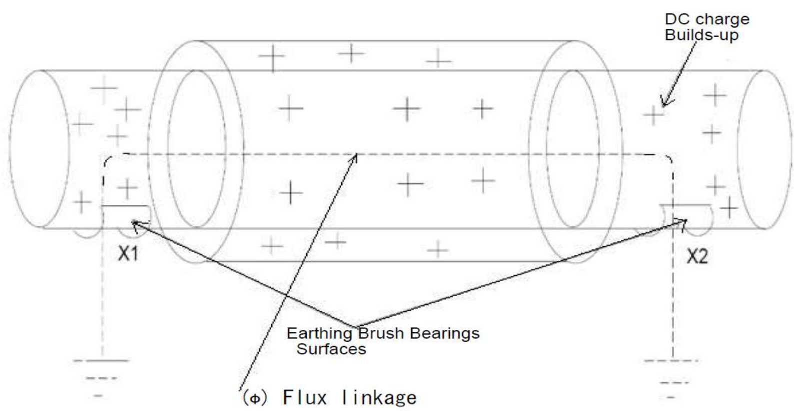

Figure 6: Electrostatic effect due to wet steam particles [1]

Figure 6 illustrates electrostatic effect due to wet steam particles. Shaft voltages from this source are most commonly generated by brushing effect of wet steam on the blades of a low-pressure (LP) turbine [1].

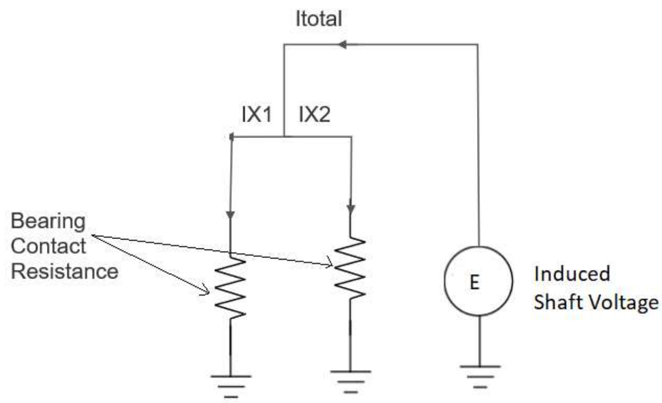

Figure 7: Electrical representation of electrostatic effect [1]

Figure 7 shows electrical representation of electrostatic charge effect. When the wet steam on the blade of the turbine in the low-pressure (LP) turbine comes into contact with the blades, causes the blades to pick up electrons and acquire a charge and, hence, a voltage [16]. Electrostatic voltage will be generated across the oil film in the generator's bearing between the rotor shaft and the inner casing. If this electrostatic charge build-up is not controlled, the electrical charge will result in the breakdown of the oil film's resistance and cause discharges at peak voltages causing a type of bearing damage known as pitting [1] [16]. This condition causes the oil dielectric strength to be compromised resulting in easier current discharges through the bearing surfaces.

3.2.2 Magnetic dissymmetry

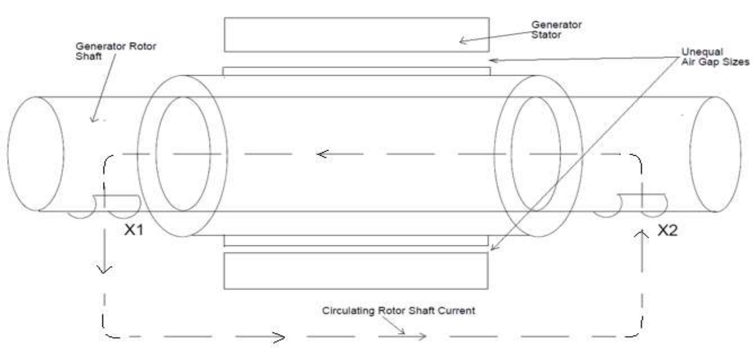

Figure 8: Magnetic dissymmetry effect [1]

Figure 8 illustrates magnetic dissymmetry effect associated with small dissymmetries in the generator rotor. Dissymmetry of magnetic fields caused by design, air gaps eccentricity, manufacturing imperfection and rotor winding inter-turn faults. It occurs because no electrical machines can be designed and manufactured with perfect symmetry. There are always differences in air gaps sizes, plate thicknesses and core-plates, as well as eccentricity in the rotor [20]. This slight deviation in electrical properties of core plates, plate thickness and physical parts of the machine will lead to unbalanced distribution of magnetic flux patterns. In summary, magnetic dissymmetry generally occurs due to the following [1] [17]:

- Slight deviations from the electrical rotating machine manufacturer's tolerances
- Design tolerance variations in different components
- Eccentricity of the stator and rotor causing variations in the air-gap
- Rotor and stator sagging
- Rotor static and dynamic eccentricity
- Split rotor and stator cores
- Misaligned laminations

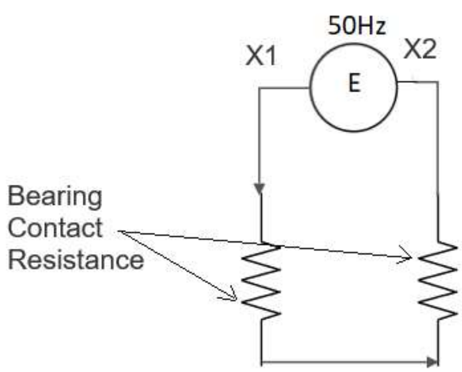

Figure 9: Electrical representation of magnetic asymmetry effect [1]

Figure 9 shows an electrical representation of the magnetic asymmetry effect. The flux component results in induced shaft voltages being generated between the ends of the generator rotor shaft. This condition will result in shaft circulating currents flowing down the centreline of the rotor as shown in *Figure 8.*

The shaft voltage signal generated from magnetic fields dissymmetry effect of a generator, such as manufacturing imperfections, rotor misalignment and rotor winding shorted turns, introduces high nominal values of 5^{th} and 6^{th} harmonics [6].

3.2.3 Shaft magnetisation

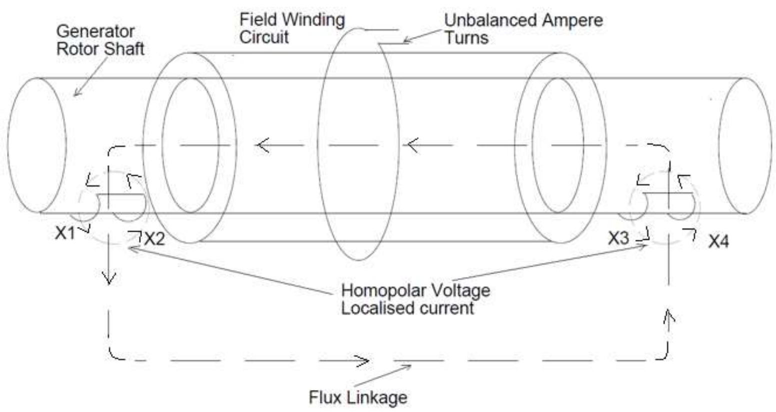

Figure 10: Shaft magnetisation [1]

Figure 10 shows how a magnetised shaft generates localized homopolar (DC) voltages on the bearing surface. Homopolar shaft based signals are DC voltage signals and, as a result, only affect the DC component of the shaft-voltage power spectrum (V_{dc}) [20]. If these homopolar (DC) voltages are not controlled, will leads to localised bearing currents that will discharges the oil film between the bearing and rotor shaft [1] [2]. Then eventually result to a bearing failure. Shaft magnetisation occur due to the following:

- Strongly magnetised components
- Insufficient shaft demagnetisation
- Application or use of strong magnetic tools

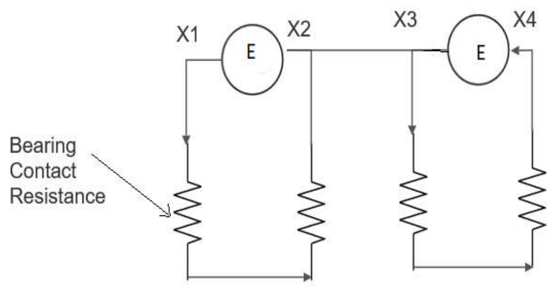

Figure 11: Electrical representation of shaft magnetisation effect [1]

Figure 11 shows electrical representation of shaft magnetisation effect. When a magnetic circuit is established, small unipolar current will be generated forming a self-excitation circuit around the bearing. The induced homopolar voltages will generate magnetic field around each bearing case with equal magnitudes as shown in *Figure 11* [1] [2]. Therefore, these induced homopolar voltages will cause localised bearing current to be generated within the rotor-shaft bearing casing. If these localised bearing currents are not controlled will discharges through the bearing surfaces and damage the bearing. These homopolar voltages can be reduced to very low values along the shaft by demagnetization of the rotor before it is placed in the turbine-generator [20].

3.2.4 Excitation system developed shaft voltage

The excitation system developed potentials are another means of causing damaging shaft currents to flow through the oil film and ultimately the generator bearing [1] [25] [17].

External voltage source supplied through excitation system can also induce shaft currents/voltages and harmonics in this voltage source can influence the frequency characteristics of the shaft voltage signal. The shaft voltage signal has a large 3rd harmonic (150 Hz) ripple voltage component relative to its fundamental counterpart. When the field winding insulation is in good condition, it acts as a capacitive impedance between the field windings and the rotor forging. [6] [25]

This ripple voltage component can range from 10-60 volts and is capable of producing 20 milliamps of shaft current when any bearing oil film is in a conducting condition. As with the generator excitation system, a shaft voltage of approximately 10 volts will damage the generator bearings. [1] [25]

Ammann et al. [25] presented a paper on shaft voltages in generator with static excitation system. They discovered that shaft voltages from excitation systems are of rectangular form with frequencies of three times the fundamental counterpart. A diagrammatic illustration and electrical circuit are shown in *Figure 12* and *Figure 13* respectively.

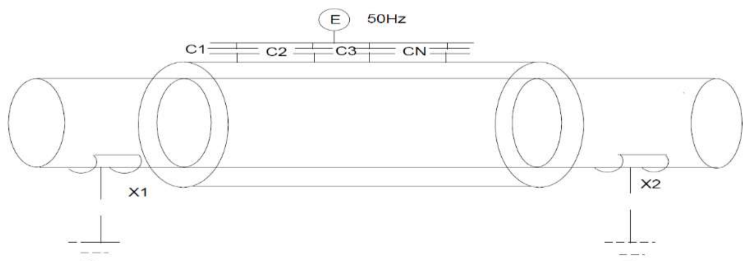

Figure 12: Generator excitation induced shaft voltage [1]

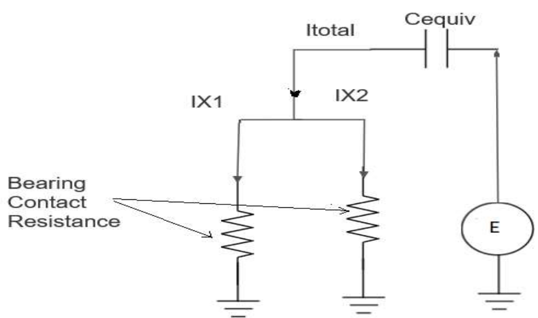

Figure 13: Electrical representation of excitation system induced voltage [1]

Figure 13 shows electrical representation of electrical representation of excitation system induced shaft voltage. The induced shaft voltages from excitation system result to a circulation shaft current to flow through the bearing oil film and then eventually discharges through the bearing casing.

3.3 Conclusion

In this chapter, background information is given on the four main causes of shaft voltages/currents in a synchronous turbine generator. Basic theoretical concept is provided on shaft voltages/currents generation and electrical representation form of the four main causes (i.e., electrostatic charge (Direct Current), magnetic asymmetry, excitation system developed shaft voltages, and shaft magnetisation) of shaft voltages and currents in a synchronous generator.

Chapter 4 Miniature Synchronous Experiment Set-up

4.1. Introduction

This chapter focused on determining the effects of different earth-brush faults on the shaft voltages/currents through physical measurements and experiments using a two-pole, 20 kVA synchronous generator. Different types of brush faults were investigated on the machine to determine their effects on establishing an earth point along the rotor shaft while the machine is in operation.

The second phase of the study evaluated different shaft-signal based fault detection techniques to determine condition of earth-brushes when the machine is in operation. This chapter is broken into sections that describe experimental set-up, measurement techniques, measurement uncertainty, analysis and interpretation methods.

4.2 Experimental Set-Up

Figure 14 shows a miniature synchronous generator on the test bed with a driving motor. The experimental set-up of an induction motor (as prime mover) is coupled to a synchronous generator with shaft brushes on the test bed. The two-pole mini-generator synchronous generator rated at 20 kVA, 3 000 rpm, 50 Hz was designed to mimic a typical 600 MW turbine generator machine was used as a test machine for this experiment.

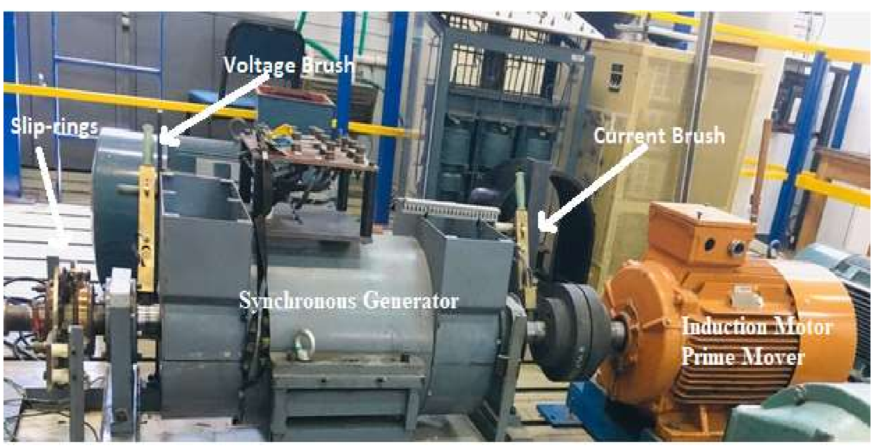

Figure 14: Picture of fully assembled experimental setup

The current earth-brush includes a shunt resistance with the following specifications: 0.0496 Ω, 150 A, 1 100 W. *Table 3* indicates, in summary, the synchronous generator constructional details.

Table 3: Technical specification of the mini-generator machine

Parameter	Mini-Generator
Power Rating	20 kVA
Number of poles	Two-pole,
Rotor rotational speed	3000 RPM
Damper bars	48
Shaft diameter	67 mm
Rotor diameter	178.5 mm
Excitation current	60 A
Frequency	50Hz

4.3 Measurement Techniques

Various techniques have been investigated and developed to measure and monitor shaft earthing currents and voltages in Stone [3], Posedel [12], and Nippes [14] [22]. The IEEE 112 standard for the test procedure for generators in IEEE Standard 112 [26] provides a standard approach for shaft voltage and current measurement. The standard states that shaft voltages can be measured by ammeter method. However, it has been pointed out that the ammeter method described in IEEE Standard 112 is not suitable for this application and does not reflect the true shaft current [18] [21].

Ong [22] has also compared different shaft-voltage and current measurement techniques. Mounting a Rogowski coil around the generator shaft to measure shaft voltage including the circulating current has been investigated before [27] [21]. However, this method needs a complex generator preparation and is not easily applicable in the field [18]. A simple but intrusive way to measure the shaft voltage with a high bandwidth, is the usage of shaft brushes [3] [14] [18] (refer to *Figure 14*).

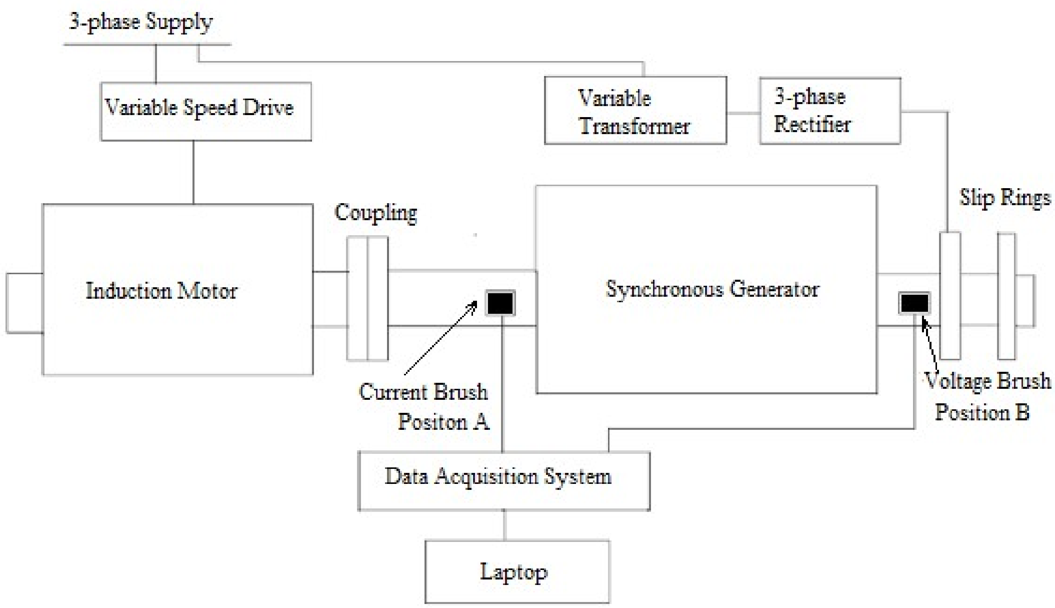

Figure 15: High-level schematic experimental/ layout with associated instrumentation systems used to measure shaft current-voltage signals [6]

Figure 15 shows a shaft earthing voltage and current measurement method, rotor shaft earthing brush configuration with shaft current and voltage brushes mounted on the synchronous generator drive and non-drive ends respectively. The voltage brush is fitted on the non-drive end (NDE) and the shaft current brush on the drive end (DE) of the generator to the measuring equipment (PicoScope).

The measuring equipment connected to the personal computer (PC)-based acquisition system is used to gather, process and display shaft voltage and shaft current information. The data acquisition system in *Figure 15* is made up of the four channel PicoScope with the signal generator.

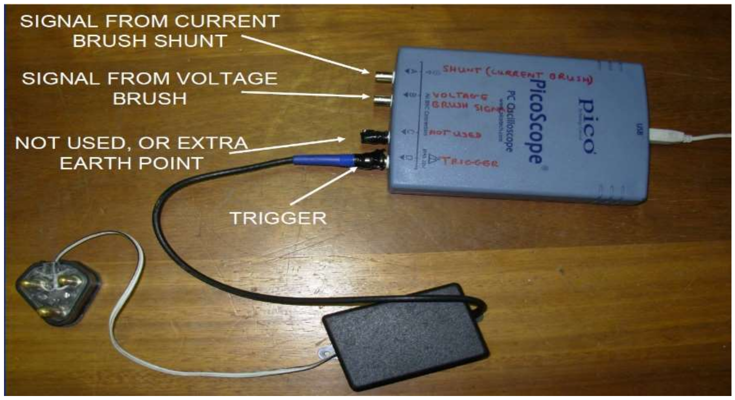

Figure 16: The four-channel Pico-scope

Figure 17: Wideband RFCT and voltage probe to measure shaft voltages

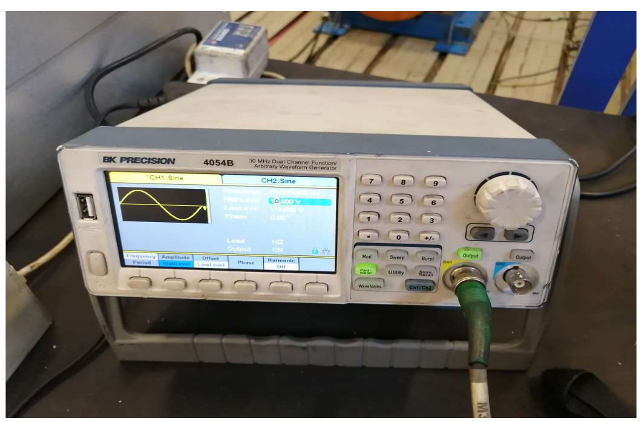

Figure 18: Signal generator as trigger

The four-channel Picoscope provided acquisition, analysis and display of raw shaft voltage and current waveform signals. The wideband RFCT as shown in *Figure 17* is used to measure the current brush currents with voltage probe to measure shaft voltages. The signal generator used as a trigger is shown in *Figure 18* and is used as a data acquisition system.

4.4 Low-Resistance/Shunt Earthing Method

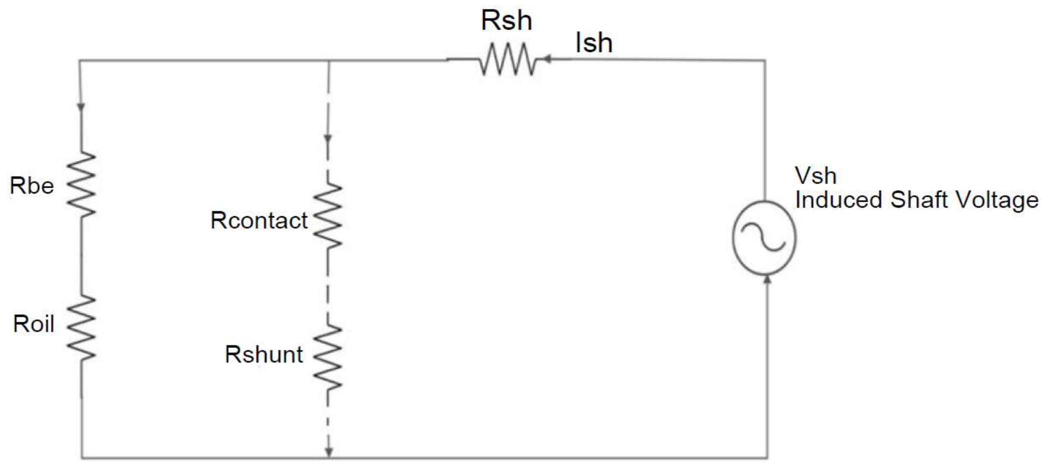

Figure 19: Simplified representation of generator under test [26]

Figure 19 indicates the application of a low-resistance/shunt earthing method of the synchronous generator under test according to IEEE Standard 112 to measure shaft currents/voltages [26]. This method shows a path for shaft earthing conducting circuit introduced through a dashed line that provides a low resistance path to earth through the shunt and current-brush resistance.

When applying Kirchhoffs law to circuit in *Figure 19*, when the machine is without the earthing brush system, we obtain:

$$V_{sh} = I_{sh}\,(R_{sh} + R_{be} + R_{oil}) \qquad (3.1)$$

where,

V_{sh} is the induced shaft voltage

I_{sh} is the induced shaft current

R_{shunt} is the resistance of the shunt in order of milli-ohms

R_{sh} is the resistance of the rotor shaft in order of micro-ohms

R_{be} is the insulation resistance of the bearing in order of kilo-ohms

R_{oil} is the resistance of the oil film in order of kilo-ohms and

$R_{contact}$ is the current brush contact resistance

Since shaft resistance is negligible, in the order of micro-ohms, equation (3.1) above can be simplified as:

$$V_{sh} = I_{sh} (R_{be} + R_{oil}) \tag{3.2}$$

Applying Kirchhoff's law to the circuit in *Figure 19*, when the machine is connected to the earthing brush system, we obtain

$$V_{sh} = I_{sh} (R_{sh} + R_{contact} + R_{shunt}) \tag{3.3}$$

With the negligible magnitude of the shaft resistance R_{sh}, the voltage current relationship can be obtained as:

$$V_{sh} = I_{sh} (R_{contact} + R_{shunt}) \tag{3.4}$$

Where R_{shunt} is the shunt resistance or the ammeter resistance and $R_{contact}$ the current brush contact resistance.

4.5 Measurement Error Analysis

All measurements have some degree of uncertainty as there is a wide range of errors and inaccuracies that could happen in the experimental process [28]. Measurements should be conducted with due diligence to reduce the possibility of error and inaccuracies as much as possible.

Blunders/mistakes are not considered a source of uncertainty since they can be removed by careful work and quality control [28]. There are two types of experimental uncertainties, namely systematic and random uncertainties, which are defined as follows:

- Random uncertainty deals with the precision of an experiment
- Systematic uncertainty deals with the accuracy of an experiment.

Systematic uncertainties are due to faults in the measuring instrument and the techniques used in the experiment. Systematic measurement is influenced by limited accuracy of the measuring devices and the habitual perceptions of the person operating the measuring equipment.

Random uncertainties are due to a deficiency in defining the parameters that are being measured [28]. Random uncertainty is due to imperfect connections between data acquisition system and shaft earth-brushes and an imprecise measurement methodology may cause random fluctuations in the magnitudes of the shaft currents and voltages.

Before the test, experimental test control conditions are put in place to verify the accuracy of the shaft earthing system of the shaft current/voltage measurement. These test conditions are developed to minimise any known effects on the magnitudes of shaft current and voltages:

- The PicoScope is calibrated on the rotor shaft before the test.
- Any bearing alignment or lubrication problem in the bearings is addressed by running the generator for half an hour before each occasion that measurements are taken.

4.6 Shaft Voltage Analysis and Interpretation

As presented in Nippes [14], Stone [3], Higgins [9] it was discovered that the shaft voltage fast Fourier transform (FFT) plot was very useful for monitoring and detecting impending machine faults. This was concluded from the fact that shaft voltages are connected to magnetic field asymmetry and that every machine fault is associated with magnetic field perturbations [3] [9] [14].

The analysis and interpretation of the earthing brush signals is done by analysing the frequency harmonic content. The fast Fourier Transform (FFT) plot is used to analyse and interpret the shaft voltage signals in the frequency domain, while the current brush scatter plot will exhibit the brush current performance in the time domain. The current brush scatter plot is time domain measurements of the current brush signals.

4.7 Conclusion

In this chapter, details of experimental set-up, instrumentation layout, measuring equipment and measurement techniques were presented. *Figures 16 -18* show a photograph of the measuring instrumentation. The theoretical analysis of the simplified machine under test was presented to provide the reader with further understanding of machine shaft voltages and earthing system relationship. The experimental test conditions for shaft current/voltage measurement were presented, and the results and interpretation method for shaft earthing current and voltages were discussed. The analysis and interpretation of the signals from the shaft earthing system will be done by analysing the frequency harmonic content and current scatter plot.

Chapter 5 Test Performance and Results

5.1 Introduction

The key objective of the research was to evaluate different shaft-signal based techniques to determine, *in situ,* earth-brush performance while online. The study further investigated the effects of earth-brush performance from shaft voltages/currents characteristics. This was accomplished through physical measurements and experiments on a 2-pole, 20 kVA synchronous generator. The results were obtained and analysed by using signal-processing techniques on the measured generator shaft-signals (i.e. shaft currents and voltages).

5.2 Test Performance and Results

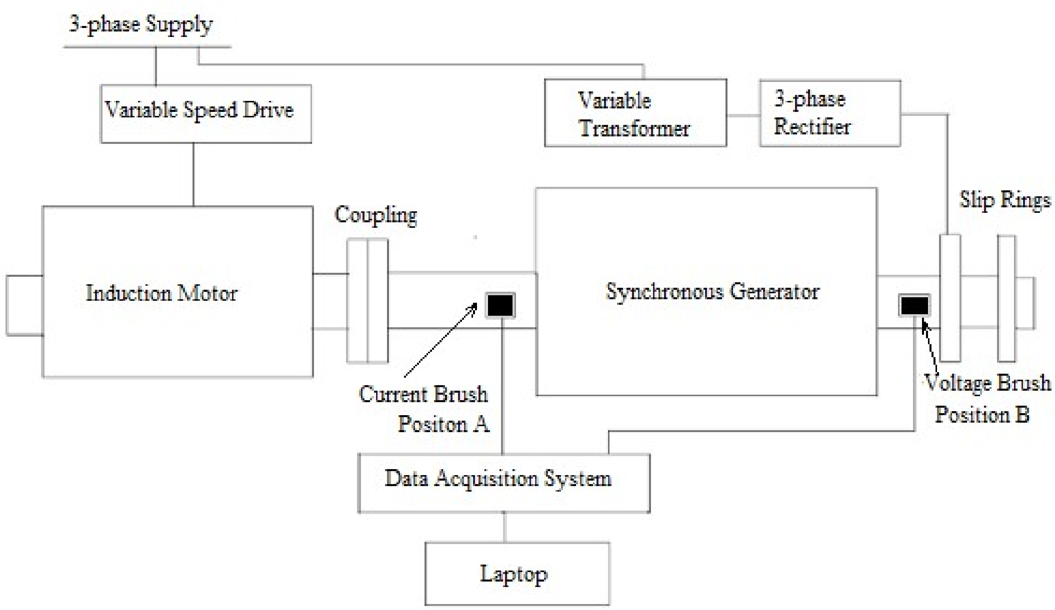

Figure 20: Coupled miniature synchronous-generator and a driving motor

Figure 20 shows an experimental set-up of a coupled miniature 2-pole synchronous generator rated at 20 kVA, and 3000 rpm, with operational frequency of 50 Hz. The synchronous generator is designed to mimic a full-sized 600 MW turbo-generator machine. The synchronous generator on the test-bed is connected to a driving induction motor.

The experimental set-up is fitted with shaft current and voltage brushes with a data acquisition system to capture the voltage and current brush signatures. The earthing system incorporates the current brush on the drive-end side of the synchronous generator and the voltage brush mounted on the non-drive end, near the exciter. The brush at Position B at the non-drive end is used to pick up a shaft voltage (this is the signal brush) and the brush at Position A on the drive-end side was used to reliably ground the shaft to the earth (grounding brush). The brushes used were manufactured by Mersen SA and are of the shaft riding carbon type.

5.3 Performance Test Scenarios

The first phase of the study investigated the effects of earth-brush fault types on shaft voltages and currents. The investigation studied shaft voltage and current behaviour under brush fault scenarios. The following test scenarios were conducted, based on the study's key research questions set out in Section 1.4:

A. Baseline Test

Test #1: In *Figure 20*, the brush at Position A is in, the brush at Position B is in. All brushes are in-service.

B. Lost Shaft Ground Circuit

Test #2: In *Figure 20*, brush at Position A in, brush at Position B out.
Test #3: In *Figure 20*, brush at Position A out, brush at Position B in.

C. Poor Earthing Performance Brush Systems

Test #4: In *Figure 20*, brush at Position B is replaced with a worn-out brush

D. Earthing brushes are exposed to oil and dust

Test #5: In *Figure 20*, brush at Position A exposed to oil and dust
Test #6: In *Figure 20*, brush at Position B exposed to oil and dust

5.4. Measured Results

5.4.1 Baseline Test

Test#1 was conducted as a baseline test with the current earth-brush at Position A and voltage earth-brush at Position B, all brushes in service. This test was conducted to establish how well the earthing brushes are making contact on the rotor shaft surface and establishing ground points along the shaft. The results from this test are defined as the baseline values for typical earthing brush performance. *Table 4* presents the RMS shaft voltage quantities ($V_{rms\_average}$ and V_{rms_peak}). These shaft voltage quantities provides a clear indication of whether the shaft voltage is increasing or decreasing.

Table 4: Shaft voltage quantities when both brushes at Position A and B are in service

Description	Values
V_{rms_peak}	1.93 V
$V_{rms\_average}$	1.91 V
V_{DC}	0.02 V

Parameter definitions in *Table 4*

V_{DC} is the DC voltage appearing on the voltage harmonics (*Please note V_{DC} is a zero-order harmonic)*

$V_{rms_{peak}}$ is the RMS peak voltage of the voltage brush

$V_{rms\_average}$ is RMS average voltage of the voltage brush

Figures 21 and *22* show shaft voltage brush waveform and corresponding shaft voltage fast Fourier Transform (FFT) plot.

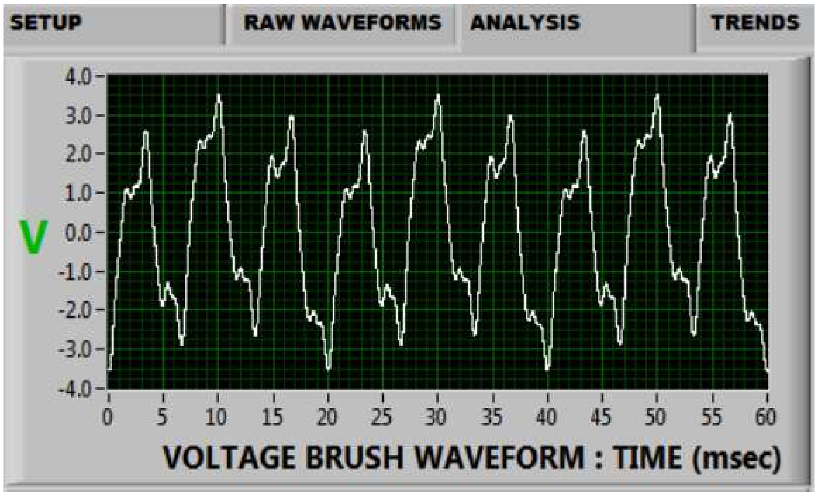

Figure 21: Shaft voltage brush waveform (V)

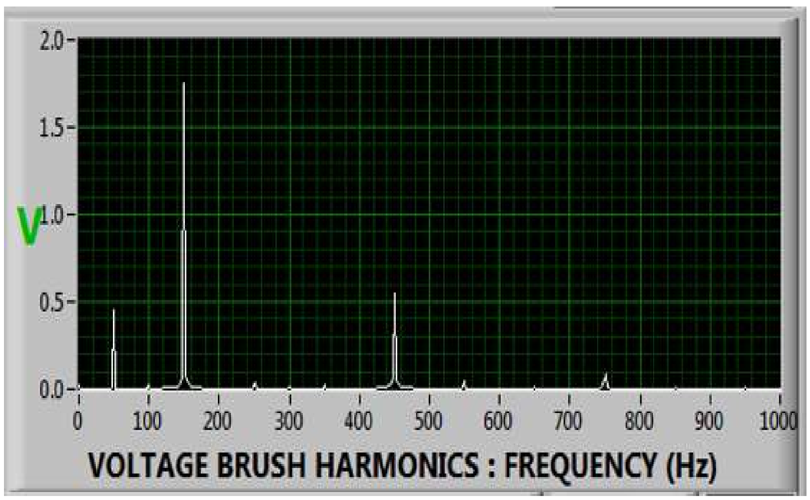

Figure 22: Shaft voltage brush harmonics (Hz) (FFT)

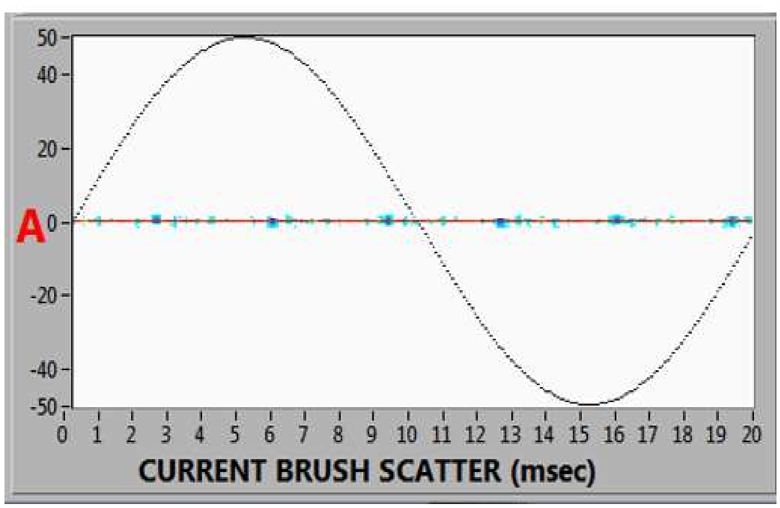

Figure 23: Current brush scatter plot (A)

Figure 23 shows the current brush scatter plot, which illustrates the current performance of the current brush.

Table 5 shows the RMS shaft-current quantities when both brushes at Position A and B are in service.

Table 5: The shaft current quantities

Description	Values
I_{rms_peak}	0.75 A
$I_{rms\_average}$	0.73 A

Parameters definition in Table 5

I_{rms_peak} is the RMS peak current in the current earthing brush

$I_{rms\_average}$ is a RMS average current in the current earthing brush

5.4.2 Lost shaft ground circuit or no earthing continuity

After the completion of Test #1 with both earthing brushes at Position A and B in service, Test #2 was introduced by lifting the earthing brush at Position B (voltage brush) and maintaining the contact point with earthing brush at Position A (current brush) only. This was done to establish earthing brush performance when the voltage brush is floating or not making contact.

Figures 24 – 29 shows the plot of the experimental shaft-voltage brush waveform, shaft-voltage frequency harmonics spectral (FFT), current scatter plot under brush fault condition when the voltage brush is out service.

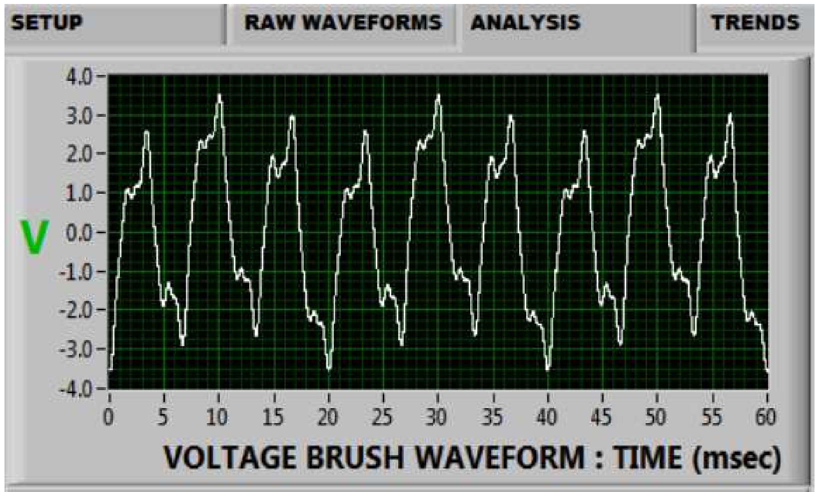

Figure 24: Shaft voltage brush waveform (V) for baseline test (Test#1)

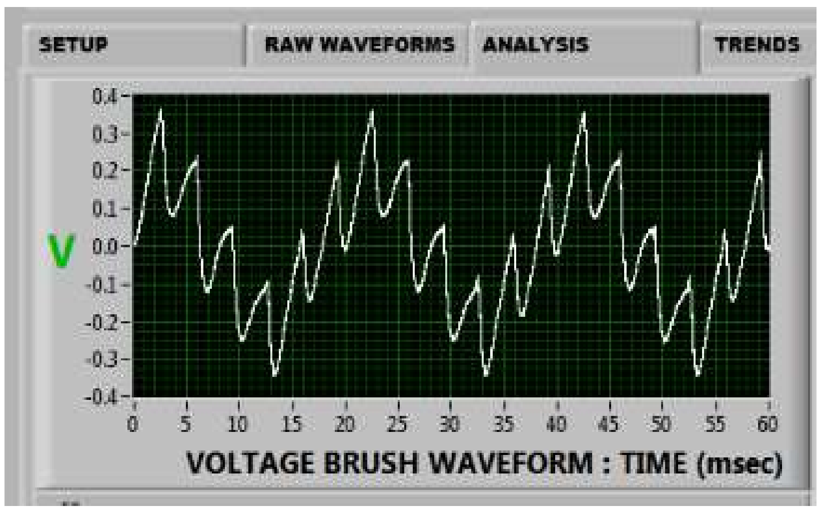

Figure 25: Shaft voltage brush waveform (V) for floating brushes (Test#2)

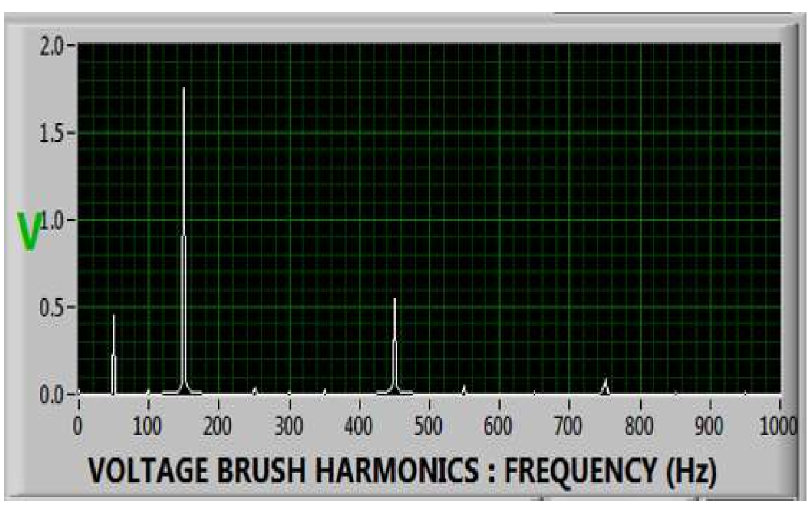

Figure 26: Shaft voltage brush harmonics (Hz) (FFT) for baseline test (Test#1)

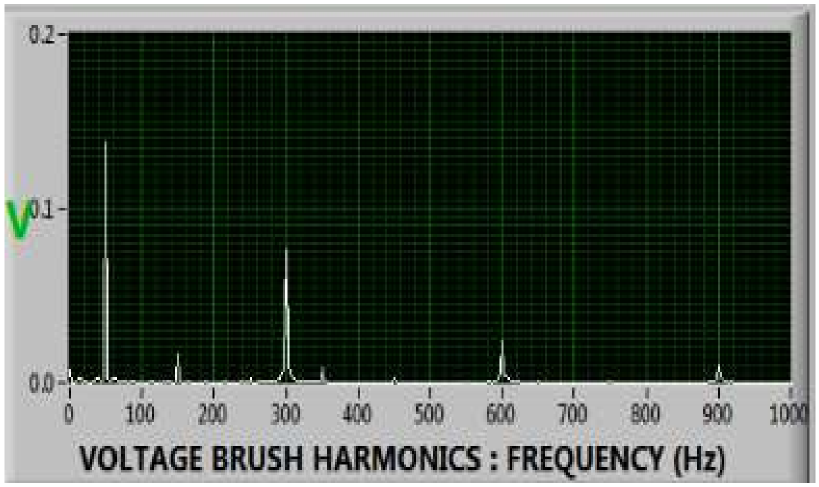

Figure 27: Voltage brush power spectrum (FFT) for floating voltage brush for floating brushes (Test#2)

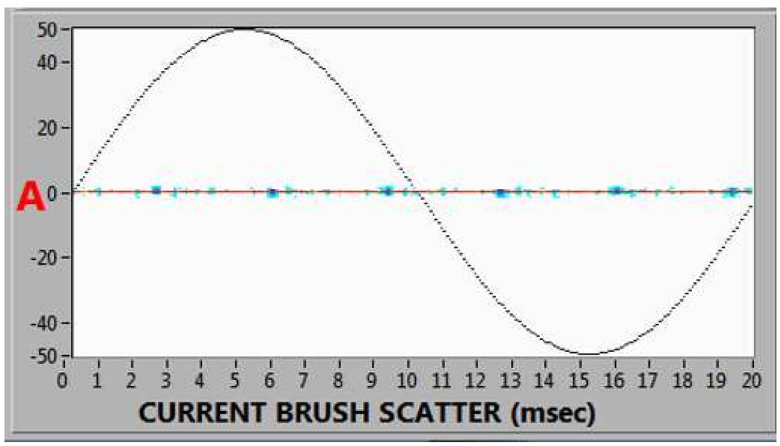

Figure 28: Current brush scatter plot (A) for baseline test (Test#1)

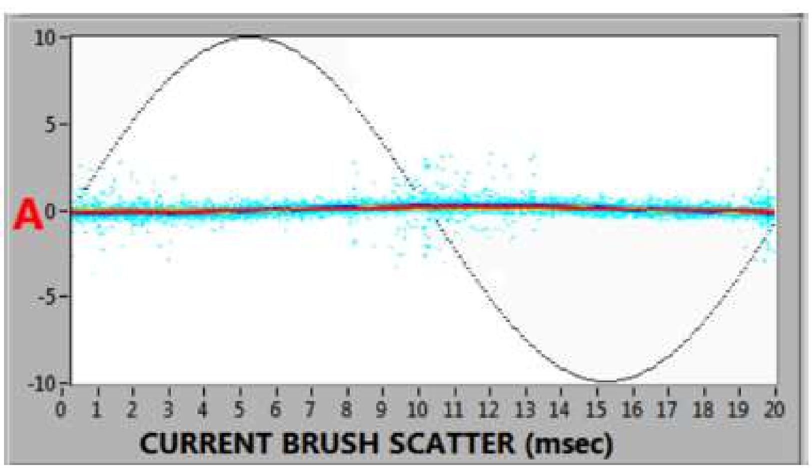

Figure 29: Current brush scatter plot (A) for floating brushes (Test#2)

Table 6: Shaft voltage quantities when the brush at Position B is out of service

Description	#Test 1 Shaft Voltage Values	#Test 2 Shaft Voltage Values
V_{rms_peak}	1.94 V	0.31 V
$V_{rms\_average}$	1.91 V	0.16 V
V_{DC}	0.02 V	0.01 V

Table 7: The shaft-current quantities when the brush at Position B is out of service

Description	#Test 1 Shaft Current Values	#Test 2 Shaft Current Values
I_{rms_peak}	0.75 A	3.86 A
$I_{rms\_average}$	0.73 A	1.40 A

Table 6 shows the shaft voltage RMS values of the shaft voltage ($V_{rms\_average}$ and V_{rms_peak}) have significantly decreased in relative magnitude when compared to the Test#1 when the voltage earth-brush was lifted from the shaft. This is an indication that the brush at Position B is ineffective and is not producing a solid earth point on the shaft. This is indicated by significantly low levels of shaft voltage quantities than the normal condition scenario.

Table 7 shows the current earth-brush quantities in values when the voltage earth-brush was lifted from the shaft. The experimental current brush quantities such as I_{rms_peak} and $I_{rms\_average}$ are significantly increased relative to Test#1 scenario when the voltage earth-brush was lifted from the shaft due to the ineffective voltage brush.

The shaft-voltage power spectrum (FFT) plot in *Figure 27* shows a distinctive dominant 50 Hz frequency component when compared to Test#1 scenario in *Figure 26.*

Under the same scenario B, Test #3 was implemented by lifting the earthing brush at Position A (current brush) and maintaining the contact point with the earthing brush at Position B (voltage brush) only. This test was conducted to establish the loss of continuity on the earthing brush circuit at Position A.

Figures 30 - 35 show the experimental shaft-voltage brush waveform, voltage brush frequency harmonics (FFT) and current scatter plot when the current brush is out of service.

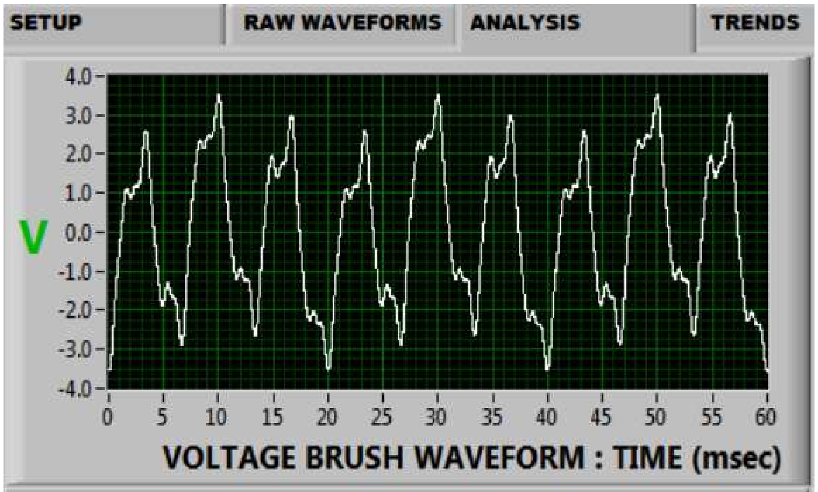

Figure 30: Shaft voltage brush waveform (V) for baseline test (Test#1)

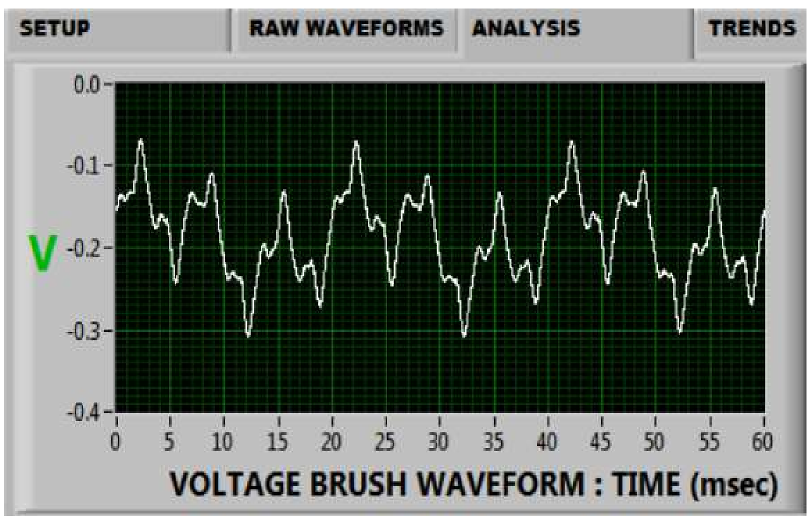

Figure 31: Shaft voltage brush waveform (V) when the current brush is out of service (Test#3)

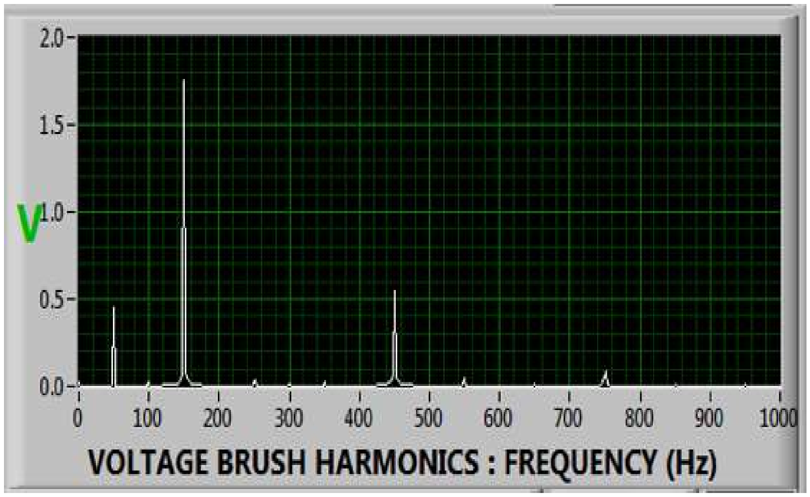

Figure 32: Shaft voltage brush harmonics (Hz) (FFT) for baseline test (Test#1)

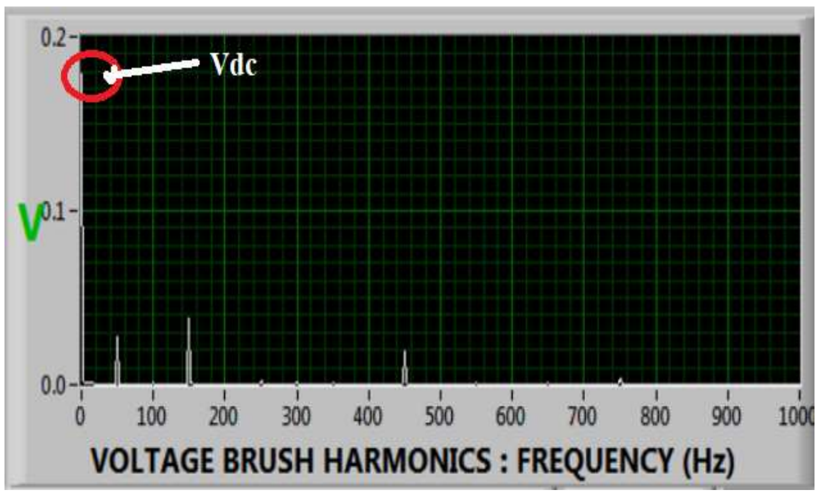

Figure 33: Voltage brush harmonic content (Hz) (FFT) when the current brush is out of service (Test#3)

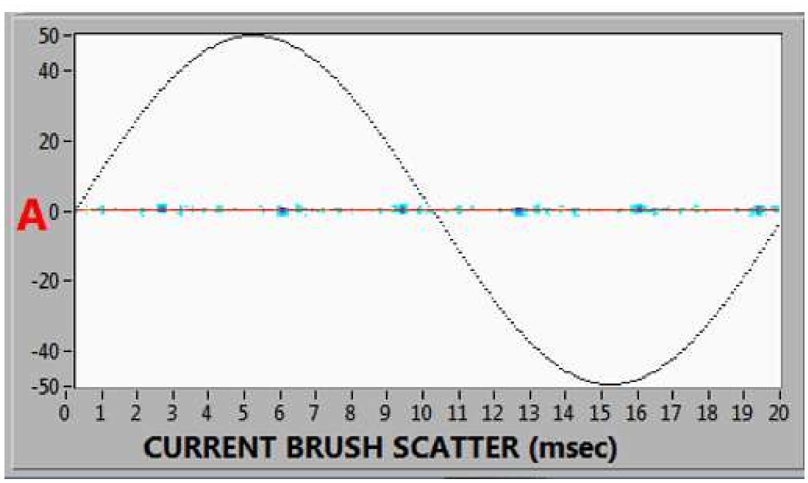

Figure 34: Current brush scatter plot (A) for baseline test (Test#1)

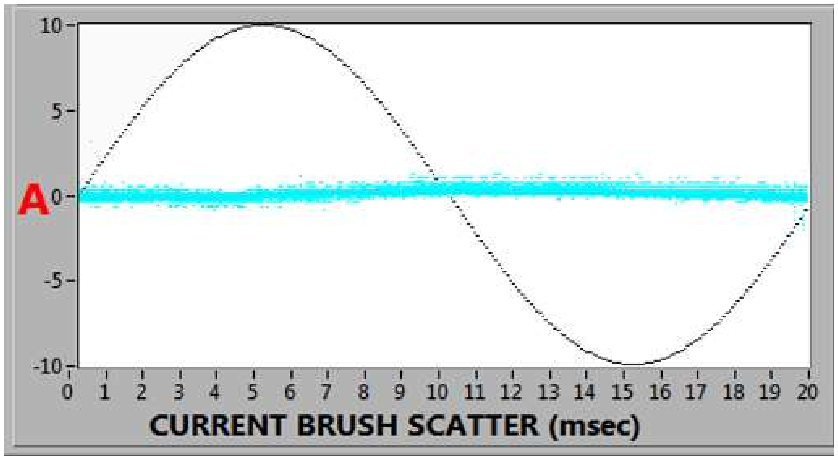

Figure 35: Current brush scatter plot (A) when the current brush is out of service (Test#3)

This test created an ungrounded condition on the generator shaft between the drive end side and driving motor. The current earth-brush at Position A was ineffective and produced an ungrounded generator shaft. *Table 8* shows the shaft voltage quantities when the earth-brush at Position A is out of service.

Table 8: Shaft voltage quantities when the brush at Position A is out of service

Description	#Test 1 Shaft Voltage Values	#Test 3 Shaft Voltage Values
V_{rms_peak}	1.94 V	1.86 V
$V_{rms\_average}$	1.91 V	0.15 V
V_{DC}	0.02 V	0.15 V

Table 9: The shaft current quantities when the brush at Position A is out of service

Description	#Test 1 Shaft Current Values	#Test 3 Shaft Current Values
I_{rms_peak}	0.75 A	1.22 A
$I_{rms\_average}$	0.73 A	0.11 A

The shaft voltage brush frequency harmonics (FFT) plot in *Figure 33* shows an increase in the relative magnitude of the DC voltage harmonic component or zero order harmonic (V_{DC}) to 0.15 V when compared to Test#1. The RMS average shaft voltage value $V_{rms\_average}$ significantly dropped by 1.72 V.

The RMS average value of the shaft current $I_{rms\_average}$ dropped significantly, by 0.62 A, a big decrease in the relative magnitude when compared to Test#1. Significant drops in average brush current and voltage values indicate poor current brush ground contact on the rotor shaft surface.

From the described current and voltage measurements and the FFT plot, it was appropriate to conclude that a disconnected current brush can be identified by the substantial increase in the relative magnitude of V_{DC} and a significant decrease in the relative magnitude of RMS average value of the shaft voltage $V_{rms\_average}$. This is an indication that the current earth-brush is ineffective and not making shaft contact.

Likewise, it can be concluded that a disconnected voltage brush can be identified by the predominant 50 Hz frequency component and a substantial decrease in the relative magnitude of the RMS average value of the shaft voltage $V_{rms\_average}$. This is an indication that the voltage brush is floating and not establishing a ground contact along the shaft.

5.4.3 Poor (worn out) earth-brush performance brush systems

Test #4 was introduced by replacing the voltage earth-brush at Position B with a worn-out earth-brush. This test was implemented to establish the earthing-brush performance when the brush is worn out.

Figures 36 - 41 show the experimental shaft-voltage brush waveform, shaft-voltage frequency harmonics spectral (FFT) and current scatter plot when the voltage brush is worn out.

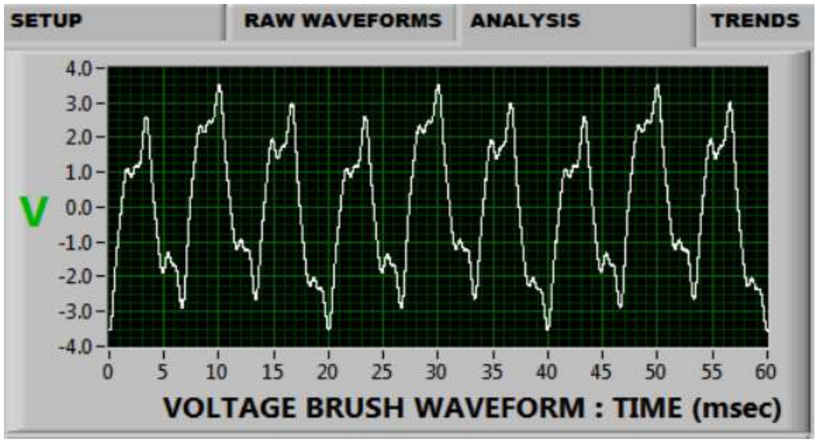

Figure 36: Shaft voltage brush waveform (V) for baseline test (Test#1)

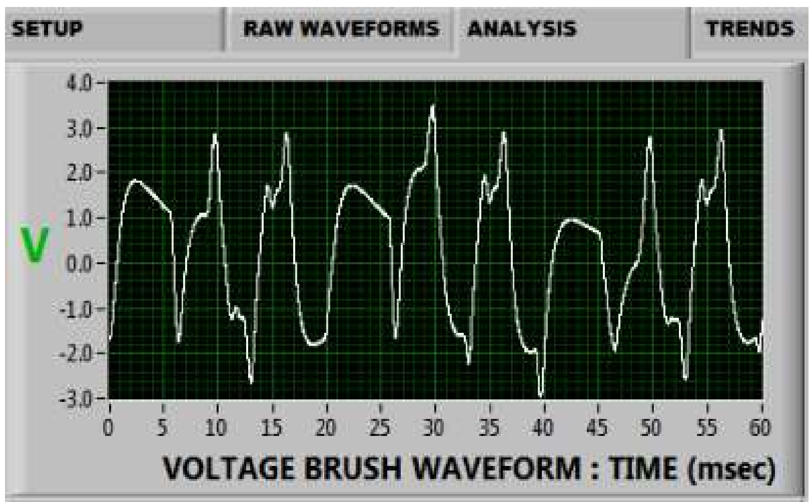

Figure 37: Shaft voltage brush waveform (V) when the voltage brush is worn out (Test #4)

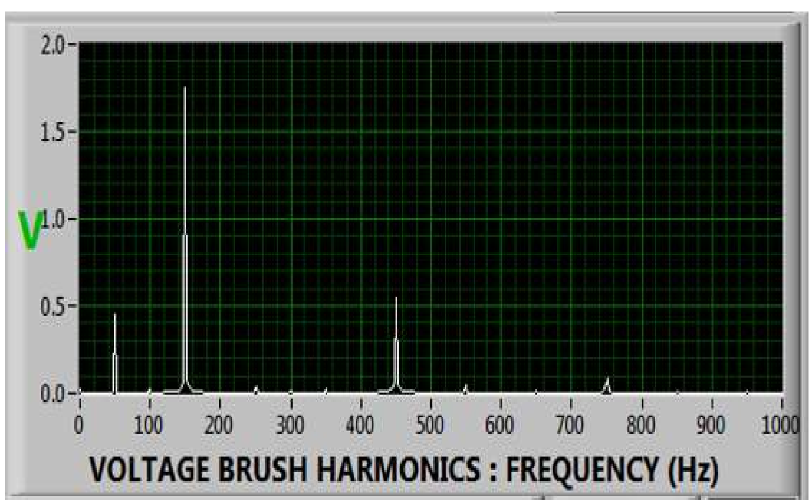

Figure 38: Shaft voltage brush harmonics (Hz) (FFT) for baseline test (Test#1)

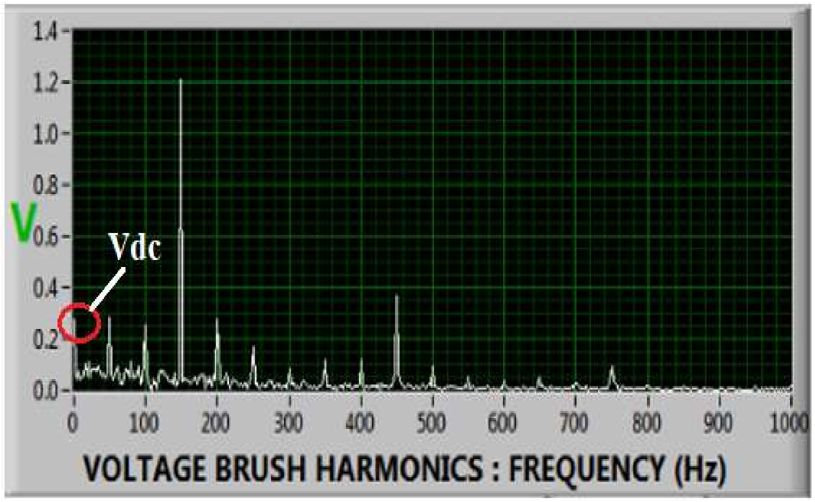

Figure 39: Shaft voltage brush harmonics (Hz) (FFT) when the voltage brush is worn out (Test#4)

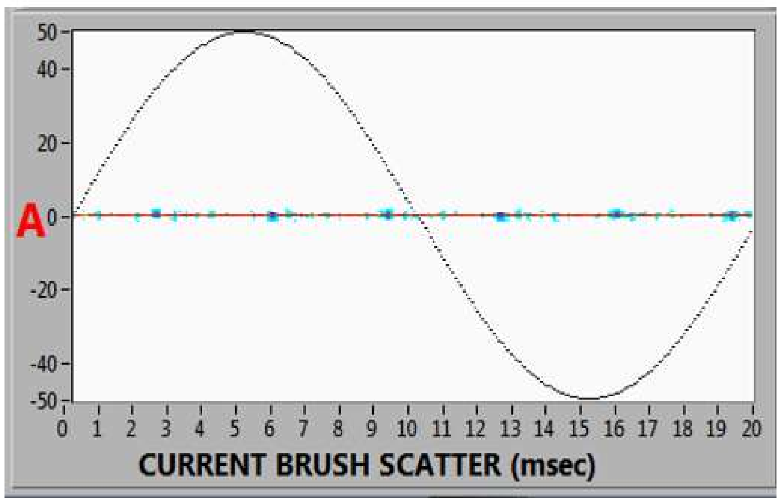

Figure 40: Current brush scatter plot (A) for baseline test (Test#1)

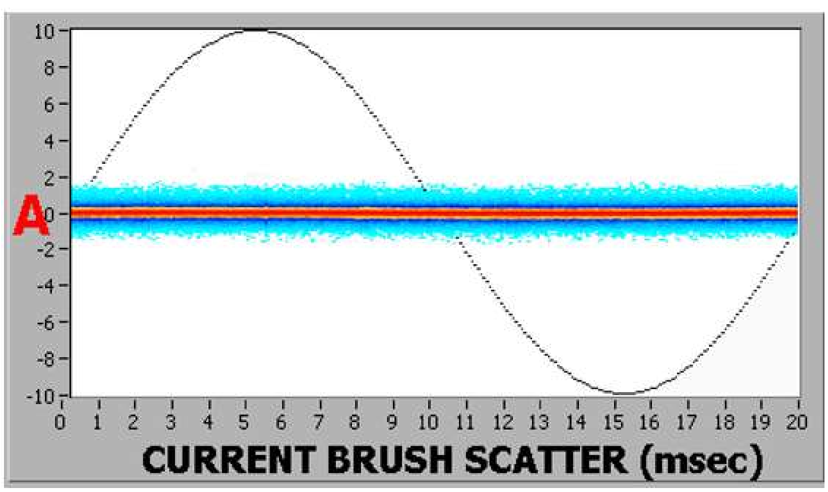

Figure 41: Current brush scatter plot (A) when the voltage brush is worn out (Test#4)

This test created an erratic shaft-voltage waveform signature as shown in *Figure 37*. *Figure 39* shows the dominant frequency components in the shaft voltage. The shaft voltage brush FFT plot in *Figure 39* shows an increase in the relative magnitude of the DC voltage harmonic component (V_{DC}) when compared to the Test#1 in *Figure 38.* The harmonics of the shaft voltage of the above-mentioned brush fault scenario show a relative increase of the 2nd and 4th harmonics.

Table 10: Shaft voltage quantities when the voltage brush at Position B is worn out

Description	#Test 1 Shaft Voltage Values	#Test 4 Shaft Voltage Values
V_{rms_peak}	1.94 V	1.85 V
$V_{rms\_average}$	1.91 V	0.60 V
V_{DC}	0.02 V	0.28 V

Table 11: The shaft current measured quantities

Description	#Test 1 Shaft Current Values	#Test 4 Shaft Current Values
I_{rms_peak}	0.75 A	1.22 A
$I_{rms\_average}$	0.73 A	0.74 A

Table 11 shows a significant increase of RMS peak value of the shaft voltage (I_{rms_peak}) when compared to the Test#1. This an indication that the worn out current brush is making poor ground contact on the surface of the rotor shaft. Significant increase in peak brush current indicates poor current brush ground contact on the rotor shaft surface. The shaft current quantities results presented in *Table 11*.

Under the described shaft voltage measurements and FFT plot, there was substantial increase in the relative magnitude of the even harmonics such as DC voltage harmonic or zero order harmonic component (V_{DC}), second harmonic (100 Hz), fourth harmonic (200 Hz) and a substantial decrease in the relative magnitude of the RMS average value of the shaft voltage $V_{rms\_average}$. It was appropriate to conclude that poor earthing performance or worn-out brush can be identified by substantial rise of even harmonics, shaft DC voltage harmonic component and erratic shaft voltage waveform.

5.4.4 Earthing brushes are exposed to oil and dust

Test #5 and Test#6 was implemented by introducing oil and dust on the current and voltage earth-brushes at Position A and B. This test was conducted to establish the earthing brush performance when the current and voltage brush are exposed to oil and dust.

Figures 42 – 47 show the experimental shaft-voltage brush waveform, shaft-voltage frequency harmonics spectral (FFT) and current scatter plot when the current brush exposed to dust and oil.

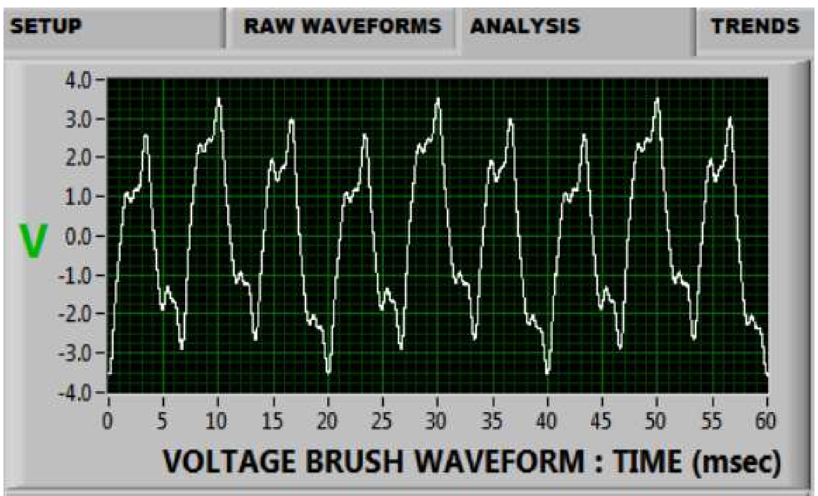

Figure 42: Shaft voltage brush waveform (V) for baseline test (Test#1)

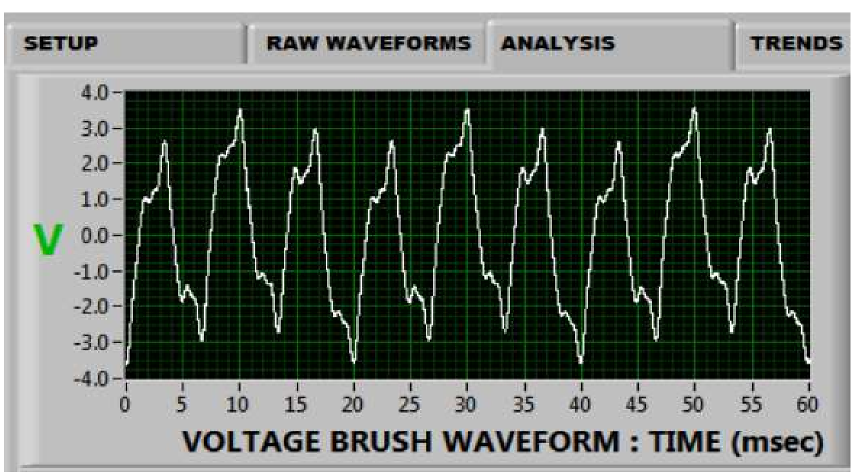

Figure 43: Shaft voltage brush waveform when the current brush exposed to dust and oil (Test#5).

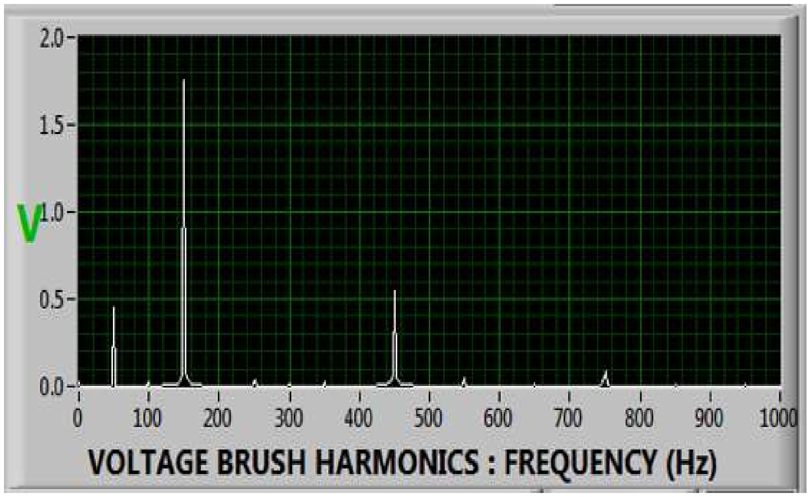

Figure 44: Shaft voltage brush harmonics (Hz) (FFT) for baseline test (Test#1)

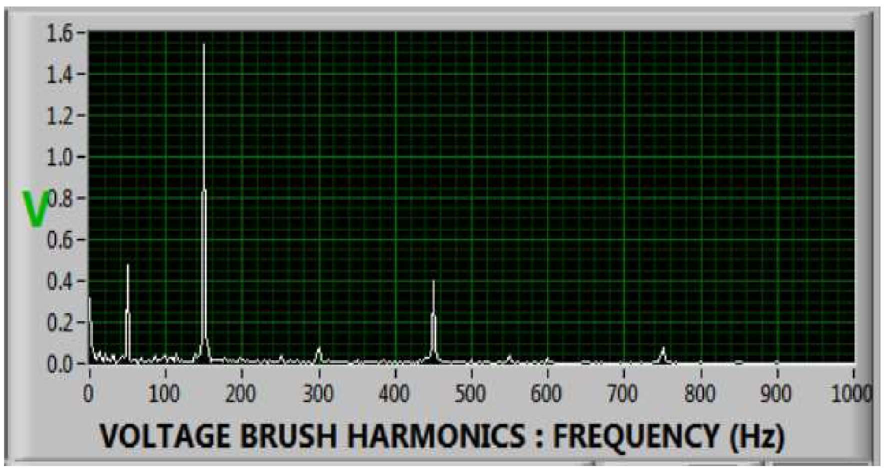

Figure 45: Voltage brush harmonic content (Hz) (FFT) when the current brush exposed to dust and oil (Test#5).

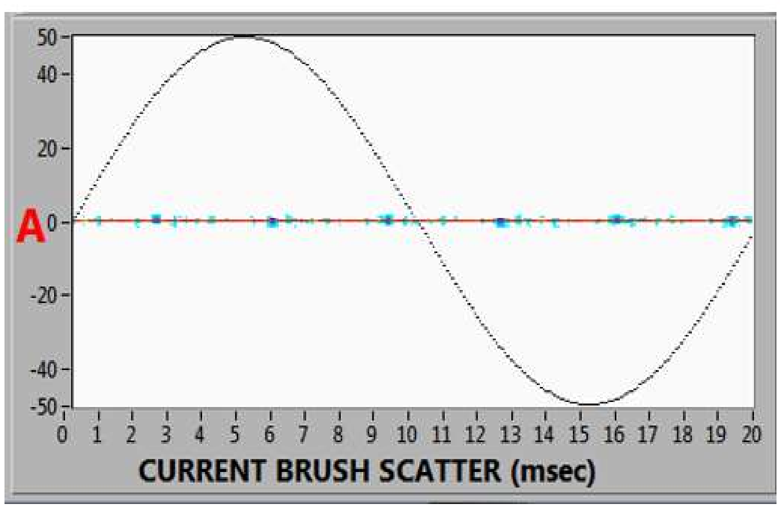

Figure 46: Current brush scatter plot (A) for baseline test (Test#1)

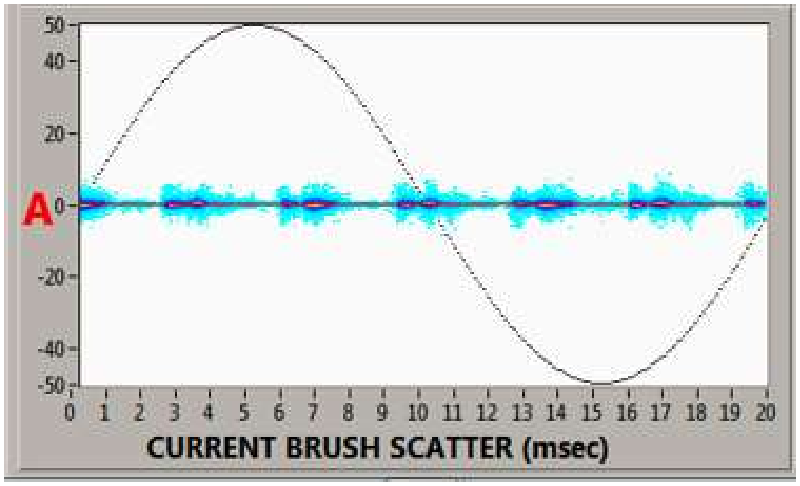

Figure 47: Current brush scatter plot (A) when the current brush exposed to dust and oil (Test#5).

This test created substantial increase in shaft currents and an erratic current signature developed on the current brush scatter plot. Therefore, the earthing brush at Position A was only poorly effective while in service. This was revealed by an erratic signature with peaks of approximately 6 A on the current scatter plot in *Figure 47*.

The shaft voltage quantities are shown in *Table 12.*

Table 12: Shaft voltage quantities when brush at Position A is exposed to oil and dust

Description	#Test 1 Shaft Voltage Values	#Test 5 Shaft Voltage Values
V_{rms_peak}	1.94 V	1.91 V
$V_{rms\_average}$	1.91 V	1.74 V
V_{DC}	0.02 V	0.32V

Table 13: The shaft current quantities when brush at Position A is exposed to oil and dust

Description	#Test 1 Shaft Current Values	#Test 5 Shaft Current Values
I_{rms_peak}	0.75 A	6.52 A
$I_{rms\_average}$	0.73 A	5.09 A

The shaft voltage brush FFT plot in *Figure 45* shows an increase in the relative magnitude of the V_{DC} when compared to the Test#1 in *Figure 44*.

The RMS average value of the shaft current $I_{rms\_average}$ and the RMS peak value of the shaft current I_{rms_peak} have substantially increased in the relative magnitude when compared to the Test#1. The significant increase in shaft current quantities was due to high resistance developed at Position A because of oil and dust presence on the shaft.

Under the described shaft voltage-current measurements, and current brush scatter plot, it was appropriate to conclude that oil and dust exposure on the current brush can be identified by the substantial increase in the relative magnitude of the current brush shaft currents, V_{DC}, and an erratic signature on the current brush scatter plot.

Another Test#6 performed under the same scenario by introducing oil and dust on the voltage brush at Position B. This test done to establish the earthing brush performance when the voltage brush exposed to oil and dust.

Figures 48 to 53 show the experimental shaft-voltage brush waveform, shaft-voltage frequency harmonics spectral (FFT) and current scatter plot when the voltage brush was exposed to dust and oil.

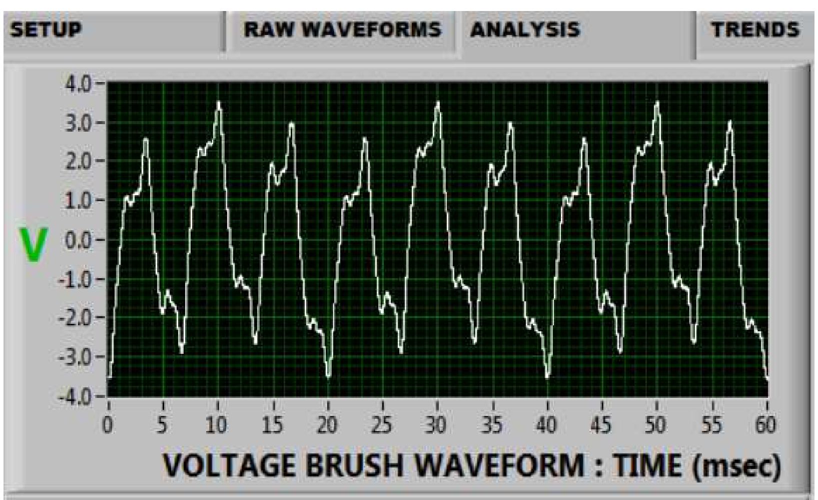

Figure 48: Shaft voltage brush waveform (V) for baseline test (Test#1)

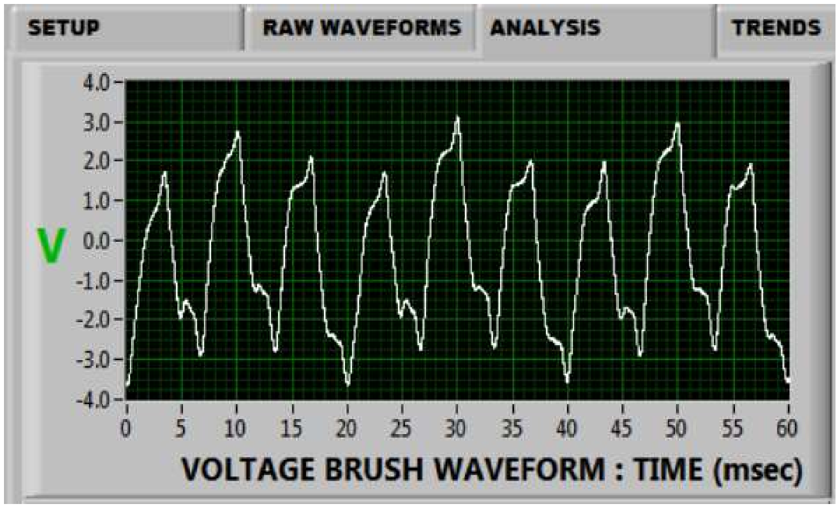

Figure 49: Shaft voltage brush waveform (V) when the voltage brush was exposed to dust and oil (Test#6).

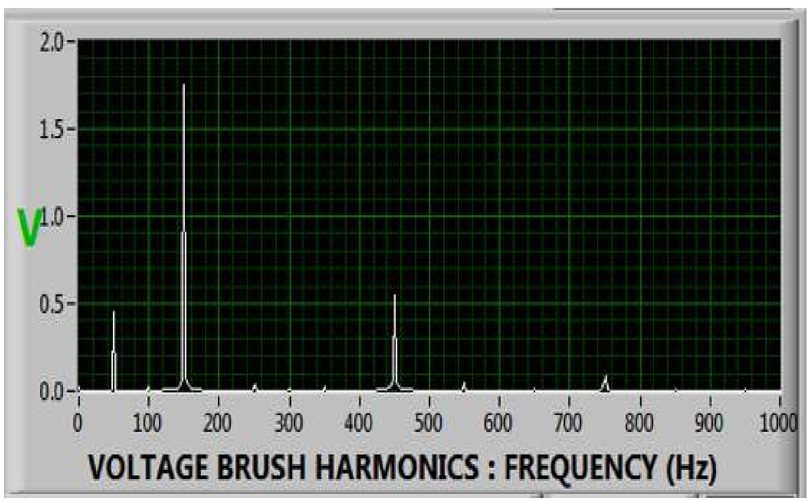

Figure 50: Shaft voltage brush harmonics (Hz) (FFT) for baseline test (Test#1)

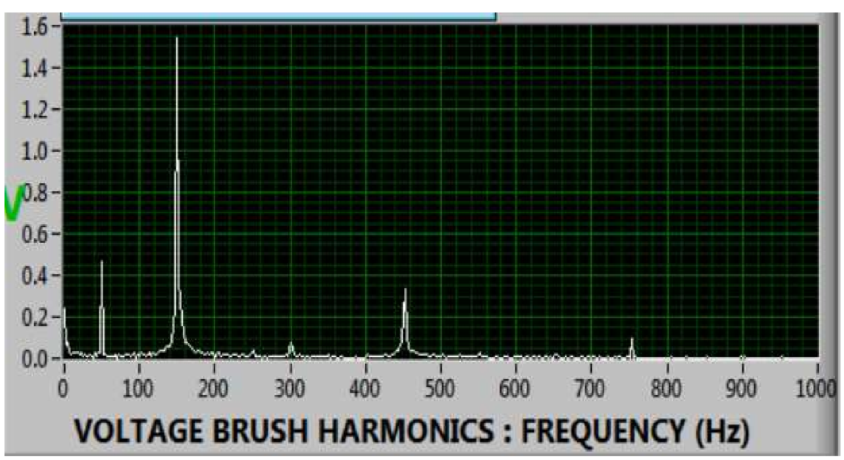

Figure 51: Voltage brush harmonic content (FFT) when the voltage brush was exposed to dust and oil (Test#6).

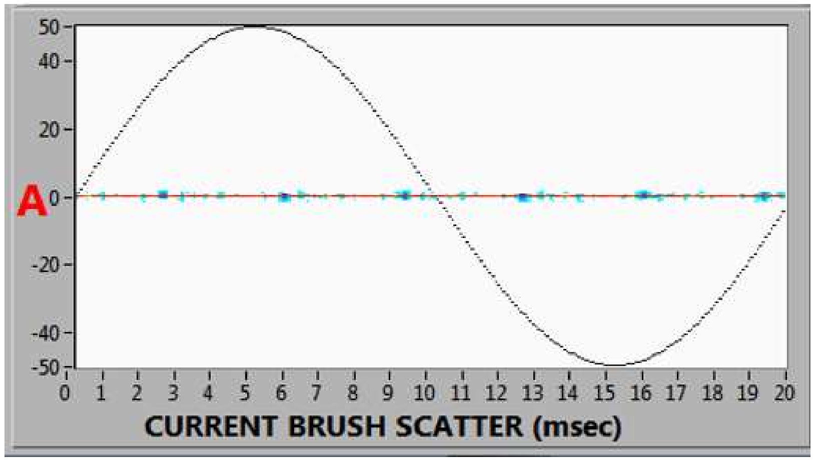

Figure 52: Current brush scatter plot (A) for baseline test (Test#1)

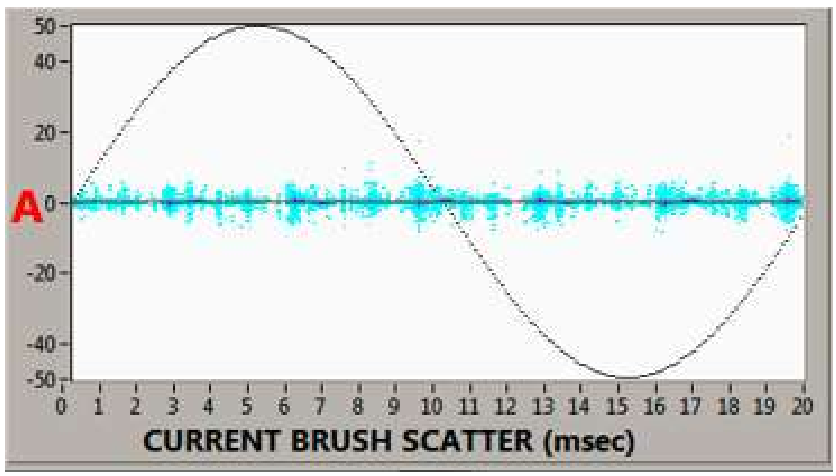

Figure 53: Current brush scatter plot (A) when the voltage brush was exposed to dust and oil (Test#6).

This test created substantial increase in shaft currents and an erratic current signature on the current brush scatter plot as shown in *Figure 53.* The shaft voltage brush FFT in *Figure 51* shows a substantial increase in the relative magnitude of the V_{DC}, and I_{rms_peak} when compared to the Test#1 in *Figure 50*. This revealed an erratic signature with peaks of approximately 5 A on the current scatter plot in *Figure 53.*

The shaft voltage quantities results are shown in *Table 14.*

Table 14: Shaft voltage quantities when brush at Position A is exposed to oil and dust

Description	#Test 1 Shaft Voltage Values	#Test 6 Shaft Voltage Values
V_{rms_peak}	1.94 V	1.91 V
$V_{rms\_average}$	1.91 V	1.88 V
V_{DC}	0.02 V	0.24 V

Table 15: The shaft current quantities when brush at Position A is exposed to oil and dust

Description	#Test 1 Shaft Current Values	#Test 6 Shaft Current Values
I_{rms_peak}	0.75 A	5.31 A
$I_{rms\_average}$	0.73 A	1.70 A

Under the described shaft current quantities, current brush scatter plot and FFT plot, it was appropriate to conclude that when the voltage brush is exposed to oil and dust, can be identified by the substantial increase in the relative magnitude of the V_{DC}, I_{rms_peak} , I_{rms_average} and an erratic current signature on the current brush scatter plot.

5.4.5 Effect of the generator excitation on shaft voltages

The rotor winding excitation current was reduced from 60 A to 40 A. *Figures 54 – 65* shows comparison plot of shaft-voltage brush waveform, and shaft-voltage frequency harmonics spectral (FFT) plot for different excitation currents with different earthing brush fault conditions.

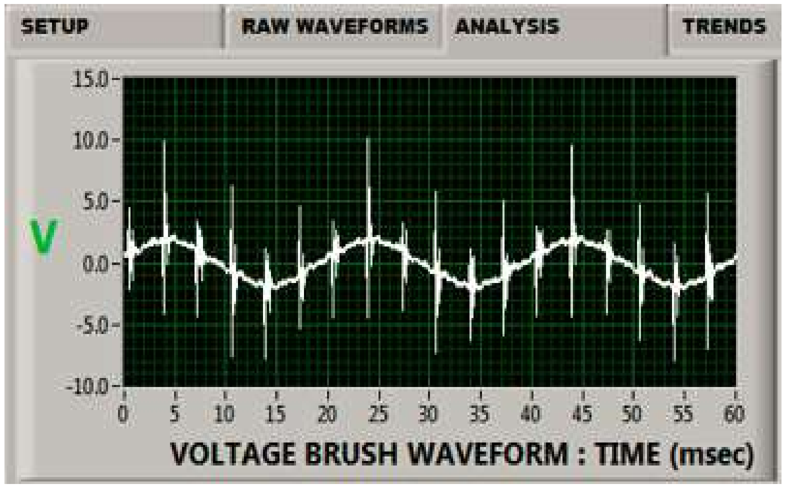

Figure 54: Shaft voltage brush waveform (V) at 60 A excitation with no earth brush continuity

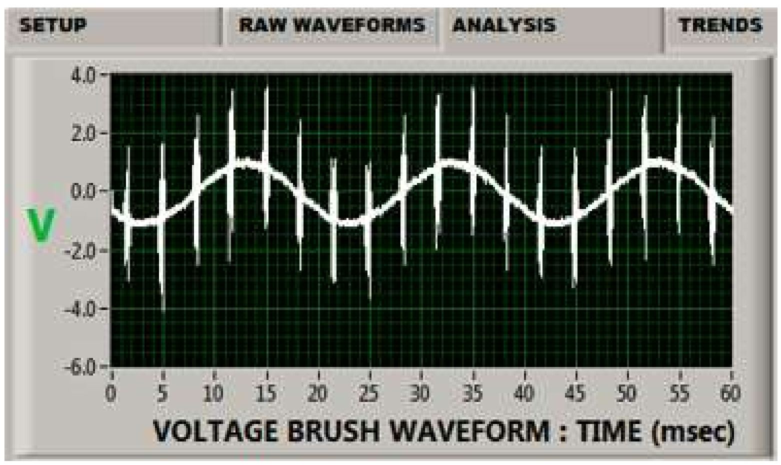

Figure 55: Shaft voltage brush waveform (V) at 40 A excitation with no earth brush continuity

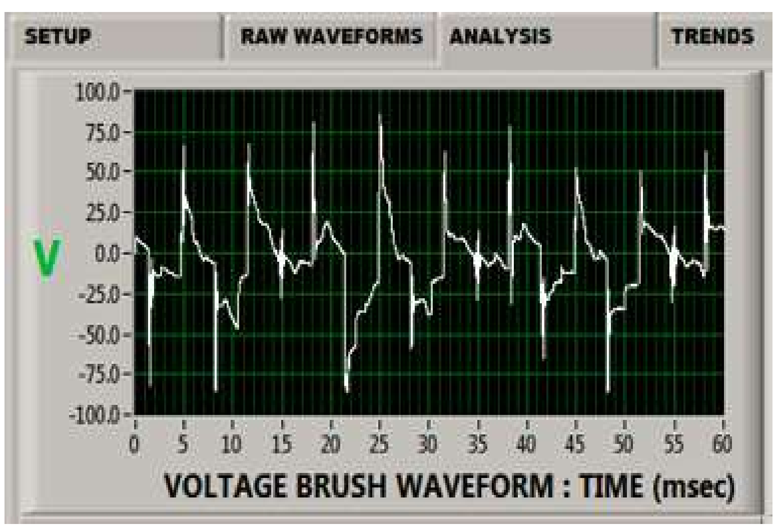

Figure 56: Shaft voltage brush waveform (V) at 60 A excitation with worn out brushes

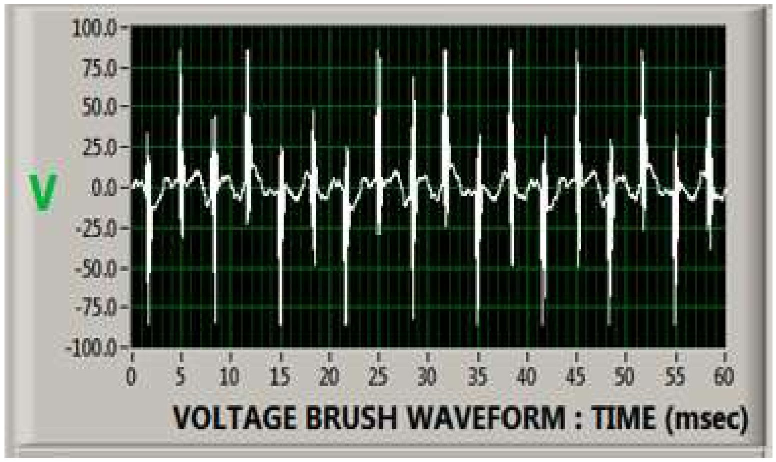

Figure 57: Shaft voltage brush waveform (V) at 40 A excitation with worn out brushes

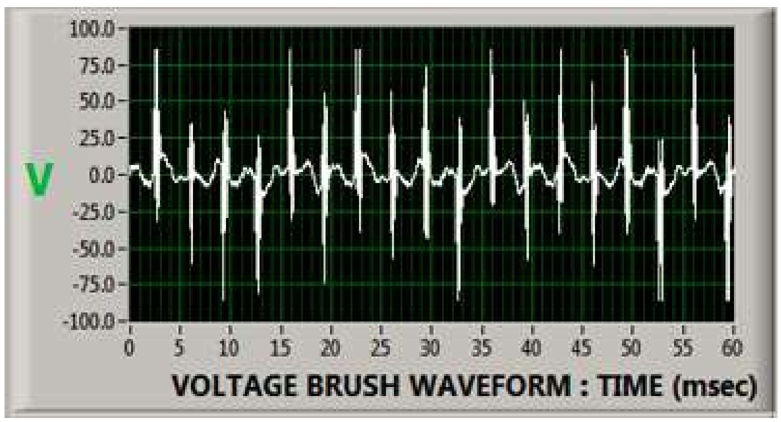

Figure 58: Shaft voltage brush waveform (V) at 60 A excitation with brushes exposed to dust and oil

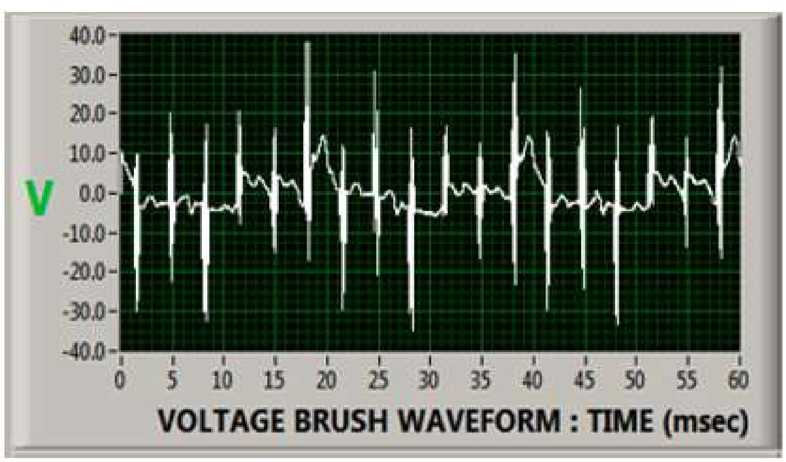

Figure 59: Shaft voltage brush waveform (V) at 40 A excitation with brushes exposed to dust and oil

Figures 60 – 65 shows comparison plot of shaft voltage power frequency spectrum for different excitation current with different earth brush fault conditions

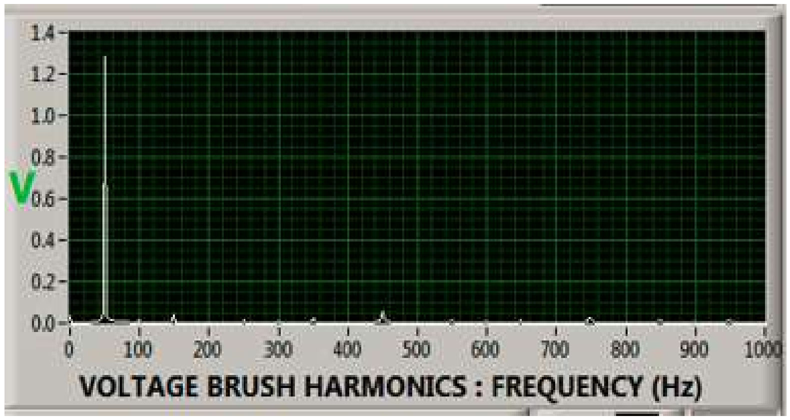

Figure 60: Shaft voltage brush harmonics (Hz) (FFT) at 60 A excitation with floating brushes

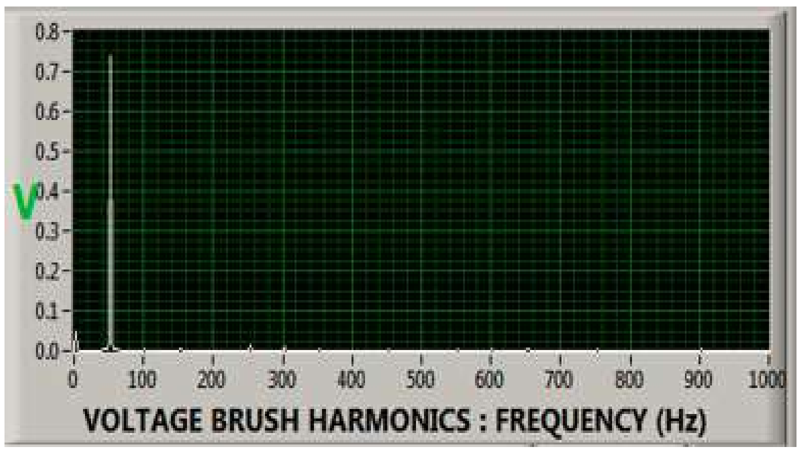

Figure 61: Shaft voltage brush harmonics (Hz) (FFT) at 40 A excitation with floating brushes

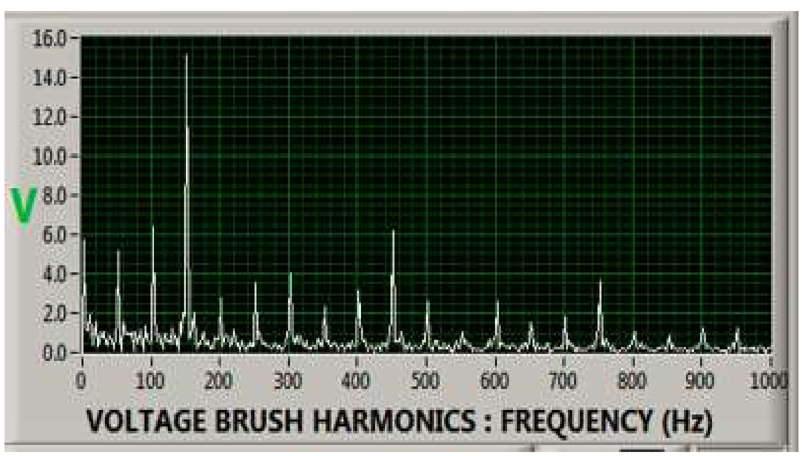

Figure 62: Shaft voltage brush harmonics (Hz) (FFT) at 60 A excitation with worn out brushes

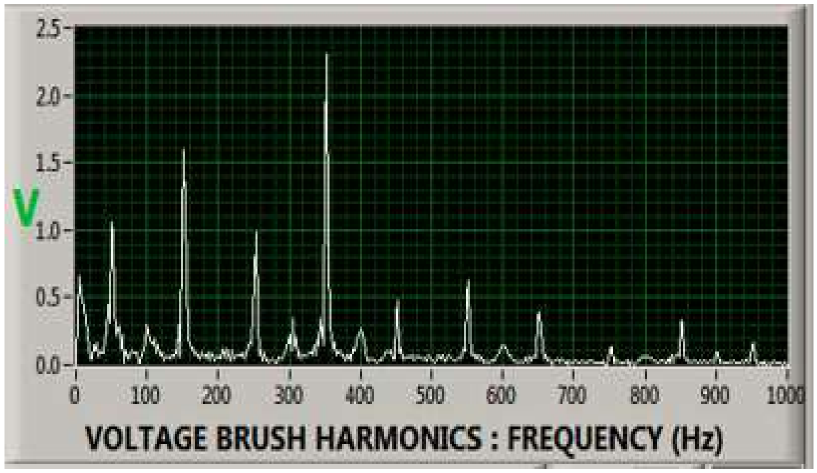

Figure 63: Shaft voltage brush harmonics (Hz) (FFT) at 40 A excitation with worn out brushes

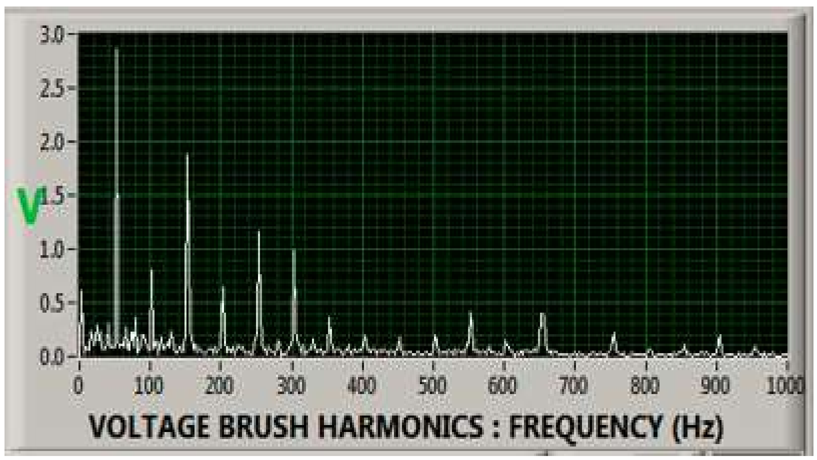

Figure 64*:* Shaft voltage brush harmonics (Hz) (FFT) at 60 A excitation with brushes exposed to dust and oil

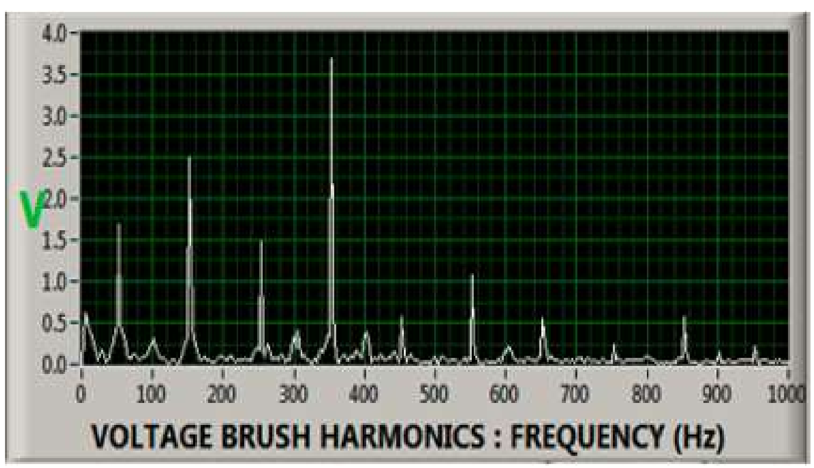

Figure 65: Shaft voltage brush harmonics (Hz) (FFT) at 40 A excitation with brushes exposed to dust and oil

Table 16: Shaft voltage quantities with different excitation currents with floating brushes

Description	Full Load Excitation (60A)	Reduced Excitation (40A)
V_{rms_peak}	24.97 V	2.45 V
$V_{rms\_average}$	0.78 V	2.09 V
V_{DC}	0.05 V	0.03 V

Table 17: Shaft voltage quantities with different excitation currents and with worn out brushes

Description	Full Load Excitation (60A)	Reduced Excitation (40A)
V_{rms_peak}	24.97 V	24.97 V
$V_{rms\_average}$	24.97 V	4.73 V
V_{DC}	5.72 V	0.34 V

Table 18: Shaft voltage quantities with different excitation currents and with brushes exposed to dust and oil

Description	Full Load Excitation (60A)	Reduced Excitation (40A)
V_{rms_peak}	24.97 V	7.60 V
$V_{rms\_average}$	4.73 V	7.06 V
V_{DC}	0.61 V	0.32 V

Figures 60 - 65 shows comparative illustrations of the shaft voltage brush harmonics with no earth continuity, worn out brushes and brushes exposed dust and oil. Under the described shaft voltage quantities, and FFT plot, it was appropriate to conclude that a reduced excitation current greatly reduces the shaft voltage. A change of 20% of the excitation field with worn-out produces substantial distortion of the shaft voltage waveform, through the decrease of a 3rd harmonic. However, it can be seen that the 7th harmonic still increases relative to the other significant harmonics when brushes is exposed to dust and oil.

5.4.6 Effect of rotational speed on shaft voltages

The rational speed of the shaft was reduced by 20% from 3000 rpm to 2400 rpm. The experiments were then performed with floating brushes, worn earth brush and with brushes exposed to dust and oil. *Figures 66 – 71* show comparison plot of shaft-voltage brush waveform for different rotational speed with different earthing brush fault conditions.

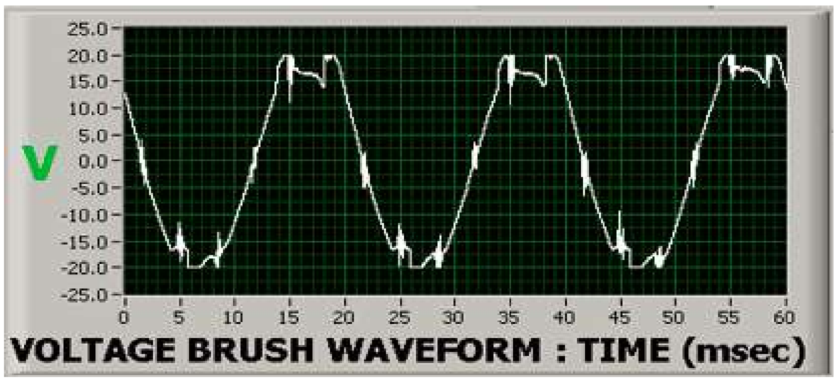

Figure 66: Shaft voltage brush waveform (V) at full speed with floating brushes

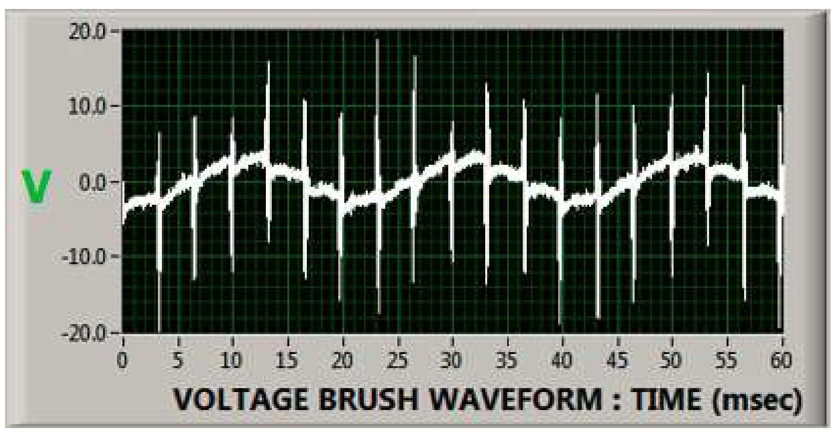

Figure 67: Shaft voltage brush waveform (V) at 80% speed with floating brushes

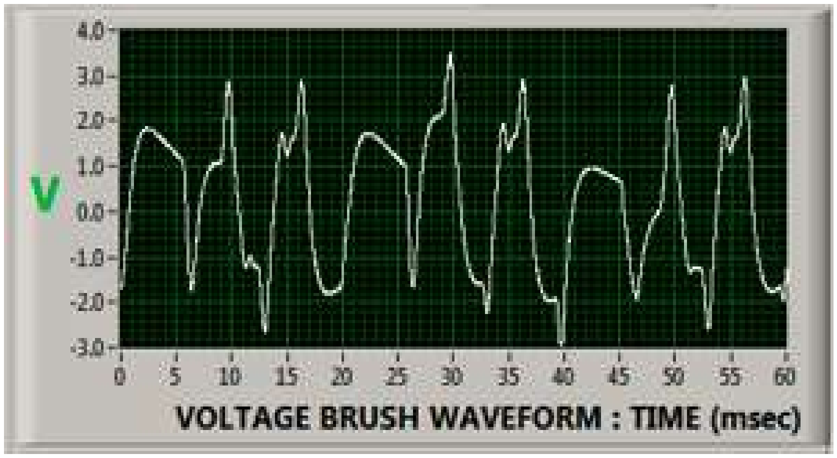

Figure 68: Shaft voltage brush harmonics (Hz) (FFT) at full load speed with worn out brushes

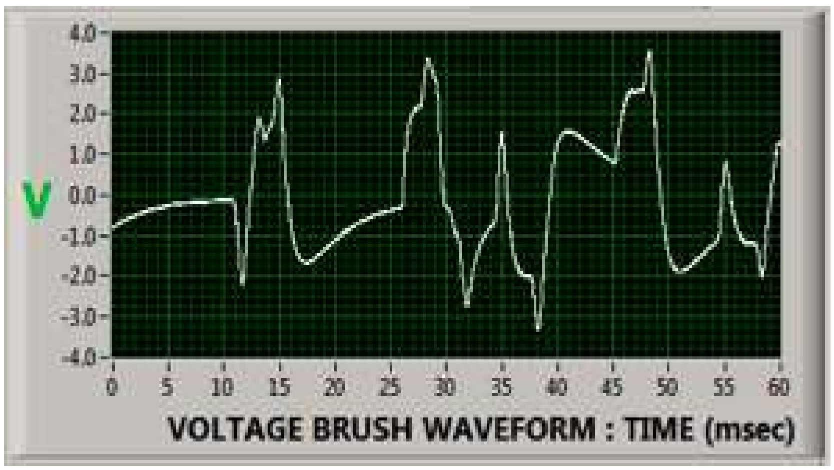

Figure 69: Shaft voltage brush harmonics (Hz) (FFT) at 80% speed with worn out brushes

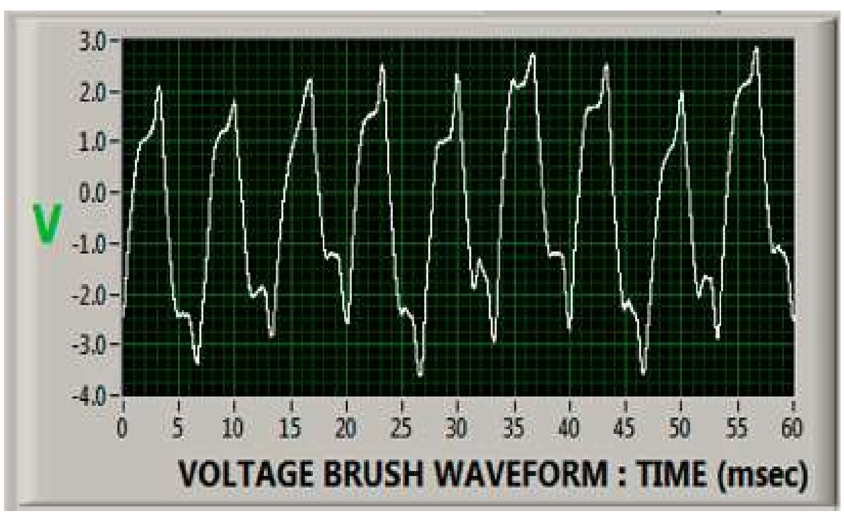

Figure 70: Shaft voltage brush harmonics (Hz) (FFT) at full load speed with worn out brushes

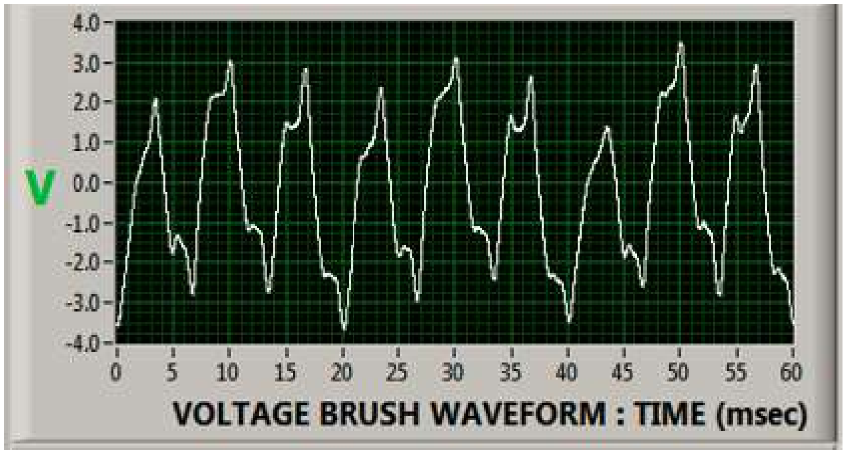

Figure 71: Shaft voltage brush harmonics (Hz) (FFT) at 80% speed with worn out brushes

Figures 72 – 77 shows comparison plot of shaft-voltage frequency harmonics spectral (FFT) for different rotational speeds with different earth brush fault conditions.

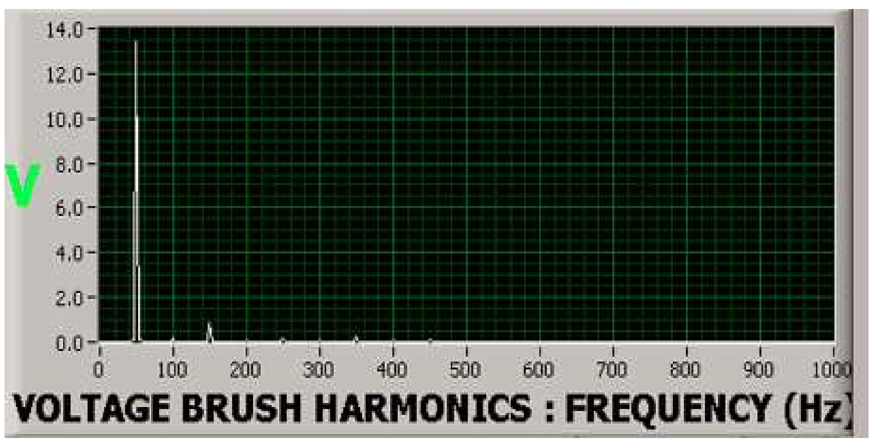

Figure 72: Shaft voltage brush harmonics (Hz) (FFT) at full speed with floating brushes

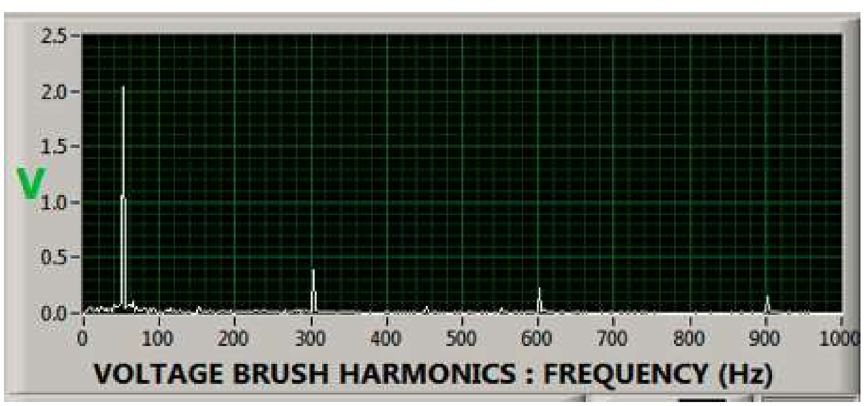

Figure 73: Shaft voltage brush harmonics (Hz) (FFT) at 80% speed with floating brushes

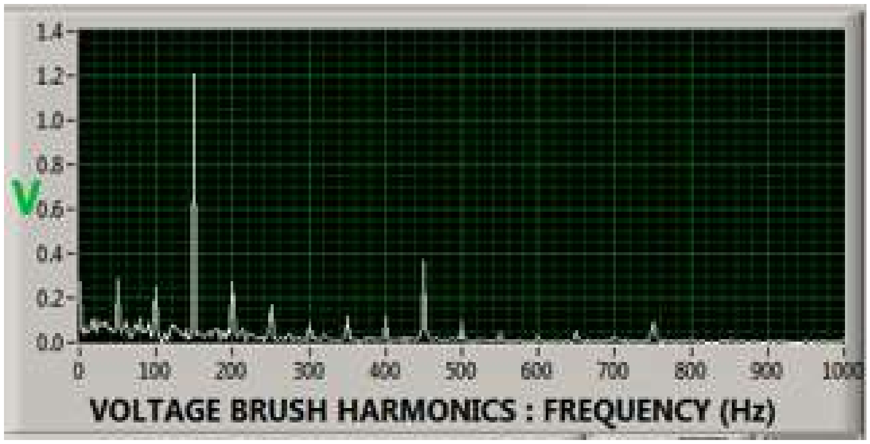

Figure 74: Shaft voltage brush harmonics (Hz) (FFT) at full load speed with worn out brushes

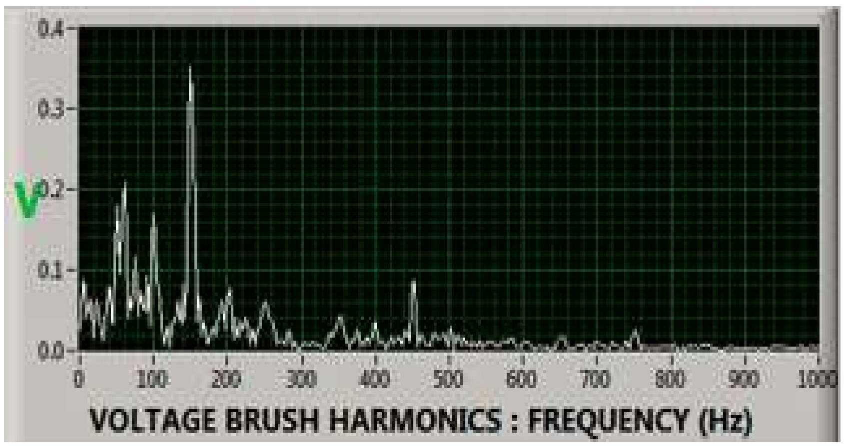

Figure 75: Shaft voltage brush harmonics (Hz) (FFT) at 80% speed with worn out brushes

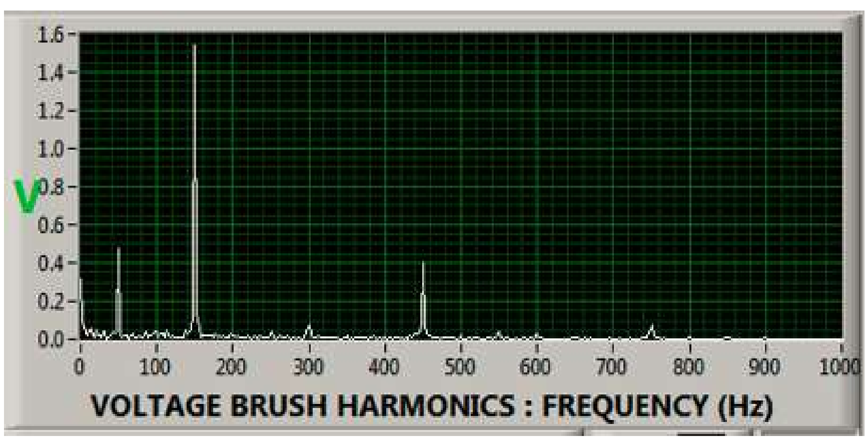

Figure 76: Shaft voltage brush harmonics (Hz) (FFT) at full load speed with exposed to oil and dust

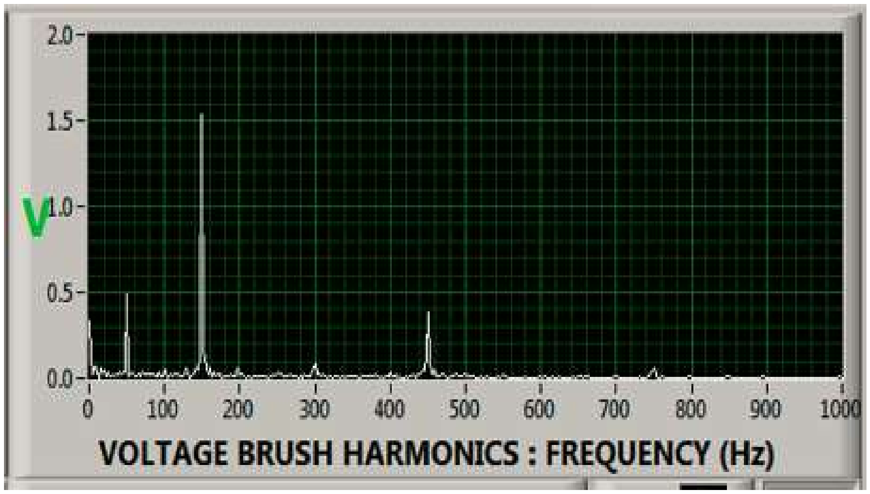

Figure 77: Shaft voltage brush harmonics (Hz) (FFT) at 80% speed with brushes exposed to oil and dust

Table 19: Shaft voltage quantities for different rotational speeds with floating earth brushes

Description	Full Load (3000RPM)	80% Speed (2400RMP)
V_{rms_peak}	1.01 V	0.92 V
$V_{rms\_average}$	0.95 V	0.72 V
V_{DC}	0.03 V	0.01 V

Table 20: Shaft voltage quantities for different rotational speeds with worn out brushes

Description	Full Load (3000RPM)	80% Speed (2400RMP)
V_{rms_peak}	1.85 V	1.85 V
$V_{rms\_average}$	1.75 V	0.65 V
V_{DC}	0.28 V	0.05 V

Table 21: Shaft voltage quantities for different rotational speeds with brushes exposed to dust and oil

Description	Full Load (3000RPM)	80% Speed (2400RMP)
V_{rms_peak}	1.91 V	1.91 V
$V_{rms\_average}$	1.79 V	1.74 V
V_{DC}	0.34 V	0.32 V

Tables 19 - 21 show the experimented RMS shaft voltages with different shaft rotation speeds at different earthing brush fault conditions. From the experiment it is clear that a slower rotational speed results in lower shaft voltages. A comparison between the shaft-voltage frequency harmonics spectral (FFT) for the three earth brush fault conditions is shown in *Figures 72-77*. It can be clearly seen that the 5th harmonic decreases significantly for worn out brushes. The harmonics of the shaft voltage for each of the abovementioned cases also show a definite trend for the 3rd, 5th, and 9th harmonics.

5.5 Conclusion

The results of an investigation of the shaft voltage and current effects, under different earth-brush fault conditions were presented. The results indicate that the shaft voltages and current characteristics have effects on earth-brush fault types. Therefore, it is possible to determine the earth-brush condition from shaft voltage and current measurement given that baseline information is available.

Floating or disconnected *voltage* brushes can be identified by the predominant 50 Hz frequency component and a substantial decrease in the relative magnitude of the RMS average value of the shaft voltage $V_{rms\_average}$. This is an indication that the voltage brush is floating and not establishing a ground contact along the shaft.

A disconnected *current* brush can be identified by the substantial increase in the relative magnitude of the DC voltage harmonic component V_{DC} and a significant decrease in the relative magnitude of the average RMS value of voltage brush $V_{rms\_average}$. This is an indication that the current earth-brush is ineffective and not making a shaft contact.

A worn-out *voltage* brush performance can be identified by a substantial rise of even harmonics, shaft DC voltages and erratic shaft voltage waveform.

A *voltage* brush exposed to oil and dust, can be identified by the substantial increase in the relative magnitude of the DC voltage harmonic V_{DC}, RMS peak value of the shaft current I_{rms_peak} , RMS average value of the shaft current I_{rms_average} and an erratic current signature on the current brush scatter plot.

A *current* brush exposed to oil and dust can be identified by the substantial increase in the relative magnitude of the current brush shaft currents and an erratic signature on the current brush scatter plot. Current scatter plot signature provides significant information that can used to determine the condition of the current brush when exposed to oil and dust.

From the experiment it was appropriate to conclude that a reduced excitation current greatly reduces the shaft voltage. A change of 20% of the excitation field with worn-out produces substantial distortion of the shaft voltage waveform, through the decrease of a 3rd harmonic

It is clear that a slower rotational speed results in lower shaft voltages. It can be clearly seen that the 5th harmonic decreases significantly for worn out brushes. The harmonics of the shaft voltage show a definite trend for the 3rd, 5th, and 9th harmonics. It can therefore be concluded that a small variation in rotational speed does influence which harmonic is significant in the diagnosis of an earth brush system.

Chapter 6 Evaluating Online Fault Detection Techniques

6.1 Introduction

The second phase of the study evaluated techniques for classifying earth-brush faults. These methods used shaft current and voltage characteristics to determine online, *in situ,* earth-brush performance. The synchronous generator earth-brush fault types are classified according to shaft-signal performance. Combinations of shaft-signals according to the type of the earth-brush fault provide a clearer understanding of how these faults should be detected.

Online detection techniques are necessary for analysis and interpretation of earth-brush performance without interrupting the operation of the synchronous generator. These techniques provide the data on earth-brush performance needed to plan remedial actions to mitigate any developing earth-brush faults and premature generator component failures.

The techniques were applied to the test performance and results obtained in Chapter 5 and are evaluated and compared in the context of the application. Three online earthing brush fault detection techniques were evaluated in this study, namely frequency spectral analysis, warning criteria and threshold checking techniques [9] [11] [12].

6.1.1 Warning criteria technique

Generator circulating shaft currents will always discharges through the smallest gap to earth and small clearance generator components are most vulnerable to discharges and failures (i.e. bearings, hydrogen seals and gears) [9] [29]. However, if these shaft-signal quantities are baselined and tracked, problems that could develop on a shaft can be averted.

Nippes [11] describes a generator shaft voltage/current monitoring system (VCM) that provides an indication of a potential developing problem. This shaft monitoring system uses warning criteria technique to determine the imminent or developing fault.

The warning criteria technique classifies faults by analysing the sequence of changes in shaft-signal quantities over time to provide detection/warning of any impending earth-brush problems. By monitoring the change of earthing brush shaft-signal performance, inferences can be made about the earthing system performance.

Thus, when there is a change in earth-brush fault current and voltage quantities, this technique provides detection and early warning of any developing earthing brush irregularities [11] [22].

Table 22 summarizes the various voltage and current components that were measured in Chapter 5 on the synchronous mini-generator at different brush faults scenarios.

Table 22: Warning criteria technique on different fault scenarios

Item	**A -Test #1**	**B - Test #2**	**C- Test #3**	**D -Test #4**	**E -Test #5**	**F-Test #6**
I_{rms_peak}	0.75 A	>> I_{rms_peak}	$> I_{rms\_peak}$	$> I_{rms\_peak}$	$\gg I_{rms\_peak}$	$\gg I_{rms\_peak}$
$I_{rms\_average}$	0.73 A	$\gg I_{rms\_average}$	$\ll I_{rms\_average}$	$> I_{rms\_average}$	$\gg I_{rms\_average}$	$\gg I_{rms\_average}$
V_{rms_peak}	1.94 V	$\ll V_{rms\_peak}$	$< V_{rms\_peak}$	$< V_{rms\_peak}$	$< V_{rms\_peak}$	$< V_{rms\_peak}$
V_{rms_average}	1.91 V	$\ll V_{rms\_\mathrm{average}}$	$\ll V_{rms\_\mathrm{average}}$	$\ll V_{rms\_\mathrm{average}}$	$< V_{rms\_\mathrm{average}}$	$< V_{rms\_\mathrm{average}}$
V_{DC}	0.02	$< V_{DC}$	$\gg V_{DC}$	$\gg V_{DC}$	$\gg V_{DC}$	$\gg V_{DC}$

In *Table 22:*

$<$ represents less than and $\ll$ represents much less than

$>$ represents more than and $\gg$ represents much more than

A- Test #1 Brush at Position A in, Brush at Position B in. All brushes are in-service.
B- Test #2 Brush at Position A in, Brush at Position B out.
C- Test #3 Brush at Position A out, Brush at Position B in.
D- Test #4 Brush at Position B replaced with a worn-out brush
E- Test #5 Brush at Position A exposed to oil and dust
F- Test #6 Brush at Position B exposed to oil and dust

Table 22 shows fault warning criteria for different brush fault scenarios. The shaft current and voltage quantities from Test #1's measured values were used as baseline data for reference. By looking at the change in current and voltage quantities in the table when different brush faults were set up, an algorithm can be developed for overall earthing performance and diagnosis.

Under the prescribed fault scenario B, Test#2 shows $\ll V_{rms\_\text{average}}$ is much less than baseline, provides indicative warning that there is a developing problem on the voltage brush at Position B. Fault scenarios E and F, Test#5, and Test #6 are much higher $\gg I_{rms\_\text{average}}$ and $\gg I_{rms\_\text{peak}}$, and provide a warning of developing irregularities on the current and voltage brush at Position A and B respectively. In fault scenario C, Test#3, the ratio of peak current to average current is much higher than normal, at >>1.5 and $> V_{DC}$ is high, which provides a warning that there a developing problem on the current brush at Position A.

6.1.3 Threshold checking (comparative logic) technique

Posedel in [12] describes a system for reducing the shaft voltages/currents in dynamoelectric machines, especially turbosets, in which on the non-drive shaft end of the machine. This shaft voltage/current monitoring system uses comparative technique to determine problems or predicts fault and degradation events associated with the generator earthing system [10] [12].

Threshold checking is a technique that classifies rotating machine faults based on shaft voltage and current quantities in a comparative logic form, suitable for interpretation of the rotating machine fault condition. By close examination using the comparative logic technique, a clear statement can be made about overall earthing system performance.

In the synchronous generator, whose measured values are shown in Chapter 5, threshold values are benchmarked from a baseline of key parameters from Test#1 results. This technique provides a logic output signal of 0 as long as these fault shaft current and voltage quantities remain below benchmark threshold value, and provides a logic output signal of 1 when the said threshold values are exceeded. These signals will be combined with one another and interpreted in a simple way in comparative structured evaluation logic [12]. *Table 23* shows the comparative structured logic of various voltage and current components that were measured in Chapter 5 on the synchronous mini-generator at different brush faults scenarios.

Table 23: Comparative structured logics on different fault scenarios

EARTHING BRUSHES STATUS		**ANALYSED MEASURED SIGNAL**						
Earthing Brushes Position		Voltage					Current	Fault Scenarios
Current Brush in-service (A)	Voltage Brush in-service (B)	V_{dc}	V_f	V_{3rd}	V_{9th}	$V_{rms\_average}$	$I_{rms\_average}$	State
X	X	0.02V	0.46V	1.75V	0.52V	1.91V	0.73 A	A
X	-	0	0	0	0	0	1	B
-	X	1	0	0	0	0	0	C
X	X	1	0	1	0	0	1	D
X^*	X	1	0	0	0	0	1	E
X	X^*	1	1	0	0	0	1	F

In *Table 23*

A- Test #1 Brush at position A in, brush at position B in. Thus, all brushes are in-service.

B- Test #2 Brush at position A in, brush at position B out.

C- Test #3 Brush at position A out, brush at position B in.

D- Test #4 Brush at position B replaced with a worn-out brush

E- Test #5 Brush at position A exposed to oil and dust

F- Test #6 Brush at position B exposed to oil and dust

V_f is the fundamental frequency

V_{3rd} is the third harmonic

V_{9th} is the ninth harmonic

V_{dc} is the DC voltage appearing on the voltage harmonics

X Earth brush in contact

− Earth brush out of contact

X^* Earth brush exposed to oil and dust

A binary combination 000001 (state B), signals a floating voltage brush at position B on the non-drive end, but intact current earthing brush at position A on the drive end of the machine. The binary combination 100000 (state C) signals that the current earth-brush at position A on the drive end is defective although the shaft earthing voltage brush at position B is functioning normally. The binary combination 101001 (state D) signals an intact current brush at position A on the drive end side but a defective voltage brush at position B on the non-drive end side of the machine. The binary combination 100001 (state E) signals high resistance on the current brush at position A, but effective voltage brush at position B because exposure to oil and dust. The binary combination 110001 (state F) signals high resistance on the voltage brush at position B and intact current brush at position A

6.1.5 Frequency spectral analysis technique

It has been proposed that the spectral analysis of the shaft voltage signal contains information that will allow the source of the earthing brush fault to be identified [9] [25].

In *Table 24* below, the earthing brush fault types from the experiment in Chapter 5 are classified, based on the effect of shaft voltage characteristics and current scatter plots that were measured on the synchronous mini-generator at different brush faults scenarios.

Table 24: Frequency Spectral Analysis on different fault scenarios

Source	**Characteristic component of shaft voltage**
Lost shaft ground circuit or no earthing continuity	
Test #2 Brush at Position A in, brush at Position B out.	The 50 Hz component of the harmonic spectrum is higher than other frequency components.
Test #3 Brush at Position A out, brush at Position B in.	DC component (V_{DC}) of the harmonic spectrum content is higher than other frequency components. $V_{rms\_average}$ much lower than usual.
Poor earthing performance brush systems	

Test #4 Brush at Position B replaced with a worn-out brush	Even harmonics content is high (100 Hz, 200 Hz, 300 Hz etc.), many other harmonics and erratic shaft-voltage waveform.
Earthing brushes are exposed to oil and dust	
Test #5 Brush at Position A exposed to oil and dust	Erratic current scatter current plot and DC component of the harmonic spectrum is much higher. $I_{rms_{\text{-peak}}} \gg, I_{rms\_\text{average}} \gg$ much higher than usual.
Test #6 Brush at Position B exposed to oil and dust.	Irregular or erratic shaft current scatter plot. $I_{rms_{\text{-peak}}} \gg, I_{rms\_\text{average}} \gg$ much higher than usual.

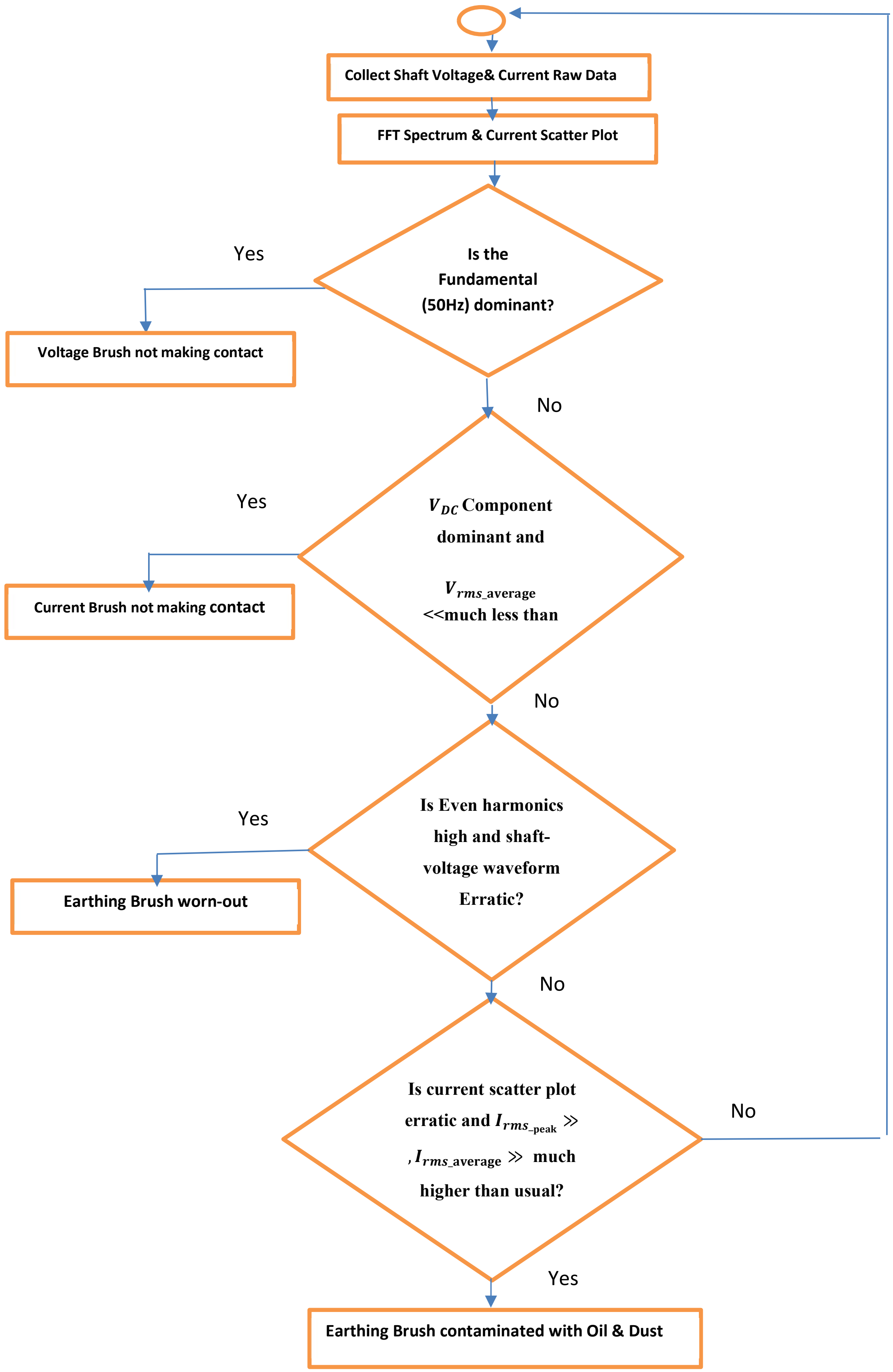

Figure 78: Flowchart with simplified approach for online Earth-brush fault detection

The steps involved in earthing brush fault detection are as shown by the flowchart in *Figure 78.* The frequency spectral analysis and current scatter plot have been considered for analysis of the earth-brush condition.

The approach easily categorises different earth-brush faults types according to the source of the fault (i.e. voltage brush and current brush). The objective of this detection is to clearly separate brush faults according to the effect the fault has on the measurable parameters (i.e. shaft currents and voltage quantities, and frequency spectral characteristics).

From the earthing brush fault detection flowchart, it is evident that earthing brush fault types directly affect shaft voltage and current quantities, although in different ways. These effects are often reflected in the FFT, current scatter plot and shaft voltage waveform.

This technique culminates in a flowchart process for earth brush fault detection when earthing brushes are in service. Fault types are identified *in situ* through the process flowchart without disrupting the operation of the synchronous generator.

6.2 Evaluating Online Detection Techniques

The previous section illustrated online shaft-signal based techniques that can be employed to provide an overview of earth-brush performance using shaft voltage and current measurement results obtained from Chapter 5. *Table 25* compares the various techniques which were described.

Table 25: Comparison of online fault detection techniques

Techniques	Advantages	Disadvantages
Frequency spectral analysis technique	No set values or benchmark values are required in order to analyse and interpret the earth-brush condition	Intimate/specialised knowledge of shaft-signal analysis and interpretation
	Comprehensive earth-brush fault analytical methodology (i.e. holistic analysis of the shaft voltages/current quantities, current scatter plots and FFT)	Intimate/specialised knowledge fast Fourier Transform (FFT) and shaft current scatter plots
	Effective flowchart with streamlined process for online earth-brush fault detection	
Threshold checking (comparative logics) technique	Provides historical profile of earthing brush performance	Fault detection on a generator depends on extensive expert experience and knowledge
	Effective methodology for brush fault trending and monitoring	Needs initially-set values or benchmark threshold values from a new or correctly-operating generator
		Require periodic information gathering, monitoring and trending
Warning criteria technique	Provide early warning of any developing earth-brush faults	Needs specially-trained observer that understands shaft voltages signal failure profiles system to make sense of the raw data
	Effective methodology for proactive maintenance	Shaft current and voltage benchmark thresholds or initially set parameters are required
		Require periodic information gathering, monitoring and trending

The warning criteria technique offers early warning of developing earth-brush faults but needs a specially-trained observer that understands system failure profiles to interpret/analyse the raw data signals. The warning criteria technique requires online measurement of voltage/current data associated with the condition of the earthing system. Although earthing system raw data are measured online but data analysis and interpretation can only be done offline. This process is ineffective and impractical in most generation plants with a large number of generators operating simultaneously.

The next technique, the threshold checking/comparative logic technique, can identify earth-brush development problems but only when the benchmark threshold values of the measured shaft-signal quantities are initially set for when the generator is in a good operating condition. The major disadvantage about threshold checking is that data analysis and interpretation must be carried out manually and is based on completely expert knowledge. This manual exercise is susceptible to human error and blunders, therefore is not appropriate for critical plant condition monitoring applications. Furthermore, for a large 600 MW turbine generator will generate numerous monitored parameter values, which can overstretch the operators and complicate fault detection.

Frequency spectral analysis technique classifies earth-brush faults types based on characteristic components of shaft voltages/currents. The analysis shows that shaft-signals display certain patterns that correspond to specific types of earth-brush faults. The harmonics given by shaft voltage fast Fourier Transform (FFT) analysis, displayed in Chapter 5, are the characteristic components that enable the identification of the earth-brush fault types. The frequency spectral analysis shaft-signal based technique provides a more comprehensive fault detection approach than others, and it does not depend on any benchmark or initially set values.

The evaluation of the three techniques suggests that the technique using frequency spectral analysis of shaft-signals is best suited for the analysis and interpretation of the earth-brush performance. Based on the analysis and comparisons, evaluation of these techniques indicate that the frequency spectral analysis shaft-signal based technique is the most suitable technique for earth-brush fault condition monitoring it provides a comprehensive analysis of earth-brush performance and does not depend on benchmark values of the measured quantities. Furthermore, this technique offers the operators a simplified flowchart approach that streamlines earth-brush fault detection process.

Chapter 7 Conclusion

7.1 Introduction

This chapter provides a general overview and conclusions of the research presented in this dissertation. A summary of suggested future research projects is also presented.

7.2 Overview and Conclusions

A description of the research problem, utilities' operational experience and background of the historical application of shaft-based signal techniques to diagnose and detect impending earthing brush faults were presented. Section 1.1 in Chapter 1 provided the key research objectives as follows:

- Investigate the effect of good and poor contact earth-brush systems from shaft voltage and current measurements
- Investigate the effect of a lost shaft ground circuit or no earthing continuity on shaft voltage and current measurements
- Investigate the effect of earth-brushes' exposure to oil and dust on shaft voltage and current measurements
- Evaluate an effective online shaft-signal based technique for monitoring the condition of the shaft earthing system
- Developed a method for online Earth-brush fault detection

In particular, the key research objective was to investigate the effects of shaft earthing brush faults from the shaft voltages/currents and evaluate online analysis and interpretation techniques to establish online, *in situ,* the condition of earth-brushes. The experimental generator was a 2-pole, 20 kVA miniature generator, with a data acquisition system and experiments were conducted on this set-up. The signal-processing technique was performed on the measured shaft currents and voltages. It was found that shaft voltages and current characteristics can indicate earth-brush faults. Therefore, it is possible to determine the earth-brush condition from shaft voltage and current measurements provided that baseline information is available.

A change of 20% of the excitation field with worn out brushes produces substantial distortion of the shaft voltage waveform, through the decrease of a 3rd harmonic. A reduced excitation current greatly reduces the shaft voltage. A change of 20% of the excitation field with worn-out produces substantial distortion of the shaft voltage waveform, through the decrease of a 3rd harmonic

A slower rotational speed results in lower shaft voltages. It can be clearly seen that the 5th harmonic decreases significantly for worn out brushes. The harmonics of the shaft voltage show a definite trend for the 3rd, 5th, and 9th harmonics. It can therefore be concluded that a small variation in rotational speed does influence which harmonic is significant in the diagnosis of an earth brush system.

After completion of the experiments in Chapter 5, based on the obtained results, the study further evaluated different analysis and interpretation techniques for shaft earthing system condition monitoring.

The warning criteria technique gives early warning of any developing earth-brush faults. The threshold checking/comparative logic technique identifies developing earth-brush problems but only when the benchmark threshold values of the measured shaft-signal quantities are initially set for the generator when the generator is in a good operating condition.

Spectral analysis technique clearly separates earth-brush faults according to the effect the fault has on the measurable parameters (i.e. shaft currents and voltage quantities, and frequency spectral characteristics). The analysis and interpretation of shaft voltages frequency characteristics lead to practical processing method in Chapter 6 for identifying shaft voltages/currents effects through analysing and interpretation of the frequency spectral components of shaft voltage/current signatures. The frequency spectral analysis technique has yielded significant information regarding the interpretation of the earth-brush condition with regards to the spectral frequency/harmonic content of the measured signals. This technique provided a clearer understanding on the interpretation of in situ earth-brush performance. This technique would provide a great insight into how earth-brush condition monitoring schemes should be applied and further improves the utility global condition monitoring system on earth-brushes.

7.3 Recommendation for Future Research Work

The research study evaluated online techniques for classifying faults based on data from shaft signals and further investigated the effects of earthing brush performance from shaft voltages/currents characteristics. Completion of this research revealed areas that need to be further research in the future. The following are recommended future research in the field of generator shaft earthing system faults detection and condition monitoring:

- Possible other faults that could possibly be introduced to the machine includes earth-brush holder misalignment and earth-brush arcing effects on the shaft voltage and currents.
- Asymmetries such as distorted rotor static or dynamic eccentricity, and joints between segmental laminations have significant effects on the shaft voltage. It is recommended that future work, where these faults are induced in the generator at different earth brush fault conditions, will produce positive results in terms of being able to distinctively identify the earth brush fault condition.
- Conduct the same experiment to evaluate performance of earth brushes after removing most practical machine features (that is no shaft key-ways, damper bars, and weld recesses) which affects the shaft voltage harmonics. What effect do the existence of these features have on the shaft voltage?
- Many variations of rotor or stator single and double earth faults should be investigated in future to test for earth brush performance for the identification of earth brush faults. It is recommended that future work, where these faults are induced in the generator at different earth brush fault conditions.
- Variation in the number of the rotor or stator slots which can occur in a synchronous machine and their effect on the shaft voltage can be analysed and quantified. What effect does a reduced number of stator slots have on the shaft voltage? Which harmonic is significant in the diagnosis of an earth brush fault evaluation?
- Perform these measurements on a running Eskom power plant turbine generator.

References

[1] B.M Ziemianek, "Steam turbine generator shaft grounding," Lehigh University, Bethlehem, United State, 1985.

[2] P.I Nippes and J.S Sohre, "Electromagnetic Shaft Currents and Demagnetization of Rotors of Turbines and Compressors," in *7th Turbomachinery Symposium*, Texas A&M University, 1978.

[3] G. Stone, B Lloyd, and M. Sasic, "Monitoring of Shaft Voltages and Grounding Currents in Rotating Machines," in *17th International Conference Electrical Machine Systems*, Hangzhou, Zhejiang University, 2014.

[4] S.J. Hoffe, "Synchronous Generator Fault Diagnosis using Shaft Signal Measurements," University of Witwatersrand, Johannesburg, South Africa , 2006.

[5] D. De Canha, "The Analysis of Shaft Voltages in a Synchronous Generator with Various Induced Faults," University of Witwatersrand, Johannesburg, South Africa, 2012.

[6] W. Doorsamy, "Processing and Inferential Methods to Improve Shaft-voltage-based Condition Monitoring of Synchronous Generators," University of Witwatersrand, Johannesburg, South Africa, 2015.

[7] P.I Nippes, P.E Elizabeth, and S. Galano, "Understanding Shaft Voltage and Ground Currents of Turbine Generators," Gaussbusters, 10 Feb. 2018. [Online]. Available: www.gaussbusters.com. [Accessed 5 Oct. 2020].

[8] J. S. Sohre, "Shaft Riding Brushes to Control Electric Stray Currents," in *20th Turbomachinery Symposium*, College Station, Texas, A&M University, 1991.

[9] S. Higgins, "Rotating Machine Shaft Signal Monitoring Method and System". United States of America Patent 2011/0313701 A1, 3 Dec. 2011.

[10] E.D Thompson, "Shaft Ground Monitoring with Diagnostic Waveform Analysis". United States of America Patent WO 2017/176401 A1, 20 Oct. 2017.

[11] P.I Nippes, "Shaft Voltage Current Monitoring System for Early Warning and Problem Detection". United States of America Patent 6,460,013, 15 Oct. 2002.

[12] Z. Posedel, "Arrangement for Reducing Shaft Voltage in Dynamoelectric Machines". United States of America Patent 4,831,295, 22 May 1989.

[13] W. Doorsamy, and W. Cronje, "Optimisation of shaft voltage based condition monitoring in generators using a Bayesian approach," in *IEEE International Conference* , Cape Town, South Africa, 2013.

[14] P.I Nippes, “Early Warning of Developing Problems in Rotating Machinery as Provided by Monitoring Shaft Voltages and Grounding Currents,” *IEEE Transactions on Energy Conversion,* vol. 19, no. 12, pp. 340-345, 2004.

[15] V.S Hameed, K.M Shameer, “Proactive condition Monitoring Systems for Power Plants,” *International Journal of Scientific and Research Publications,* vol. 3, no. 11, pp. 71-79, 2013.

[16] M. Costello, “Shaft Voltages and Rotating Machinery,” *IEEE Transaction on Industry Applications,* vol. 29, no. 2, pp. 419-426, 1993.

[17] S. D. Lange, “Management of Shaft Earthing Guideline and Related Issues Works Instruction,” Eskom Holdings, Johannesburg, South Africa, 2017.

[18] T. Plazenet, “A Comprehensive Study on Shaft Voltages and Bearing Currents in Rotating Machines,” *IEEE Transactions on Industry Applications,* vol. 54, no. 4, pp. 72-77, 2018.

[19] W. KeSheng, “Vibration Monitoring on electrical machine using Vold-Kalman Filter Order Tracking,” Unversity of Pretoria, Pretoria, South Africa, 2008.

[20] R.C Miller, and M. Twerdochlib, “Core Monitor that uses Rotor Shaft Voltages”. United States of America Patent 5032826, 20 Jul 1991.

[21] K.J Raymond, and K.J Ong, “An investigation of Shaft Current in a Large Sleeve Bearing Induction Machine,” McMaster University, Hamilton, Ontario, Canada, 1999.

[22] P. Nippes, “Early Warning and Problem Detection in Rotating Machinery By Monitoring Shaft Voltage and/or Grounding Current”. United States of America Patent 7,034,709 B1, 25 Apr. 2006.

[23] S. Higgins, “Shaft Voltage and Current Monitoring Guideline,” Eskom Holdings, Johannesburg, South Africa, 2012.

[24] T. Khan, “circuitglobe,” Electronic Instrumentation, 4 Dec. 2019. [Online]. Available: www.circuitglobe.com. [Accessed 2/11/2020].

[25] C. Ammann, K. Reichert, R. Joho, Z. Posedel, “Shaft Voltages in Generators with Static Excitation Systems - Problems and Solutions,” in *IEEE Transactions on Energy Conversion*, Massachusetts, United State, 1998.

[26] IEEE, “IEEE Standard Test Procedure for Polyphase Induction Motors and Generators,” in *112-2017* , United States, 2018.

[27] R. Ong, J.H Dymond, and R.D Findlay, “Comparison of techniques of measuring shaft voltages in rotating machines,” *IEEE Transactions on Energy Conversion (Volume: 12, Issue: 4, Dec 1997) ,* vol. 12, no. 4, pp. 363 - 367, 1997.

[28] D. Pengra, “Data Analysis and Experimental Uncertainty,” Unversity of Washington, Seattle, Washington, 2009.

[29] G.W Buckley, and R.J Corkins, "Importance of Grounding Brushes to the Safe Operation of Large Turbine Generators," in *IEEE Transactions on Energy Conversion*, Emilia, Italy, 1988.

Appendix A, Shaft voltage brush harmonics chart history

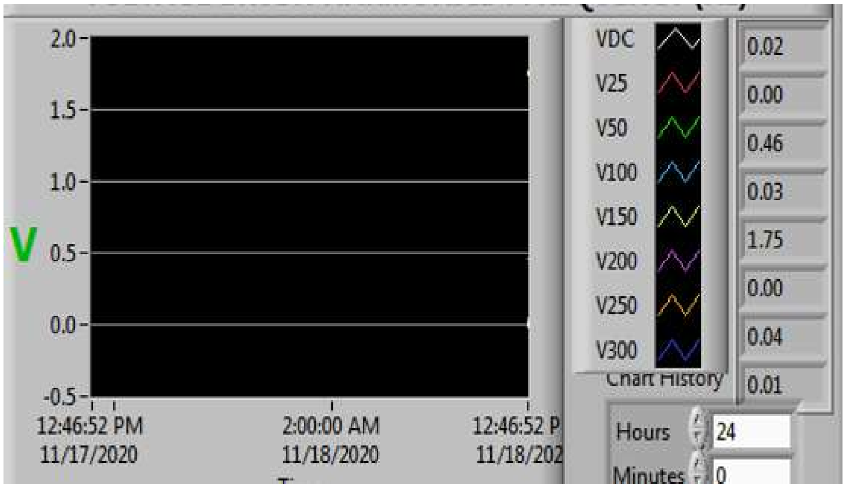

Figure 79: Voltage Brush Harmonics (Hz) Chart history for Test # 1

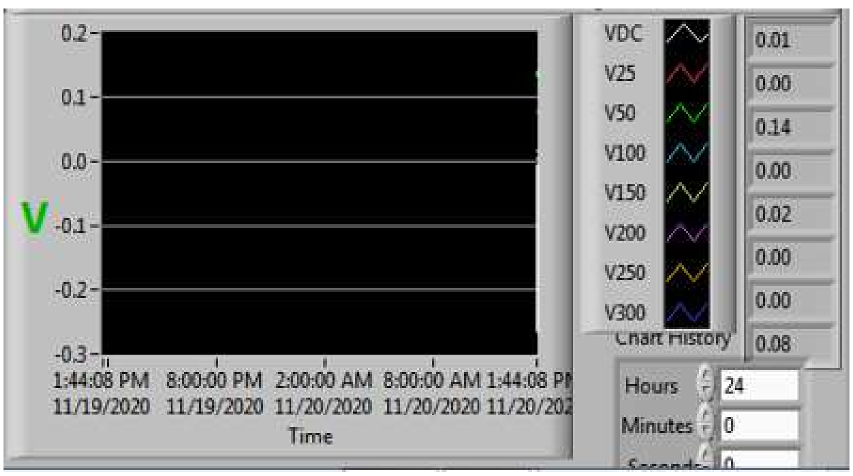

Figure 80: Voltage Brush Harmonics (Hz) Chart history for Test # 2

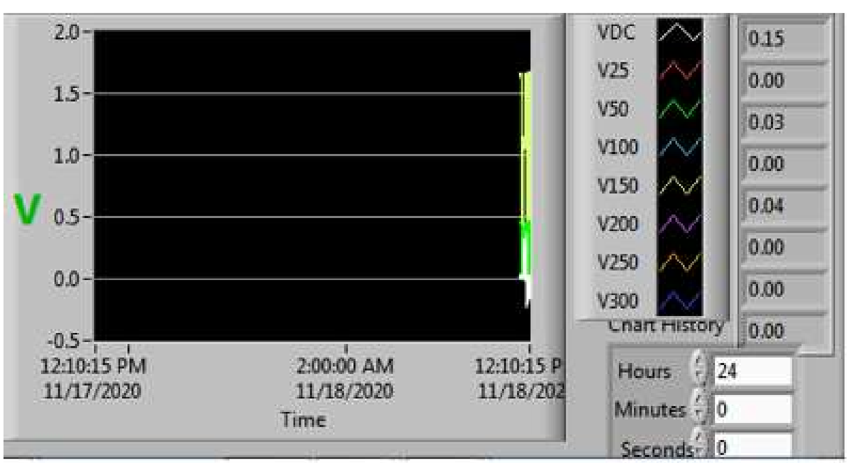

Figure 81: Voltage Brush Harmonics (Hz) Chart history for Test # 3

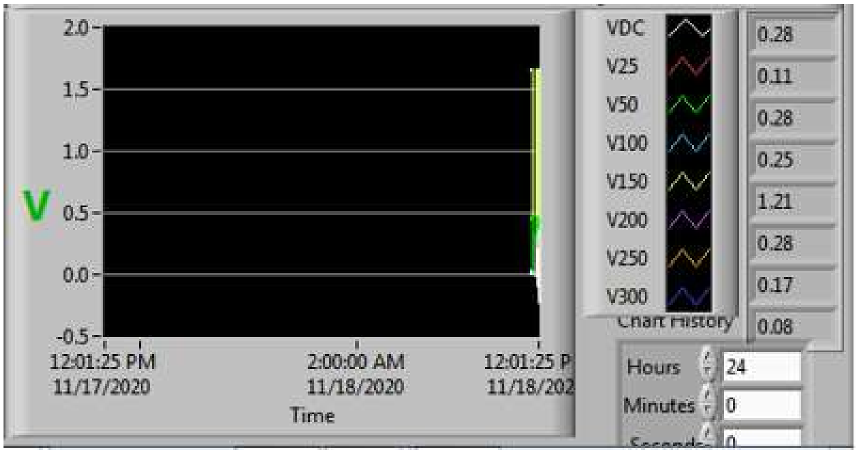

Figure 82: Voltage Brush Harmonics (Hz) Chart history for Test # 4

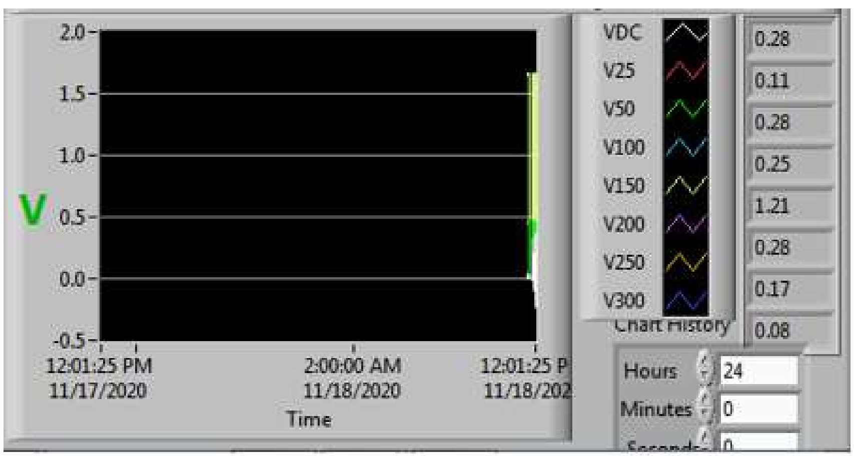

Figure 83: Voltage Brush Harmonics (Hz) Chart history for Test # 5

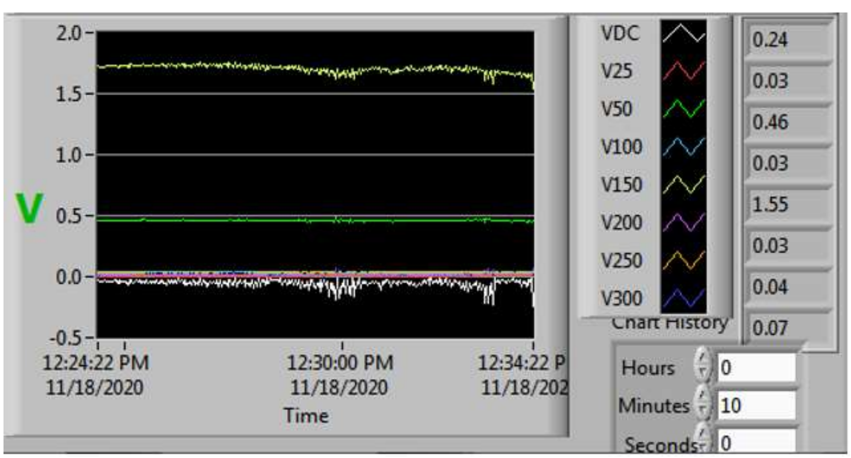

Figure 84: Voltage Brush Harmonics (Hz) Chart history for Test # 6

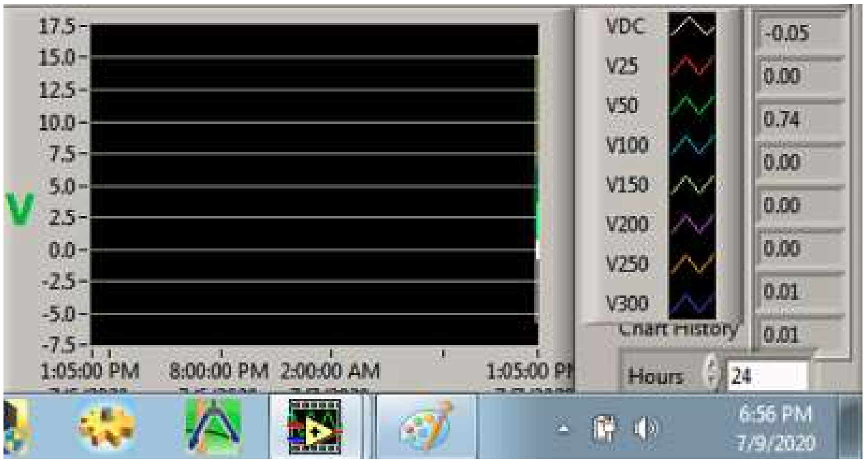

Figure 85: Voltage Brush Harmonics (Hz) Chart history at 60 A excitation with no earth brush continuity

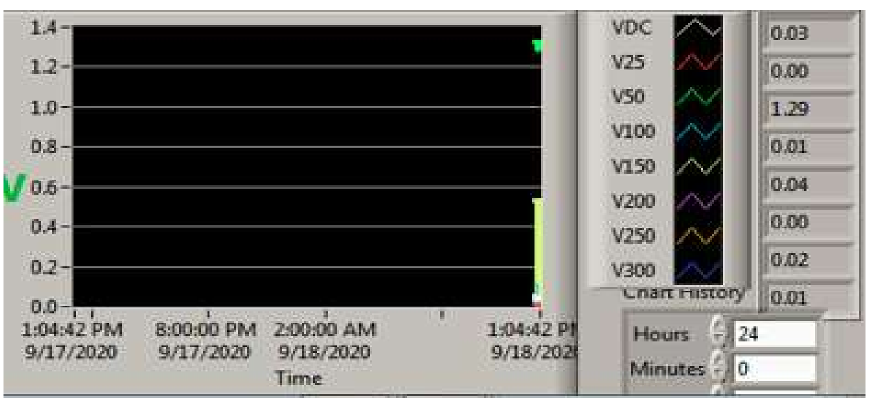

Figure 86: Voltage Brush Harmonics (Hz) Chart history at 40 A excitation with no earth brush continuity

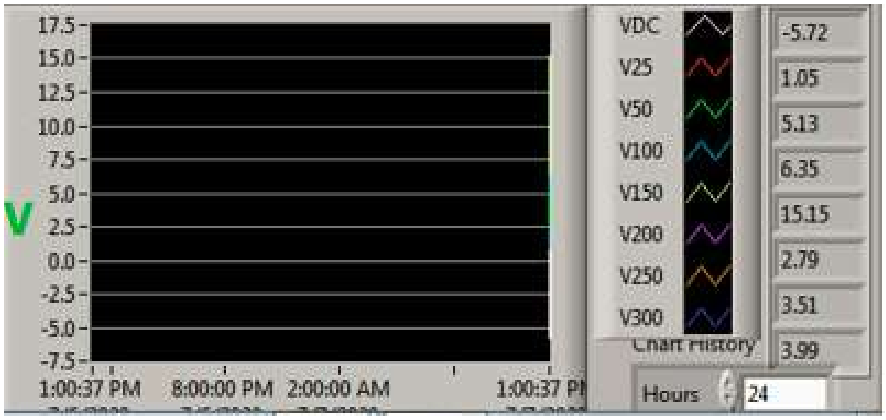

Figure 87: Voltage Brush Harmonics (Hz) Chart history at 60 A excitation with worn out brushes

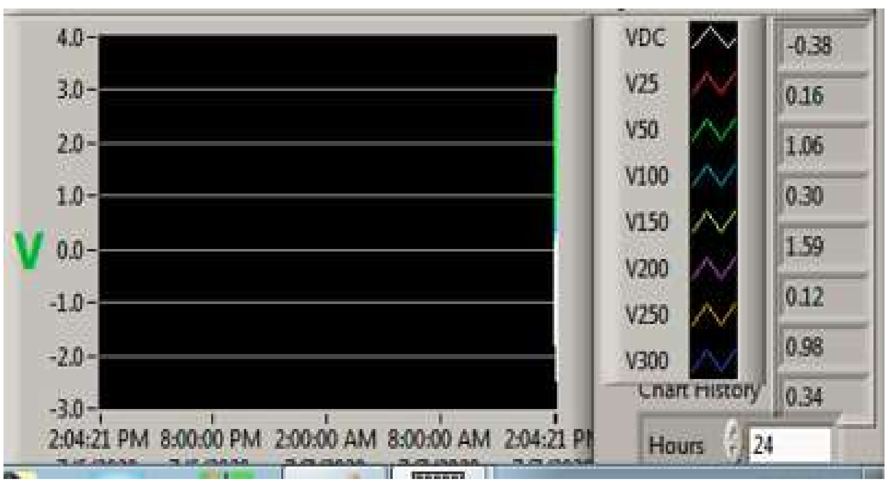

Figure 88: Voltage Brush Harmonics (Hz) Chart history at 40 A excitation with worn out brushes

Figure 89: Voltage Brush Harmonics (Hz) Chart history at 60 A excitation with brushes exposed to dust and oil

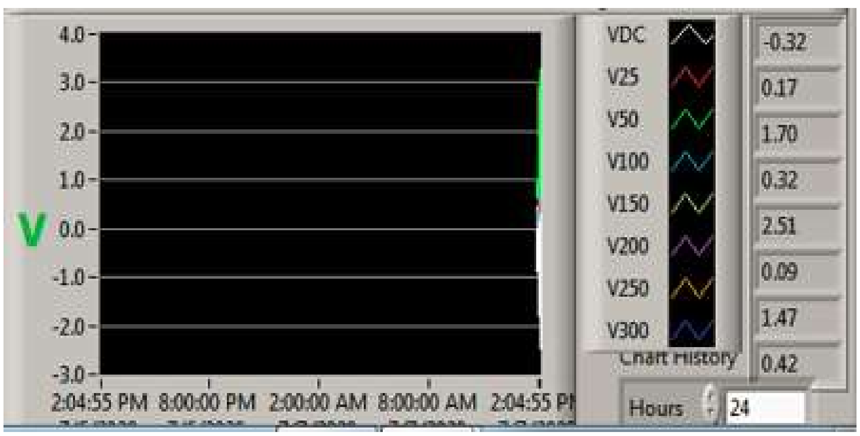

Figure 90: Voltage Brush Harmonics (Hz) Chart history at 40 A excitation with brushes exposed to dust and oil

Figures 91– 96 shows comparison plot of current brush scatter plot (A) for different excitation currents with different earth brush fault conditions

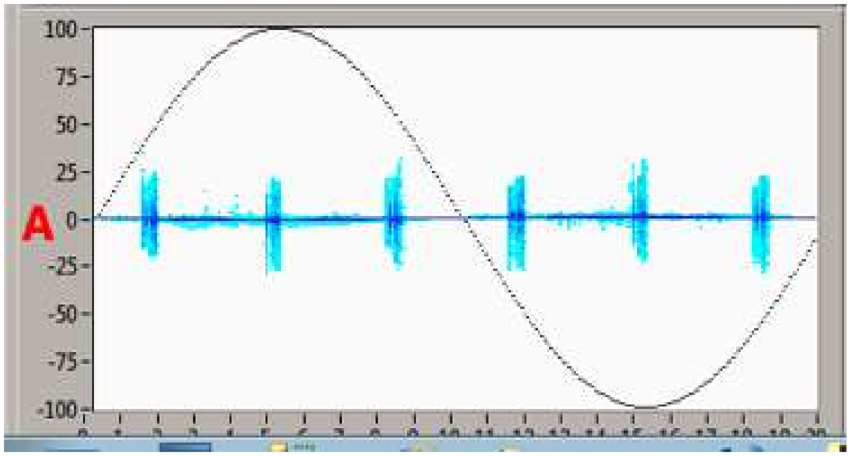

Figure 91: Current brush scatter plot (A) at 60 A excitation with no earth brush continuity

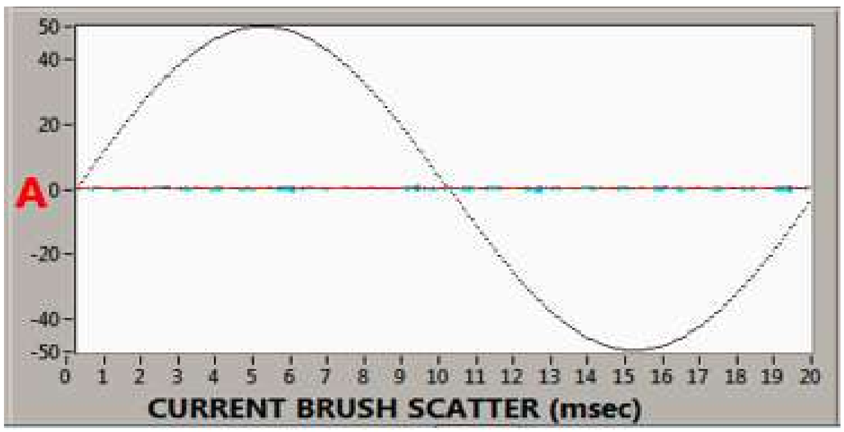

Figure 92: Current brush scatter plot (A) at 40 A excitation with no earth brush continuity

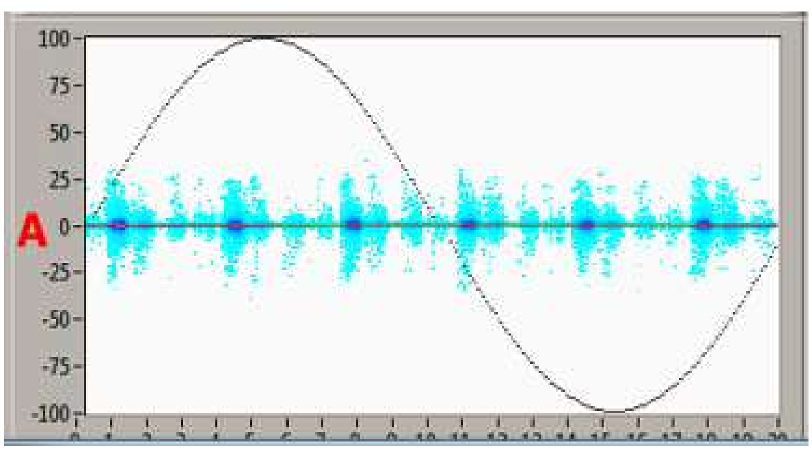

Figure 93: Current brush scatter plot (A) at 60 A excitation with worn out brushes

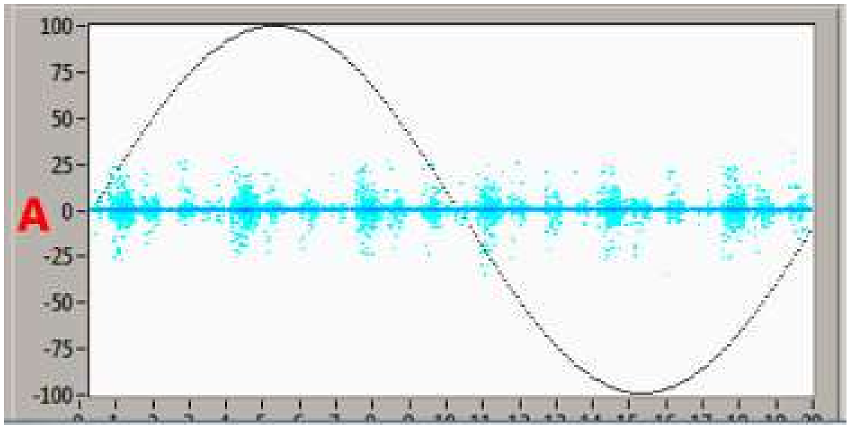

Figure 94: Current brush scatter plot (A) at 40 A excitation with worn out brushes

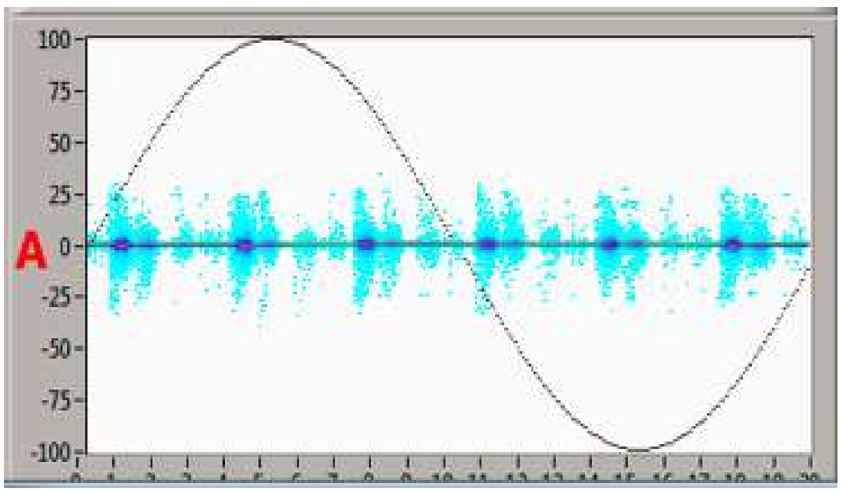

Figure 95: Current brush scatter plot (A) at 60 A excitation with brushes exposed to dust and oil

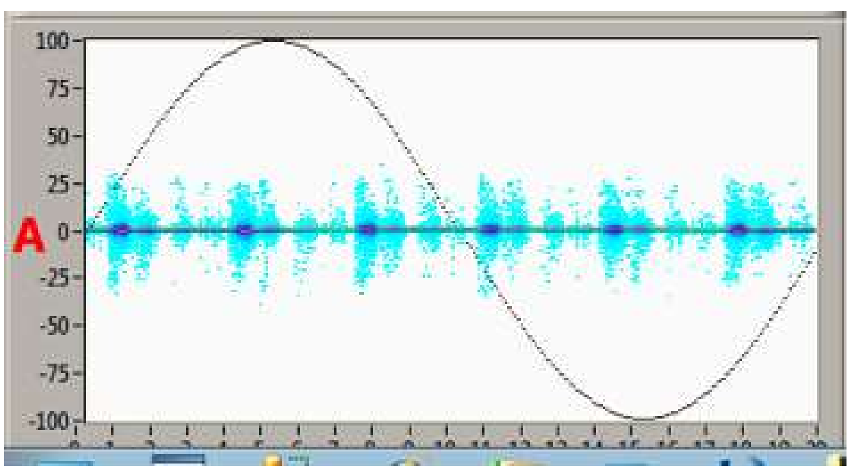

Figure 96: Current brush scatter plot (A) at 40 A excitation with brushes exposed to dust and oil

Appendix B, Testing equipment datasheet

PicoScope®
4000 Series

High-Resolution PC Oscilloscopes

Detailed waveform capture from Pico Technology

- 12-bit resolution
- 80 MS/s real-time sampling rate
- USB 2.0 interface for data and power
- 32 M sample buffer size
- Up to 4 channels

Oscilloscope

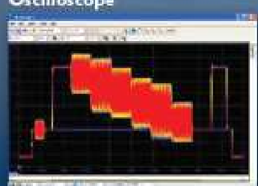

Zoomed scope views

Spectrum analyser

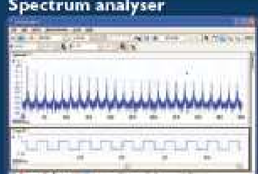

All-in-one instruments

The PicoScope 4000 Series PC Oscilloscopes are extremely versatile, with an oscilloscope and spectrum analyser included in every model.

Convenience and speed

The PicoScope 4000 Series scopes obtain their power from the USB 2.0 interface, so there's no need for an external power supply. The USB port also delivers high-speed data to your PC to give you a responsive, high-resolution display. With 80 MS/s sampling, the 4000 Series scopes are the fastest USB-powered 12-bit scopes around.

Deep memory

The 32 M sample buffer is 'always on'. There is never a compromise between buffer size and waveform update rate, because the PicoScope 4000 Series always maximises both at the same time. Now you can capture every waveform with full detail without having to think about it.

Advanced software

The scopes are bundled with the latest version of PicoScope for Windows. PicoScope is easy to use and can export data in a variety of graphical, text and binary formats. Also included are Windows and Linux drivers and example programs.

www.picotech.com

	PicoScope 4424	PicoScope 4224
Channels (vertical)		
Number of channels	4	2
Bandwidth	20 MHz (10 MHz on ±50 mV range)	
Sensitivity	10 mV/div to 20 V/div	
Full-scale ranges	±50 mV to ±100 V	
DC accuracy	1% of full scale	
Nominal input impedance	1 MΩ || 22 pF	
Overload protection	±200 V	
Input coupling	AC or DC, software-controlled	
Input connectors	4 x BNC	2 x BNC
Timebase (horizontal)		
Timebases	100 ns/div to 200 s/div	
Timebase accuracy	50 ppm	
Timebase jitter	≤ 10 ps	
Trigger		
Trigger sources	Any input channel	
Modes	Auto, repeat, single, none	
Types	Rising edge, falling edge, edge with hysteresis, pulse width, runt pulse, dropout, windowed	
Acquisition		
ADC resolution	12 bits (up to 16 bits with resolution enhancement)	
Software filtering	User-adjustable cut-off frequency and on/off control	
Sampling rate	80 MS/s, 1 or 2 channels 20 MS/s, 3 or 4 channels	80 MS/s
Buffer size	32 M samples shared between active channels	
Number of waveform segments in buffer	Adjustable from 1 to 1000	
Display		
Display styles	Real-time, digital colour, analogue intensity	
Measurements and analysis		
Rulers	2 per channel on Y axis + 2 on X axis	
Automatic measurements	26 automatic measurements in time and frequency domains	
Channel maths	Invert, add, subtract, multiply, divide, advanced equations	
FFT	Spectrum view with up to 1 M points	
General		
Operating temperature range	+0 °C to +45 °C (+15 °C to +40 °C for quoted accuracy)	
Power	Powered from USB port: 5 V @ 500 mA max.	
PC connection	USB 2.0	
PC requirements	Microsoft Windows XP (SP2) or Vista, 32-bit versions only	
Dimensions	200 mm x 140 mm x 35 mm	
Weight	< 500 g	
Approvals	FCC (EMC), CE (EMC, LVD), RoHS	

Data Sheet

Dual Channel Function/Arbitrary Waveform Generators
4050B Series

The 4050B Series Dual Channel Function/ Arbitrary Waveform Generators are capable of generating stable and precise sine, square, triangle, pulse, and arbitrary waveforms. With an easy-to-read color display and intuitive user interface with numeric keypad, these instruments offer plenty of features including linear/logarithmic sweep, built-in counter, extensive modulation and triggering capabilities, a continuously variable DC offset, and a high performance 14-bit, 150 MSa/s arbitrary waveform generator. CH1 and CH2 outputs can both be varied from 0 to 10 Vpp into 50 ohms (up to 20 Vpp into open circuit).

Easily create custom arbitrary waveforms using the included waveform editing software or use any of the 196 built-in predefined arbitrary waveforms. More than 1000 user-defined 16k point arbitrary waveforms can be saved to the instrument. Additionally, the included LabVIEW™ drivers allow users to conveniently load and save .csv or .txt file data directly into the arb memory without having to use waveform editing software.

Extensive modulation capabilities include amplitude and frequency modulation (AM/FM), double sideband amplitude modulation (DSB AM), amplitude and frequency shift keying (ASK/ FSK), phase modulation (PM), phase shift keying (PSK), and pulse width modulation (PWM).

The standard external 10 MHz reference clock input and output allows users to synchronize their instrument with another generator. Additionally, the generators offer powerful channel copy, track and combine functionality and the phase of both output channels can be synchronized conveniently with the push of a button. These handy features are typically not found in function generators at this price point.

These versatile function/arbitrary waveform generators are suitable for education and other applications that require high signal fidelity, a variety of modulation schemes, or arbitrary waveform generation capabilities.

Model	4053B	4054B	4056B
Sine and square frequency range	1 μHz – 10 MHz	1 μHz – 30 MHz	1 μHz – 60 MHz

Features & Benefits

- 14-bit, 150 MSa/s, 16k point arbitrary waveform generator
- Two independent channels with individual output On/Off buttons
- Convenient channel copy, track and combine functions
- Synchronize the phase of both channels with the push of a button
- Low-jitter square wave generation for simulating reliable clock signals, generating triggers, or validating serial data buses
- Large 4.3-inch LCD color display
- Linear and logarithmic sweep
- AM/DSB-AM/ASK/FM/FSK/PM/PSK/PWM modulation functions
- Variable DC offset
- Adjustable duty cycle
- Internal/external triggering
- Gate and burst mode
- 196 built-in predefined arbitrary waveforms
- Flash memory size of approximately 100 MB allows for storage/recall of >1000 instrument settings and user-defined arbitrary waveforms
- Built-in frequency counter
- Harmonics generator function
- LAN, USB device port (USBTMC-compliant), and front panel USB host port
- GPIB connectivity with optional USB-to-GPIB adapter
- PC software provided for arbitrary waveform editing
- Short circuit output protection

Technical data subject to change
© B&K Precision Corp. 2017

www.bkprecision.com

BK PRECISION
ELECTRONIC TEST INSTRUMENTS

Front panel

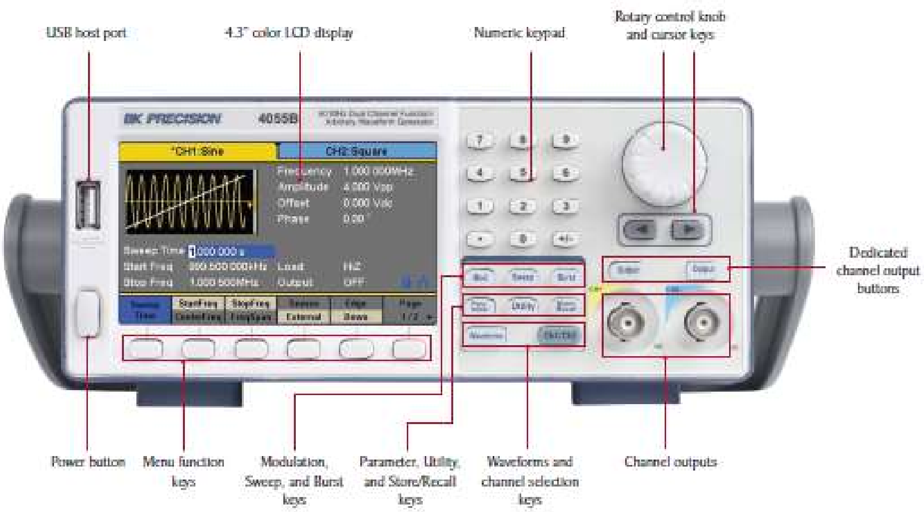

Intuitive user interface

Easily adjust all waveform parameters using the intuitive menu-driven front panel keypad with dedicated channel selection keys, numeric keypad, and rotary control knob. Connect your USB flash drive to the USB host port to quickly save and recall instrument settings and waveforms.

Rear panel

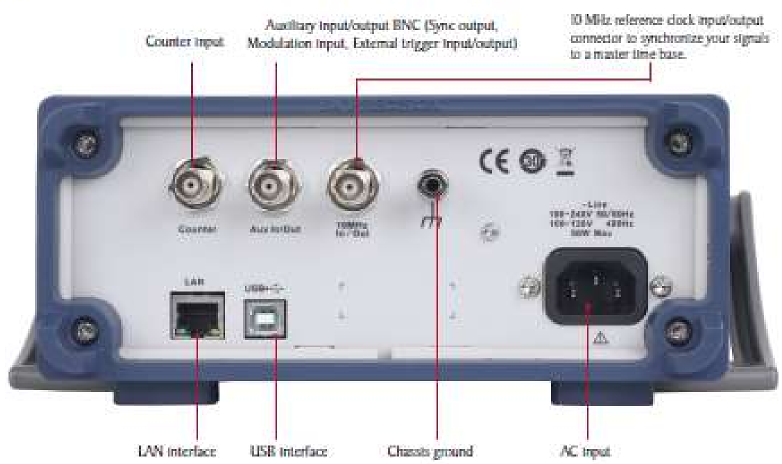

Flexible operation

Channel copy and sync function

Save time with the 4050B Series' two independent channels to output synchronous signals. With a push of a button, all waveform parameters can be quickly copied between channels to set up identical output signals. Phase between channels can also be adjusted from the front panel.

Channel tracking function

Customize your generator's channel output configuration with frequency, amplitude, and phase coupling. When enabled, CH1 and CH2 can automatically track according to the user's set frequency, amplitude, and phase deviation ratio between channels.

Channel combine function

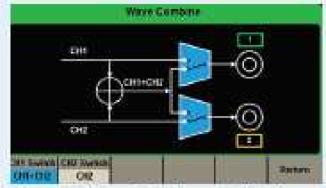

Create complex waveforms by internally adding each channel's waveform and outputting the combined waveform on channel 1 or 2.

Harmonics function

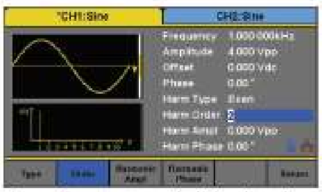

Generate harmonics up to the 10th order with independent amplitude and phase settings.

Generate arbitrary waveforms with ease

The 4050B Series features a large, non-volatile flash memory of about 100 MB, allowing users to create, store, and recall >1000 user-defined 16k point arbitrary waveforms or output any of the 196 built-in predefined arbitrary waveforms.

The provided waveform editing software can be used to create point-by-point arbitrary waveforms via freehand or waveform math functions. A standard USB interface on the rear panel allows users to easily interface with a PC to load these arbitrary waveforms into the instrument. The front panel also offers a convenient USB host port for connecting your USB flash drive to save/recall instrument settings and waveforms.

Advanced square and pulse generator

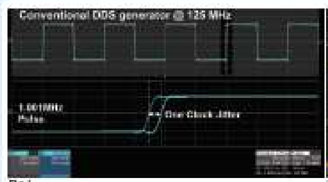

Fig 1

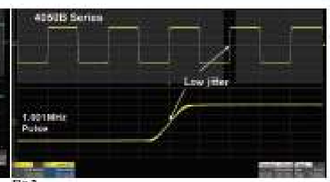

Fig 2

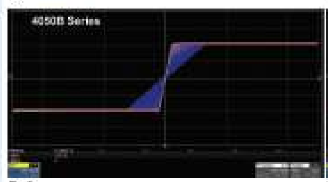

Fig 3

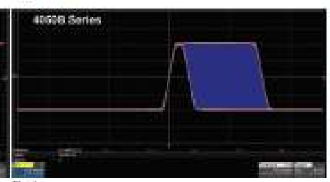

Fig 4

For applications requiring high signal integrity and edge stability, the 4050B Series can produce low jitter pulse waveforms (Fig 2) compared to conventional DDS generators (Fig 1). The instrument can also generate pulses with minimum rise/fall times of 16.8 ns (Fig 3), minimum pulse width of 32 ns (Fig 4) and maximum rise/fall times of 22.4 seconds.

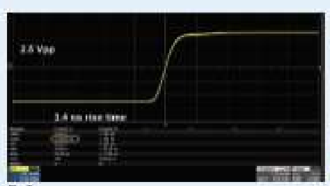

Fig 5

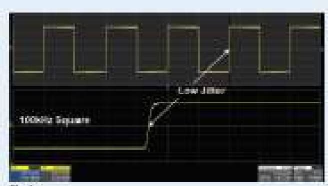

Fig 6

Generate high performance square waves with < 3.4 ns rise/fall times (Fig 5) and rms jitter < 300ps + 0.05 ppm of period (Fig 6)

Specifications

Model	4053B	4054B	4055B
Channels	2		
Frequency Characteristics			
Sine & Square	1 μHz – 10 MHz	1 μHz – 30 MHz	1 μHz – 60 MHz
Triangle, Ramp	1 μHz – 300 kHz		
Pulse	1 μHz – 12.5 MHz		
Noise (-3 dB)	> 60 MHz		
Arbitrary	1 μHz – 6 MHz		
Accuracy	± 25 ppm (1 year)		
Resolution	1 μHz		
Arbitrary Characteristics			
Built-in Waveforms	196 built-in waveforms (includes DC)		
Waveform Length	16k points / Ch		
Vertical Resolution	14 bits		
Sampling Rate	150 MSa/s		
Minimum Rise/Fall Time	6.5 ns (typical)		
Jitter (pk-pk)	8 ns (typical)		
Non-volatile Memory Storage	> 1000 16k points waveforms (100 MB in file system)		
Output Characteristics			
Amplitude Range	2 mVpp – 10 Vpp into 50 Ω (4 mVpp – 20 Vpp into open circuit), ≤ 10 MHz 2 mVpp – 5 Vpp into 50 Ω (4 mVpp – 10 Vpp into open circuit), > 10 MHz		
Amplitude Resolution	up to 4 digits		
Amplitude Accuracy (10 kHz)	± (1 % + 1 mVpp)		
Amplitude Flatness	± 0.3 dB (reference 10 kHz, 2.5 Vpp, 50 Ω load)		
Cross Talk	< -60 dBc (both channels set to 0 dBm, sine 50 Ω load)		
Offset Range (DC)	± 5 V into 50 Ω (± 10 V into open circuit)		
Offset Resolution	up to 4 digits		
Offset Accuracy	± (|offset setting value| x 1% + 3 mV)		
Channel Output Impedance	50 Ω, high impedance		
Output Protection	short-circuit protection		
Waveform Characteristics (sine, square, triangle, ramp)			
Harmonic Distortion (Sine)	DC – 10 MHz, < - 60 dBc / 10 MHz – 30 MHz < -50 dBc / 30 MHz – 60 MHz, < - 40 dBc (0 dBm input signal)		
Total Harmonic Distortion (Sine)	10 Hz – 20 kHz at 0 dBm, < 0.075%		
Spurious (non-harmonic)	DC – 10 MHz, < -65 dBc / 10 MHz – 30 MHz, < -55 / 30 MHz – 60 MHz, < -40 (0 dBm input signal)		
Rise/Fall Time (square)	< 4.2 ns (10 % – 90 %, at 1Vpp into 50 Ω)		
Variable Duty Cycle (square)	0.001% - 99.999% (depending on frequency setting)		
Asymmetry (50% duty cycle)	1% of period + 20 ns (typical,1 kHz, 1 Vpp)		
Jitter (rms) cycle to cycle (square)	300 ps + 0.00 ppm of period (typical, 1 kHz, 1 Vpp)		
Ramp Symmetry	0% – 100%		
Linearity (triangle, ramp at 1 kHz, 1 Vpp, 100% symmetry)	< 1% of peak output (typical)		

Model	4053B, 4054B & 4055B
Pulse	
Pulse Width	32.6 ns minimum, 100 ps resolution, 1,000,000 s max.
Rise/Fall Time	16.8 ns (1 Vpp, 50 10% – 90% 50 Ω load)
Duty Cycle	0.001% resolution
Overshoot	< 3 % (100 kHz, 1 Vpp)
Jitter (rms) cycle to cycle	300 ps + 0.05 ppm of period (typical, 1 kHz, 1 Vpp)
Burst	
Waveform	ine, square, ramp, pulse, arbitrary, noise
Type	cycle (1-1000000 cycles), infinite, gated
Start/Stop Phase	0 ° – 360 °
Internal Period	1 µs – 1000 s
Gated Source	internal, external trigger
Trigger Source	internal, external, manual
Phase Offset	
Range	0 ° – 360 °
Resolution	0.1 °
AM, FM & PM Modulation Characteristics	
Carrier	sine, square, ramp, arbitrary (except DC)
Source	internal, external
Internal Modulation Waveform	sine, square, ramp, noise, arbitrary (1 mHz – 20 kHz)
AM Modulation Depth	0% – 120%, 0.1% resolution
FM Frequency Deviation	0 – 0.5*bandwidth, 10 µHz resolution
PM Phase Deviation	0 – 360 °, 0.1 ° resolution
ASK & FSK Modulation Characteristics	
Carrier	sine, square, ramp, arbitrary (except DC)
Source	internal, external
Modulation Waveform	50% duty cycle square waveform (1 mHz – 50 kHz)
PWM Modulation Characteristics	
Source	internal, external
Modulation Waveform	sine, square, ramp, arbitrary (except DC)
Internal Modulation Frequency	1 mHz – 20 kHz
DSB-AM Modulation Characteristics	
Carrier	sine, square, ramp, arbitrary (except DC)
Source	internal, external
Modulation Waveform	sine, square, ramp, noise, arbitrary (1 mHz – 20 kHz)
Sweep Characteristics	
Waveforms	sine, square, ramp, arbitrary (except DC)
Sweep Shape	linear or logarithmic, up or down
Sweep Time	1 ms – 500 s
Sweep Trigger	internal, external, manual

Auxiliary Input / Output	
Modulation Input	±6 Vpp (typical) for 100% modulation Maximum input voltage: 7 V Input impedance: 10 kΩ
Sync and Trigger Out	TTL compatible *1) Output impedance 100 Ω Maximum frequency: 1 MHz Minimum pulse width: 500 ns
Trigger In	TTL compatible *2) Input impedance: 10 kΩ Minimum pulse width: 100 ns Response time 100 ns (max) in sweep mode and 600 ns (max) in burst mode
Reference Clock	
Input	Frequency Range: 10 MHz ± 1 kHz (typical) Min. Voltage Input: 1.4 V 5 kΩ input impedance
Output	Frequency Range: 10 MHz ± 25 ppm (typical) Voltage Level: 3.3 V (typical), 2 V (minimum) 50 Ω output impedance
Frequency Counter	
Measurement	frequency, period, duty cycle, positive/negative pulse width
Measurement Range	100 mHz – 200 MHz (DC coupling) 10 Hz – 200 MHz (AC coupling)
Input Range	100 mV to ± 2.5 V (< 100 MHz, DC coupling) 200 mV to ± 2.5 V (100 MHz – 200 MHz, DC coupling) 100 mV to 5 V (< 100 MHz, AC coupling) 200 mV to 5 V (100 MHz – 200 MHz, AC coupling)
Input Impedance	1 MΩ
Coupling	AC, DC, HF, REJ
Environmental and Safety	
Temperature	operating: 32 °F – 104 °F (0 °C – 40 °C) storage: -4 °F – 140 °F (-20 °C – 60 °C)
Humidity	< 86° F (30 °C), ≤ 90 % RH 104 °F (40 °C), ≤ 50 % RH
Altitude	operating: below 9,842 ft (3,000 m) storage: below 49,212 ft (15,000 m)
Electromagnetic Compatibility	EMC Directive 2004/108/EC, EN61326:2006, EN61000-3-2:2006+A2:2009, EN61000-3-3:2008
Safety	Low voltage directive 2006/95/EC, EN61010-1:2001, EN61010-031:2002+A1:2008
General	
Display	4.3" TFT-LCD display, 480 x 272
Interfaces	LAN & USBTMC (standard), GPIB (optional), USB host port
Storage Memory	Arbitrary waveforms and instrument settings share the same non-volatile storage memory of 100 MB.
Power	100 – 240 VAC ± 10%, 50 / 60 Hz 100 – 120 VAC ± 10%, 400 Hz
Power Consumption	50 W max.
Dimensions (W x H x D)	261 x 96 x 295 mm (10.3" x 3.78" x 11.6")
Weight	3.32 kg (7.32 lbs)
	Three-Year Warranty
Standard Accessories	Getting started manual, instruction manual (downloadable), AC power cord, USB type A-to-type B cable, certificate of calibration
Optional Accessories	USB-to-GPIB adapter (model AK40G)

1*) V_{OH} = 3.8 V (I_{OH} = -8 mA), V_{OL} = 0.44 V (I_{OL} = 8 mA)
2*) V_{IH}= 2 V (min) / 5.5 V (max), V_{IL}= -0.5V (min) / 0.8 V (max)

Appendix C: Mini Generator Drawings

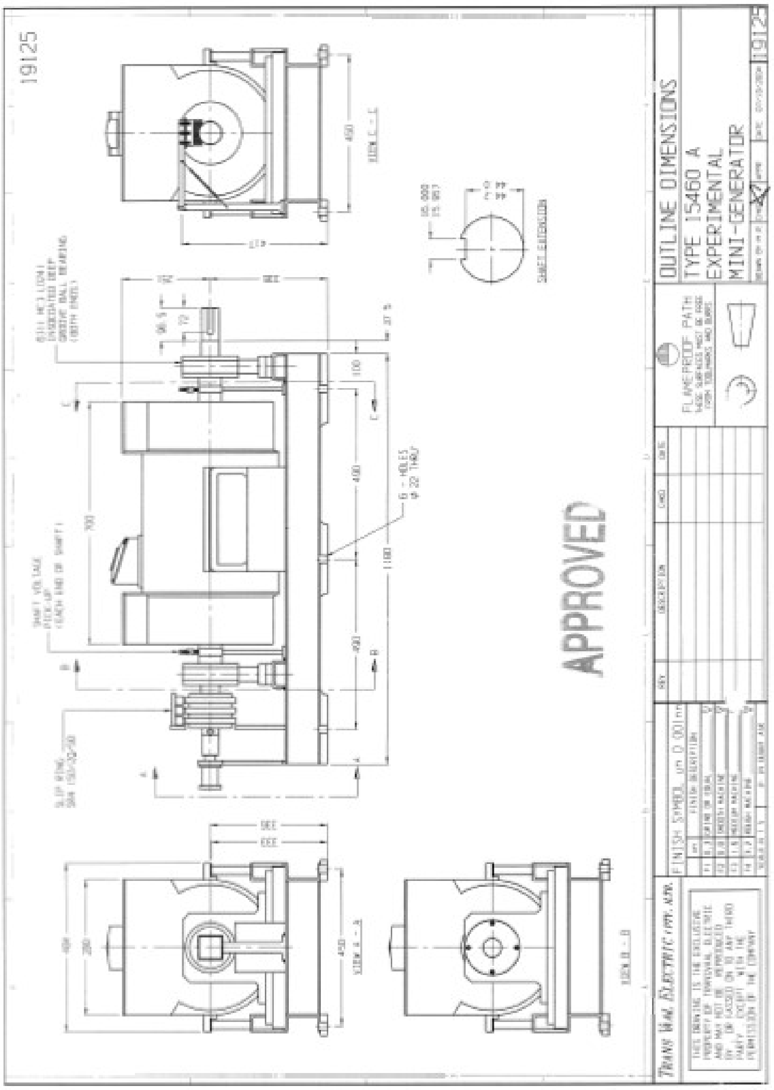

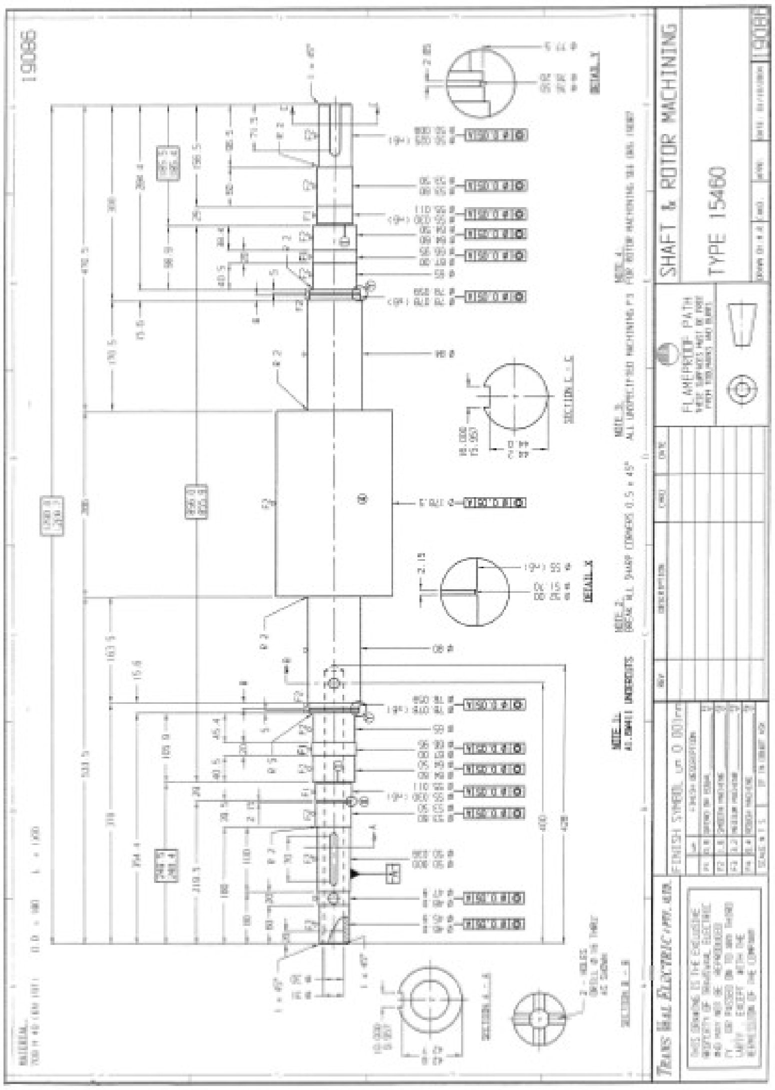
SHAFT & ROTOR MACHINING
TYPE 15460
19086

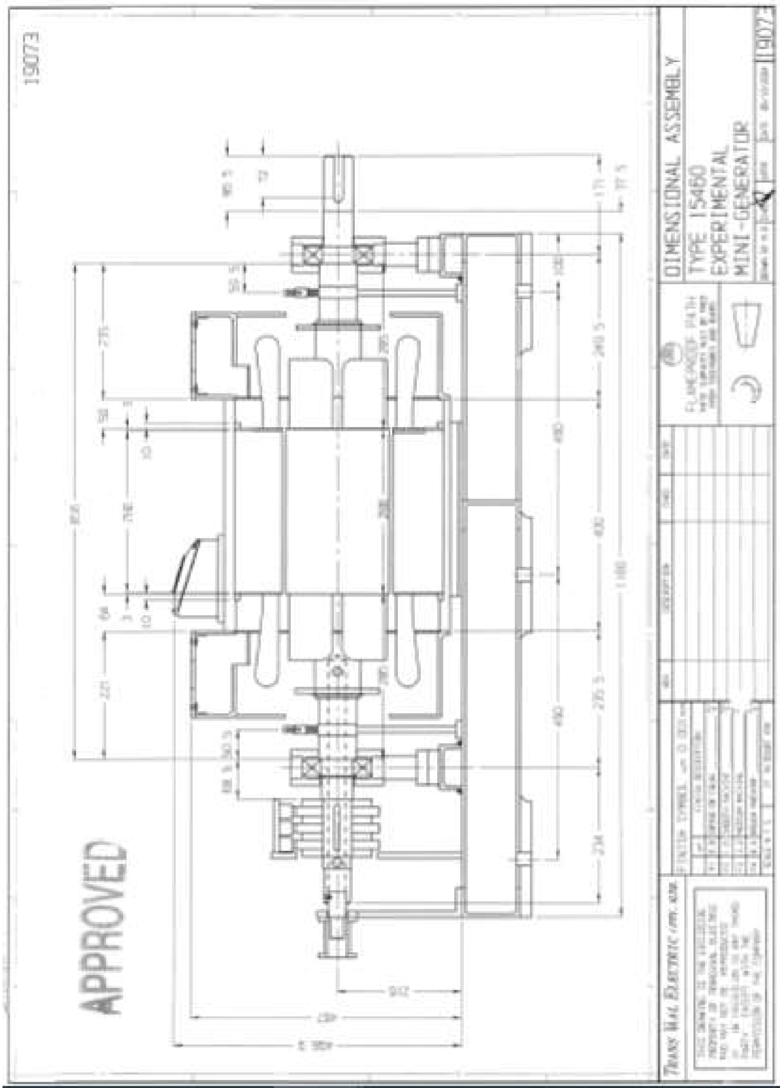
19073
APPROVED
DIMENSIONAL ASSEMBLY
TYPE 15460
EXPERIMENTAL
MINI-GENERATOR
19073

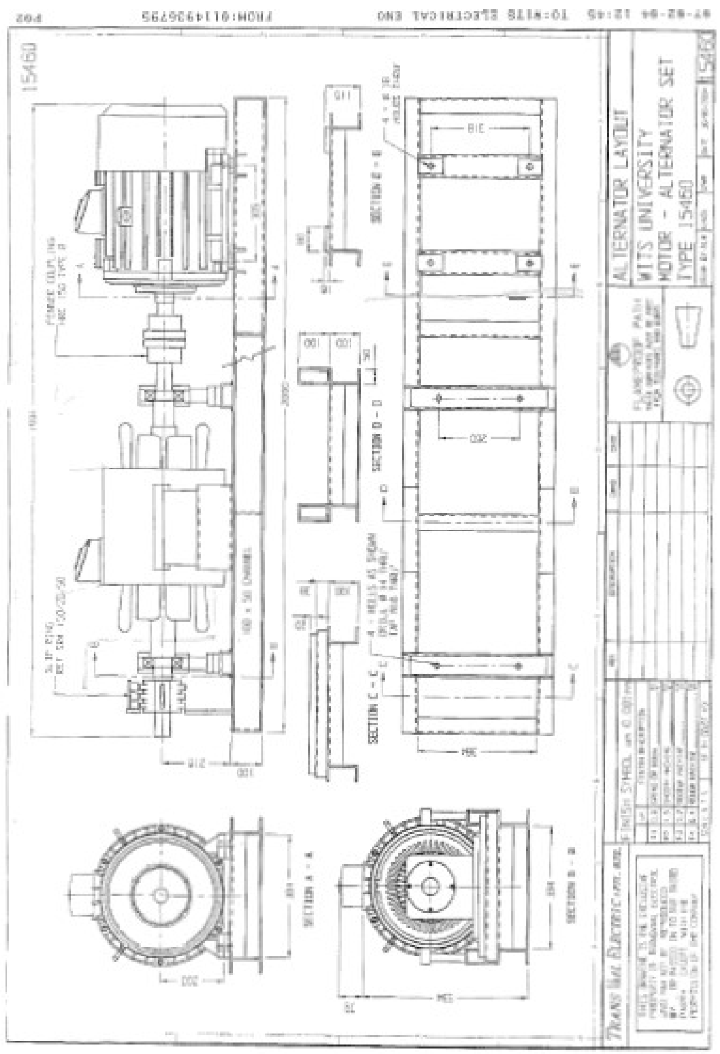
ALTERNATOR LAYOUT
WITS UNIVERSITY
MOTOR - ALTERNATOR SET
TYPE 15460